AD-A066 365 NAVAL POSTGRADUATE SCHOOL MONTEREY CALIF F/G 20/1
NEAR GRAZING SCATTERING BY SLIGHTLY ROUGH SURFACES.(U)
DEC 78 J M BAILIE

UNCLASSIFIED NL

1 OF 2
AD
A066365

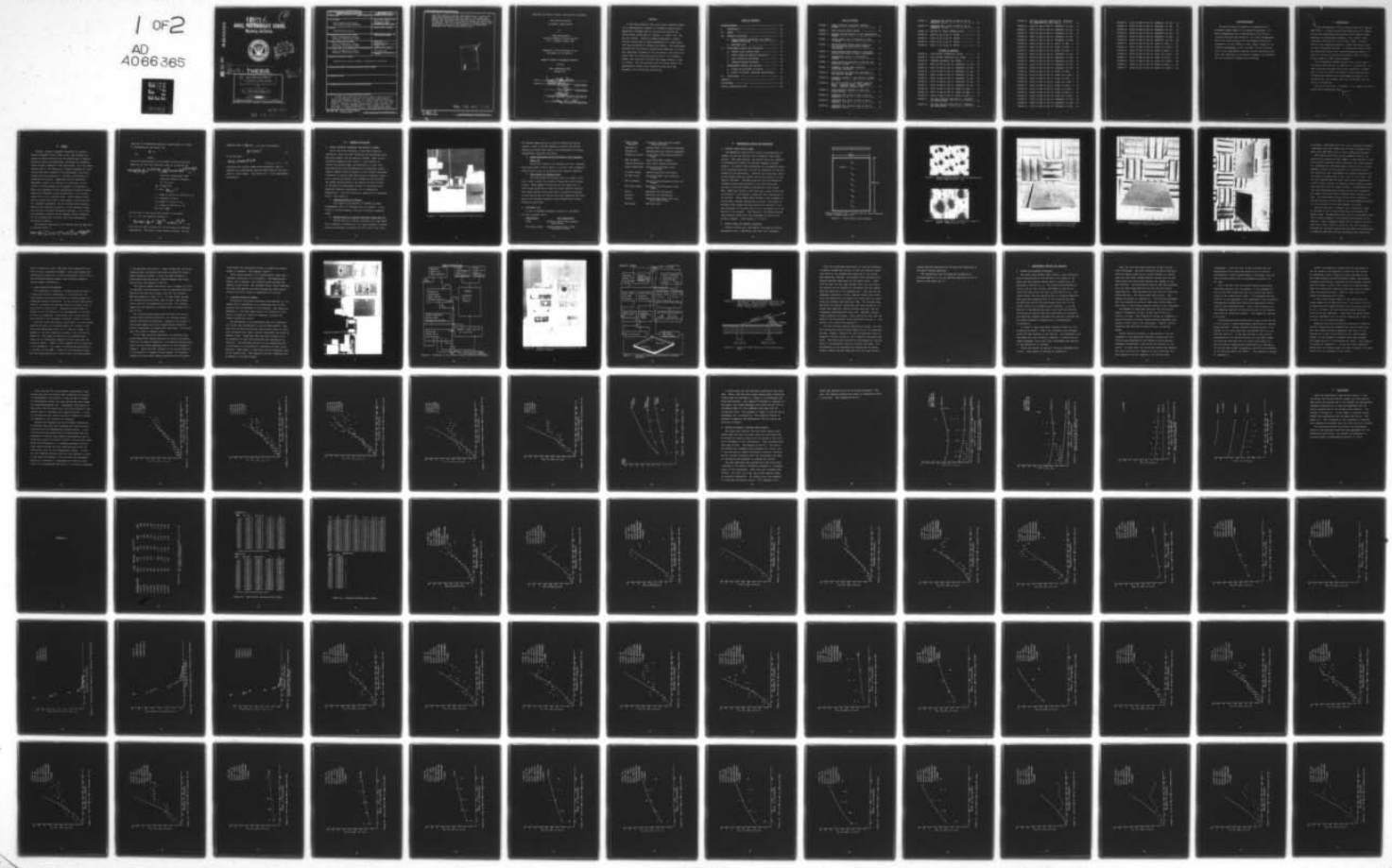

AD A066365

DDC FILE COPY

LEVEL II

(2) B.S.

NAVAL POSTGRADUATE SCHOOL

Monterey, California

DDC
RECEIVED
MAR 26 1979
C

(9) Master's THESIS,

(12) 112 p.

(6) NEAR GRAZING SCATTERING
BY SLIGHTLY ROUGH SURFACES.

by

(10) James Matthew Bailie

(11) Dec[redacted]78

Thesis Advisor: H. Medwin

Approved for public release; distribution unlimited

251 450

79 03 26 053

SECURITY CLASSIFICATION OF THIS PAGE (When Data Entered)

REPORT DOCUMENTATION PAGE		READ INSTRUCTIONS BEFORE COMPLETING FORM
1. REPORT NUMBER	2. GOVT ACCESSION NO.	3. RECIPIENT'S CATALOG NUMBER
4. TITLE (and Subtitle) Near Grazing Scattering By Slightly Rough Surfaces		5. TYPE OF REPORT & PERIOD COVERED Master's Thesis (December 1978) 6. PERFORMING ORG. REPORT NUMBER
7. AUTHOR(s) James Matthew Bailie		8. CONTRACT OR GRANT NUMBER(s)
9. PERFORMING ORGANIZATION NAME AND ADDRESS Naval Postgraduate School Monterey, California 93940		10. PROGRAM ELEMENT, PROJECT, TASK AREA & WORK UNIT NUMBERS
11. CONTROLLING OFFICE NAME AND ADDRESS Naval Postgraduate School Monterey, California 93940		12. REPORT DATE December 1978 13. NUMBER OF PAGES 111
14. MONITORING AGENCY NAME & ADDRESS(if different from Controlling Office) Naval Postgraduate School Monterey, California 93940		15. SECURITY CLASS. (of this report) Unclassified 15a. DECLASSIFICATION/DOWNGRADING SCHEDULE

16. DISTRIBUTION STATEMENT (of this Report)

Approved for public release; distribution unlimited

17. DISTRIBUTION STATEMENT (of the abstract entered in Block 20, if different from Report)

18. SUPPLEMENTARY NOTES

19. KEY WORDS (Continue on reverse side if necessary and identify by block number)

20. ABSTRACT (Continue on reverse side if necessary and identify by block number)

It has been predicted that point source radiation which is at near-grazing incidence to a slightly rough surface generates a boundary wave in the fluid as well as the better known volume wave (I. Tolstoy, J. Acoust. Soc. Am., 63, S60 (1978)). Anechoic chamber experiments, using a surface constructed of rigid hemispheres on a rigid plate, have been performed to compare with theory. The experiments confirm

DD FORM 1 JAN 73 1473 EDITION OF 1 NOV 65 IS OBSOLETE
S/N 0102-014-6601 |

SECURITY CLASSIFICATION OF THIS PAGE (When Data Entered)

that the relative boundary wave amplitude to volume wave amplitude increases as the 3/2 power of the sound frequency when the source and receiver are on the boundary. However the predicted r^2 growth with range reaches a limit at $kr \simeq 100$. For the receiver above the rough surface the experimental values of the scattered sound show some agreement with theoretical predictions.

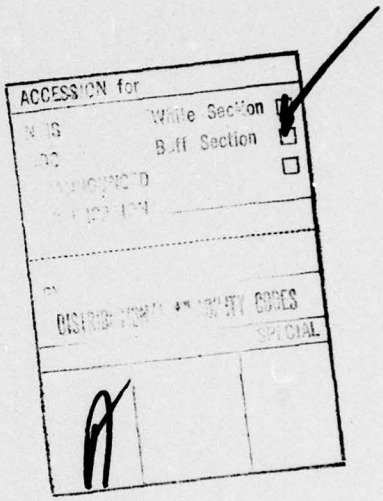

79 03 26 053

Approved for public release; distribution unlimited

Near Grazing Scattering By Slightly Rough Surfaces

by

James Matthew Bailie
Lieutenant Commander, United States Navy
B. S., Frederick College, 1966

Submitted in partial fulfillment of the
requirements for the degree of

MASTER OF SCIENCE IN ENGINEERING ACOUSTICS

from the

NAVAL POSTGRADUATE SCHOOL
December 1978

Author James Matthew Bailie

Approved by: _____
Thesis Advisor

_____
Second Reader

_____
Chairman, Department of Physics and Chemistry

William M. Tolles
Dean of Science and Engineering

ABSTRACT

It has been predicted that point source radiation which is at near-grazing incidence to a slightly rough surface generates a boundary wave in the fluid as well as the better known volume wave (I. Tolstoy, J. Acoust. Soc. Am., 63, S60 (1978)). Anechoic chamber experiments, using a surface constructed of rigid hemispheres on a rigid plate, have been performed to compare with theory. The experiments confirm that the relative boundary wave amplitude to volume wave amplitude increases as the 3/2 power of the sound frequency when the source and receiver are on the boundary. However the predicted $r^{\frac{1}{2}}$ growth with range reaches a limit at $kr \simeq 100$. For the receiver above the rough surface the experimental values of the scattered sound show some agreement with theoretical predictions.

TABLE OF CONTENTS

ACKNOWLEDGEMENTS ---------- 10

I. INTRODUCTION ---------- 11

II. THEORY ---------- 12

III. RESEARCH FACILITIES ---------- 15

A. OCEAN ACOUSTICS LABORATORY AND ANECHOIC CHAMBER FACILITIES ---------- 15

B. EQUIPMENT LIST ---------- 17

IV. EXPERIMENTAL DESIGN AND PROCEDURES ---------- 19

A. TOLSTOY ROUGH SURFACE MODEL ---------- 19

B. SOUND SOURCE AND RECEIVER SELECTION ------- 19

C. DATA COLLECTION PROCEDURES ---------- 26

D. COMPUTER PROGRAM PROCESSES ---------- 28

V. EXPERIMENTAL RESULTS AND ANALYSIS ---------- 36

A. SOURCE AND RECEIVER ON SURFACE ---------- 36

B. SOURCE ON SURFACE, RECEIVER ABOVE SURFACE - 47

VI. CONCLUSIONS ---------- 53

APPENDIX A ---------- 54

BIBLIOGRAPHY ---------- 109

INITIAL DISTRIBUTION LIST ---------- 110

LIST OF FIGURES

FIGURE 1	OCEAN ACOUSTICS LABORATORY COMPUTER SYSTEM	16
FIGURE 2	ROUGH SURFACE MODEL DRAWING	20
FIGURE 3	MAXIMUM PACKING DENSITY OF THE HEMISPHERICAL BOSSES	21
FIGURE 4	RUBBER CEMENT FILL TO EQUATORIAL PLANE OF BOSSES	21
FIGURE 5	SMOOTH SURFACE CONTROL PLATE WITH B & K 4134 MICROPHONE POSITIONED AT TWENTY CENTIMETERS	22
FIGURE 6	ROUGH SURFACE PLATE WITH B & K 4134 MICROPHONE POSITIONED AT TWENTY CENTIMETERS	23
FIGURE 7	EXPERIMENTAL PLATES IN THE ANECHOIC CHAMBER	24
FIGURE 8	OCEAN ACOUSTICS LABORATORY RECEIVING AND PROCESSING SYSTEM	29
FIGURE 9	SCHEMATIC OF THE OCEAN ACOUSTICS LABORATORY EQUIPMENT	30
FIGURE 10	TRANSMITTING AND RECEIVING EQUIPMENT IN THE ANECHOIC CHAMBER	31
FIGURE 11	SCHEMATIC DRAWING OF THE ANECHOIC CHAMBER EQUIPMENT	32
FIGURE 12	ONE CYCLE OF THE 2.5 KILOHERTZ SAWTOOTH PULSE. RECEIVED PULSE. THE SAMPLING PULSE. SAMPLING APERTURE PULSE	33
FIGURE 13	CROSS-SECTIONAL DRAWING OF THE ROUGH SURFACE MODEL	33
FIGURE 14	COMPOSITE PLOT (RATIO OF BWA TO VWA VS. FREQUENCY) 10 CM	41
FIGURE 15	COMPOSITE PLOT (RATIO OF BWA TO VWA VS. FREQUENCY) 20 CM	42
FIGURE 16	COMPOSITE PLOT (RATIO OF BWA TO VWA VS. FREQUENCY) 30 CM	43

FIGURE 17 COMPOSITE PLOT (RATIO OF BWA TO VWA VS. FREQUENCY) 40 CM ---------- 44

FIGURE 18 COMPOSITE PLOT (RATIO OF BWA TO VWA VS. FREQUENCY) 50 CM ---------- 45

FIGURE 19 BWA/VWA VS. RANGE COMPOSITE PLOT -------- 46

FIGURE 20 RATIO OF P_S TO P_6 VS. HEIGHT ---------- 49

FIGURE 21 RATIO OF P_S TO P_6 VS. HEIGHT ---------- 50

FIGURE 22 RATIO OF P_S TO P_6 VS. HEIGHT ---------- 51

FIGURE 23 RATIO OF P_S TO P_6 VS. HEIGHT ---------- 52

FIGURES IN APPENDIX

FIGURE 24 BIOT-TOLSTOY THEORETICAL VALUES --------- 55

FIGURE 25 FAST FOURIER TRANSFORM DATA FORMAT ------ 56

FIGURE 26 COMPUTER PROCESSED DATA FORMAT ---------- 57

FIGURE 27 RATIO OF BWA TO VWA VS. FREQUENCY (10 CM)- 58

FIGURE 28 RATIO OF BWA TO VWA VS. FREQUENCY (20 CM)- 59

FIGURE 29 RATIO OF BWA TO VWA VS. FREQUENCY (30 CM)- 60

FIGURE 30 RATIO OF BWA TO VWA VS. FREQUENCY (40 CM)- 61

FIGURE 31 RATIO OF BWA TO VWA VS. FREQUENCY (10 CM)- 62

FIGURE 32 RATIO OF BWA TO VWA VS. FREQUENCY (20 CM)- 63

FIGURE 33 RATIO OF BWA TO VWA VS. FREQUENCY (30 CM)- 64

FIGURE 34 RATIO OF BWA TO VWA VS. RANGE (10 KHZ)---- 65

FIGURE 35 RATIO OF BWA TO VWA VS. RANGE (20 KHZ)---- 66

FIGURE 36 RATIO OF BWA TO VWA VS. RANGE (30 KHZ) --- 67

FIGURE 37 FFT DATA RELATIVE AMPLITUDE VS. FREQUENCY FOR SMOOTH PLATE ---------- 68

FIGURE 38 FFT DATA RELATIVE AMPLITUDE VS. FREQUENCY FOR ROUGH PLATE ---------- 69

FIGURE 39 FFT DATA RELATIVE AMPLITUDE VS. FREQUENCY FOR HEMISPHERICAL BOSS REPACKS ---------- 70
FIGURE 40 RATIO OF BWA TO VWA VS. FREQUENCY (10 CM)- 71
FIGURE 41 RATIO OF BWA TO VWA VS. FREQUENCY (20 CM)- 72
FIGURE 42 RATIO OF BWA TO VWA VS. FREQUENCY (30 CM)- 73
FIGURE 43 RATIO OF BWA TO VWA VS. FREQUENCY (40 CM)- 74
FIGURE 44 RATIO OF BWA TO VWA VS. FREQUENCY (50 CM)- 75
FIGURE 45 RATIO OF BWA TO VWA VS. RANGE (10 KHZ) --- 76
FIGURE 46 RATIO OF BWA TO VWA VS. RANGE (20 KHZ) --- 77
FIGURE 47 RATIO OF BWA TO VWA VS. RANGE (30 KHZ) --- 78
FIGURE 48 RATIO OF BWA TO VWA VS. FREQUENCY (10 CM)- 79
FIGURE 49 RATIO OF BWA TO VWA VS. FREQUENCY (20 CM)- 80
FIGURE 50 RATIO OF BWA TO VWA VS. FREQUENCY (30 CM)- 81
FIGURE 51 RATIO OF BWA TO VWA VS. FREQUENCY (40 CM)- 82
FIGURE 52 RATIO OF BWA TO VWA VS. FREQUENCY (50 CM)- 83
FIGURE 53 RATIO OF BWA TO VWA VS. RANGE (10 KHZ) --- 84
FIGURE 54 RATIO OF BWA TO VWA VS. RANGE (12.5 KHZ)-- 85
FIGURE 55 RATIO OF BWA TO VWA VS. RANGE (15 KHZ) --- 86
FIGURE 56 RATIO OF BWA TO VWA VS. RANGE (17.5 KHZ)-- 87
FIGURE 57 RATIO OF BWA TO VWA VS. RANGE (20 KHZ)---- 88
FIGURE 58 RATIO OF BWA TO VWA VS. RANGE (22.5 KHZ)-- 89
FIGURE 59 RATIO OF BWA TO VWA VS. RANGE (25 KHZ)---- 80
FIGURE 60 RATIO OF BWA TO VWA VS. RANGE (27.5 KHZ)-- 91
FIGURE 61 RATIO OF BWA TO VWA VS. FREQUENCY (10 CM)- 92
FIGURE 62 RATIO OF BWA TO VWA VS. FREQUENCY (20 CM)- 93
FIGURE 63 RATIO OF BWA TO VWA VS. FREQUENCY (30 CM)- 94

FIGURE 64 RATIO OF BWA TO VWA VS. FREQUENCY (40 CM)- 95
FIGURE 65 RATIO OF BWA TO VWA VS. FREQUENCY (10 CM)- 96
FIGURE 66 RATIO OF BWA TO VWA VS. FREQUENCY (20 CM)- 97
FIGURE 67 RATIO OF BWA TO VWA VS. FREQUENCY (30 CM)- 98
FIGURE 68 RATIO OF BWA TO VWA VS. FREQUENCY (40 CM)- 99
FIGURE 69 RATIO OF BWA TO VWA VS. FREQUENCY (50 CM)- 100
FIGURE 70 RATIO OF BWA TO VWA VS. RANGE (10 KHZ) --- 101
FIGURE 71 RATIO OF BWA TO VWA VS. RANGE (12.5 KHZ)-- 102
FIGURE 72 RATIO OF BWA TO VWA VS. RANGE (15 KHZ)---- 103
FIGURE 73 RATIO OF BWA TO VWA VS. RANGE (17.5 KHZ)-- 104
FIGURE 74 RATIO OF BWA TO VWA VS. RANGE (20 KHZ)---- 105
FIGURE 75 RATIO OF BWA TO VWA VS. RANGE (22.5 KHZ)-- 106
FIGURE 76 RATIO OF BWA TO VWA VS. RANGE (25 KHZ)---- 107
FIGURE 77 RATIO OF BWA TO VWA VS. RANGE (27.5 KHZ)-- 108

ACKNOWLEDGEMENTS

The writer wishes to express his appreciation to Professor Herman Medwin of the Physics Department, U.S. Naval Postgraduate School and Professor Ivan Tolstoy, Visiting Distinguished Professor, U.S. Naval Postgraduate School for their guidance and encouragement during the preparation of this thesis; to Mrs. Jeanie Savage for her computer programming; to Mr. Tom Maris for his construction of the experimental surfaces and the associated hardware; and especially to Lieutenant Commander Joe Bremhorst for his electronic wizardry and friendship.

I. INTRODUCTION

At the 95th meeting of the Acoustical Society of America (May 1978), I. Tolstoy outlined his application of a theory by M.A. Biot describing sound scatter from slightly rough surfaces at near-grazing incidence. This theory, using a boundary condition due to Biot (Biot 1968), is first order in the roughness parameter, rather than second order as other scattering theories: it includes multiple scatter and diffraction which other theories generally ignore: it does not involve the Kirchhoff Assumption which is particularly suspect at small grazing angles.

For near-grazing forward scatter from a point source, the theory predicts that, in addition to a volume wave, coherent multiple Rayleigh scatter will generate a boundary wave in the fluid above the slightly rough rigid surface. At sufficient distances for near-grazing incidence it is predicted that the boundary wave will be greater than the direct or volume wave.

The aim of this work, in general, is to compare Tolstoy's theory with experimental data.

II. THEORY

Tolstoy, using an original formulation of coherent scatter proposed by Biot (1968, 1973), has extended the theory to obtain solutions for the scattering of transient spherical waves by rough planes, providing the roughness scale is small compared to the pulse width. Biot had demonstrated that if the spacing (h) between hemispherical boss centers was small compared to the wavelength, then these bosses could be replaced by a continuous distribution of monopoles and dipoles. Beginning with the assumption $d/\lambda < h/\lambda \ll 1$, where d is a radius of a boss and h is the center to center spacing of the bosses, he proceeded to derive the equations for the scattering of pressure pulses radiated by transient point sources above or on a rough plane (z=0) for an isotropic case. After extensive mathematics, beyond the scope of this thesis, Tolstoy arrived at a temporal expression for the boundary wave pressure. Tolstoy also carried his solution to the frequency domain with the use of Fourier transform techniques. It is here, from Tolstoy's equation for an impulse Fourier transform for the boundary wave solution, that this experimental verification starts.

The spectral amplitude of the boundary wave $P_B(\omega)$ given by Tolstoy (1979) is

$$P_B(\omega) = \frac{\epsilon}{2c^2}\left[J_o^2[\omega r/c] + Y^2[\omega r/c]\right]^{\frac{1}{2}} \omega^2 e^{-\epsilon(z+z_o)\omega^2/c^2} \quad (1)$$

where ϵ is a scattering parameter (proportional to volume of scatterers per unit area), and

$$\frac{\omega}{c} = k.$$

For

$$kr \gg 1,$$

far field substitutions for the Bessel functions allow the equation for the total scattered field to be written as:

$$P_s(f) = \frac{\epsilon}{2\pi} k^2 \left[\theta^2 + \frac{2\pi}{kr} e^{[-2\epsilon k^2 (z+z_o)]} + 2\left[\frac{2\pi}{kr}\right]^{1/2} \theta \sin(kr - \pi/4) e^{[-\epsilon k^2 (z+z_o)]} \right]^{1/2} \quad (2)$$

where for close-packed hemispherical bosses of diameter 0.2 cm in air

$\epsilon = 8.85 \times 10^{-3}$ cm

$k = \omega/c = \frac{2\pi f}{3.43 \times 10^4}$ cm^{-1}

r = range of source to receiver in cm

f = frequency in Hertz

z_o = height of source in cm

z = height of receiver in cm

$\theta = \tan^{-1} \frac{z+z_o}{r}$

For the case of the source and receiver on the plate ($z_o + z = 0$) this equation reduces to

$$P_s(f) = P_\theta(f) = \frac{\epsilon}{2\pi} k^2 \left[\frac{2\pi}{kr}\right]^{1/2} = \epsilon (2\pi r)^{-1/2} k^{3/2} \quad (3)$$

which can be readily solved for various range and frequency combinations. The direct volume acoustic arrival, for the

impulsive case is $\frac{1}{2\pi r}\delta(t - r/c)$ and its spectrum:

$$P_\delta = [2\pi r]^{-1} \tag{4}$$

It is the ratio

$$P_s / P_\delta = \epsilon (2\pi r)^{1/2} k^{3/2} \qquad \text{for } z_o = z = 0 \tag{5}$$

calculated for various ranges and frequencies, that is compared with experimental spectral amplitudes as the major effort in this thesis. (See Section IV - D for experimental procedures.)

III. RESEARCH FACILITIES

A. OCEAN ACOUSTICS LABORATORY AND ANECHOIC CHAMBER

Due to the close proximity of the Ocean Acoustics Laboratory, where the data collection and processing equipment was located, and the Anechoic Chamber, where the experimental apparatus was located, it was possible to collect the analog signal and digitize it in real time. Data acquisition and processing were accomplished using a digital computer system composed of four primary components, interfaced to provide high speed analog to digital conversion, digital processing, data storage and data printout. The design was developed by the Special Projects Section of the Naval Air Development Center in conjunction with Pinkerton Computer Consultants, Inc. of Warminster, Pennsylvania. The four individual components are described below: (see Figure 1)

1. Interdata Model 70 Computer

This digital minicomputer is FORTRAN and BASIC programmable with a 64 thousand byte core memory. In addition to the core memory, data can be stored on magnetic discs.

2. Phoenix Analog to Digital Converter, Model ADC 712

The ADC analog to digital converter is a high speed device capable of encoding ±10 volt input signals in digital form and providing an accuracy of 0.005 volts in 20 volts.

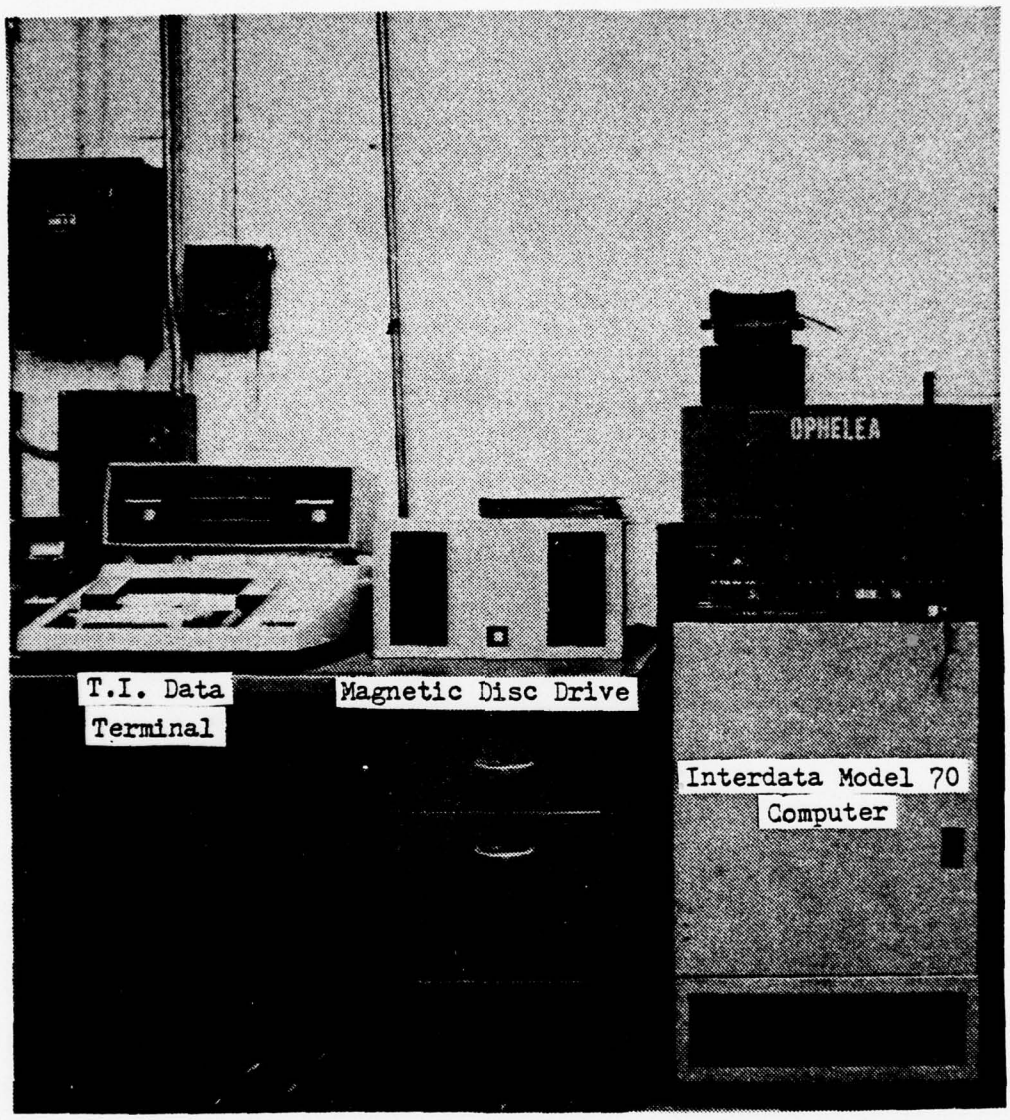

Figure 1. Ocean Acoustics Laboratory Computer System

The maximum sampling rate is 450,000 samples per second; however, rates of 256,000 samples per second and 320,000 samples per second were used in the experiment for optimum experimental frequency resolution.

3. Texas Instruments Silent Electronic Data Terminal, Model 733

The TI 733 consists of a keyboard used as a programming input/output control device, a printer, and a playback/record section used in conjunction with digital cassettes.

4. Orbis Model 76 Diskette Drive

The Orbis Model 76 Diskette Drive is a small, portable, direct access, 256 kilobyte floppy disc data storage device. These magnetic discs provide the capability to store large quantities of data for later computer analysis. The overall system facilitates rapid, accurate processing of any desired type of analog electrical signal and was used mainly for frequency analysis using standard Fast Fourier Transform algorithms.

B. EQUIPMENT LIST

A list of standard equipment referred to throughout the text is given below:

Abbreviation	Full Description
Scope	Tektronix Model 545B 4-channel Oscilloscope
HP Counter 5223L	Hewlett-Packard Model 5223L Electronic Counter

RS648 Timing Simulator	Interface Technology Model RS648 Timing Simulator
Wavetek 114	Wavetek Model 114 Function Generator
Wavetek 114	Wavetek Model 144 Function Generator
Frequency Counter	Donner Model 8050 Frequency/Period Meter
RMS Voltmeter	Fluke 8920A RMS Voltmeter
Digital Multimeter	Fluke 8000A Digital Multimeter
Pulse Transformer	North Hills Wide-Band Pulse Transformer
DC Power Supply	Lambda Regulated Power Supply
KH 3550 Filter	Krohn-Hite Model 3550 Frequency Filter
PAR 133 Preamp	Princton Applied Research Model 113 Preamp
MIC Power Supply	B&K Model 2804 Microphone Power Supply
Source	B&K Model 4134 Microphone
Receiver	B&K Model 4133 Microphone
O-scope	Hewlett-Packard Model 140A Dual Trace Oscilloscope
MIC Preamp	B&K Model 2619

IV. EXPERIMENTAL DESIGN AND PROCEDURES

A. TOLSTOY ROUGH SURFACE MODEL

The experiment required that sound at near-grazing incidence be sent and received over a slightly rough rigid surface. More specifically, the surface was to be composed of hemispherical bosses with maximum hexagonal packing density. To achieve these parameters two rectangular pieces of ¼" aluminum plate were cut with the dimension of 100 centimeters by 82 centimeters. One-half inch holes were drilled and tapped along the center line of each plate at 10 centimeter intervals. Threaded plugs and two non-conducting threaded sleeves were machined to hold the source and receiver at various distance combinations on the plates. Next, edges were fitted on one plate and a layer of #9 chilled lead shot, 2 millimeters in diameter each, was poured on the surface. Using shaker table methods on the slightly elevated plate, maximum packing was achieved. (See Figure 3) Thinned rubber cement was then poured over the shot to insure adherence to the plate and to fill the spaces up to the equator of the spheres. (See Figure 4) The smooth and the rough surface plates were then suspended by wires in the anechoic chamber. (See Figures 5, 6, and 7)

B. SOUND SOURCE AND RECEIVER SELECTION

Several sources were investigated including an Ionovac exponential horn, a B&K Model 4138 (1/8 inch) condenser

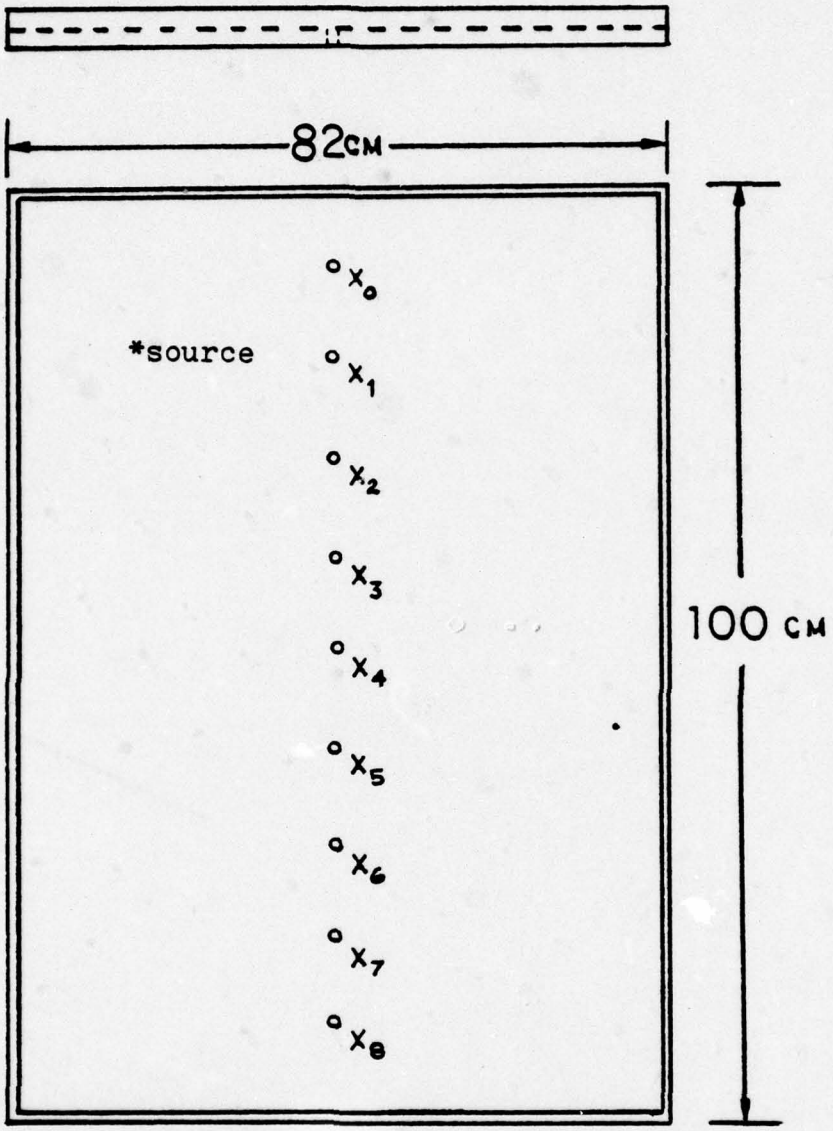

*Source located in this position for all data presented unless otherwise specified.

Figure 2. Rough Surface Model Drawing

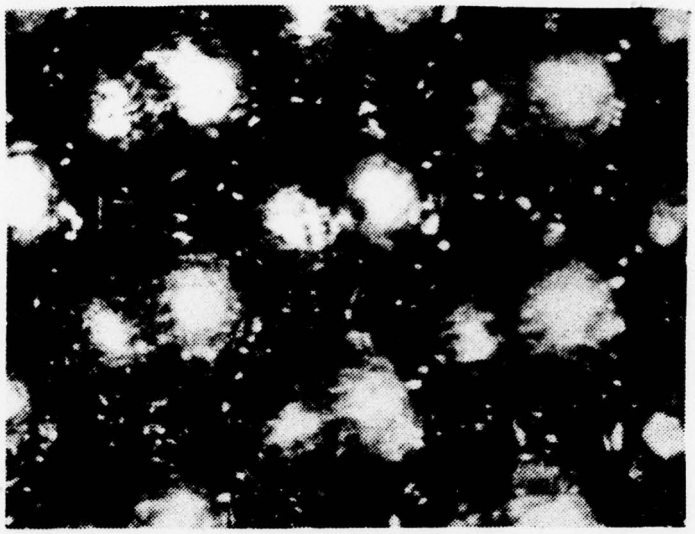

Figure 3. Maximum Packing Density Of The Hemispherical Bosses (Magnification 15x)

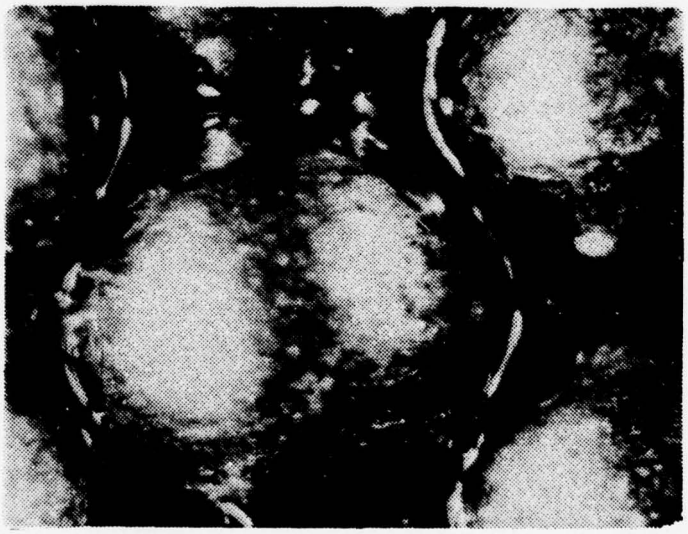

Figure 4. Rubber Cement Fill to Equatorial Plane Of Bosses (Magnification 33x)

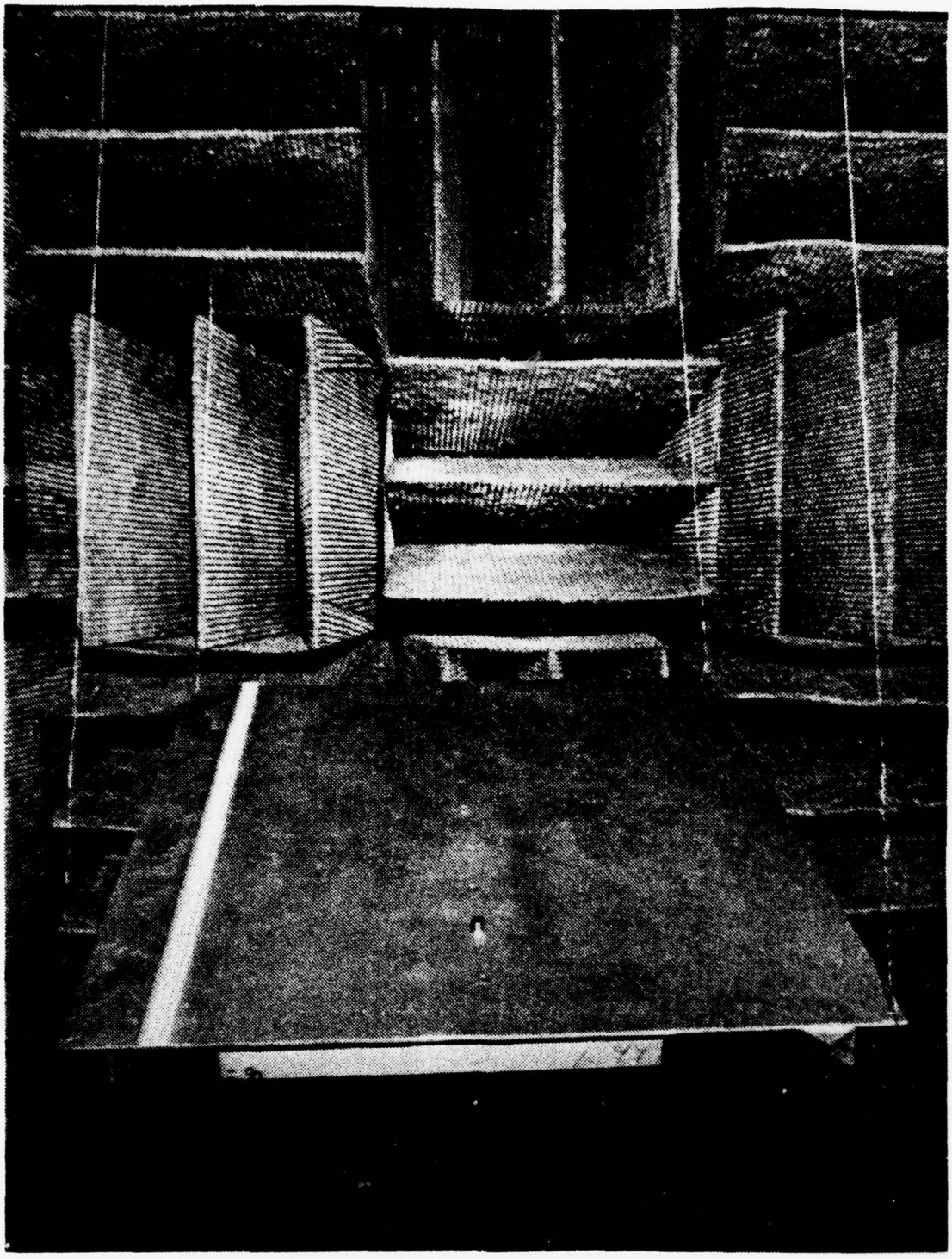

Figure 5. Smooth Surface Control Plate with B + K 4134 Microphone Positioned at Twenty Centimeters

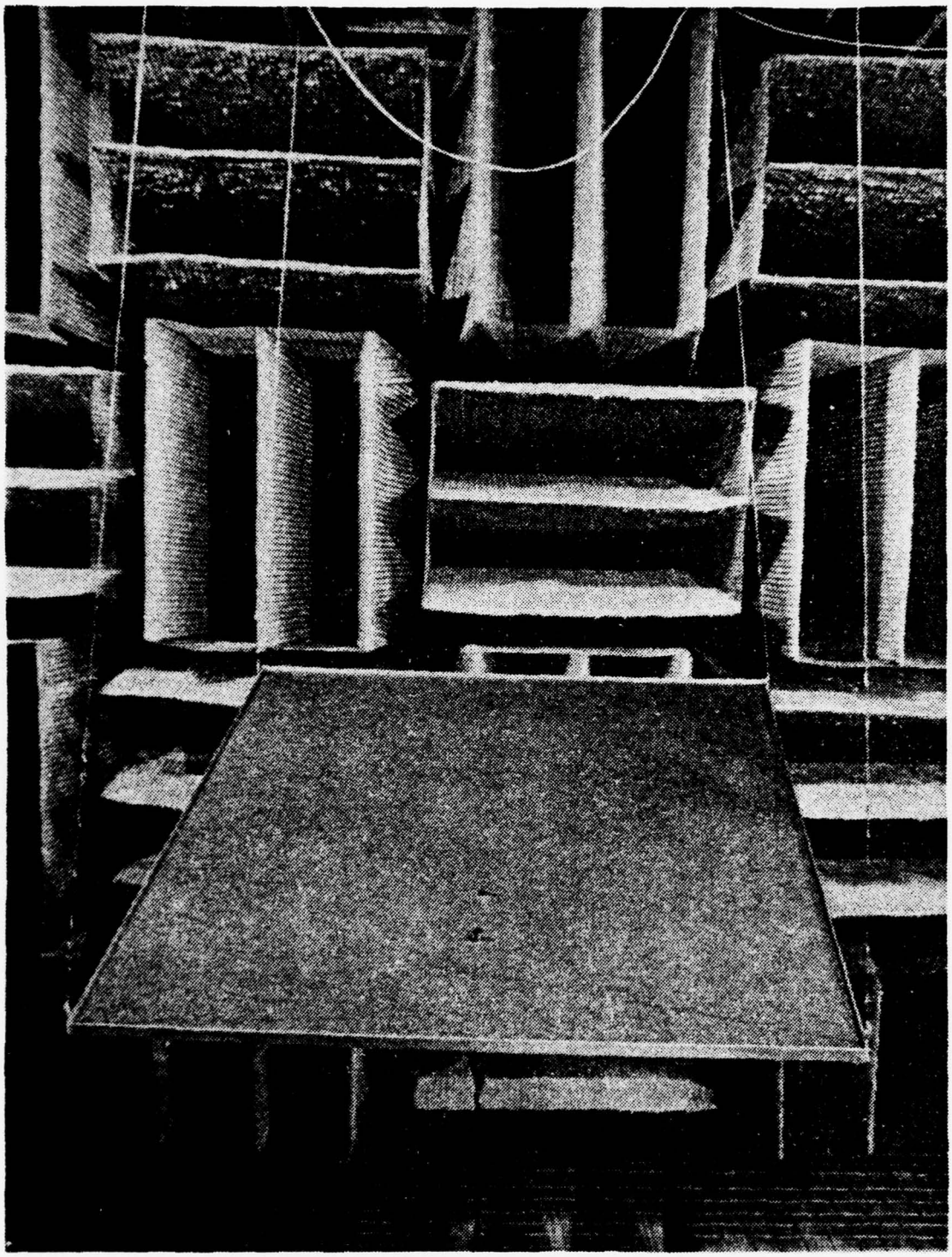

Figure 6. Rough Surface Plate With B + K 4134 Microphone Positioned at Twenty Centimeters

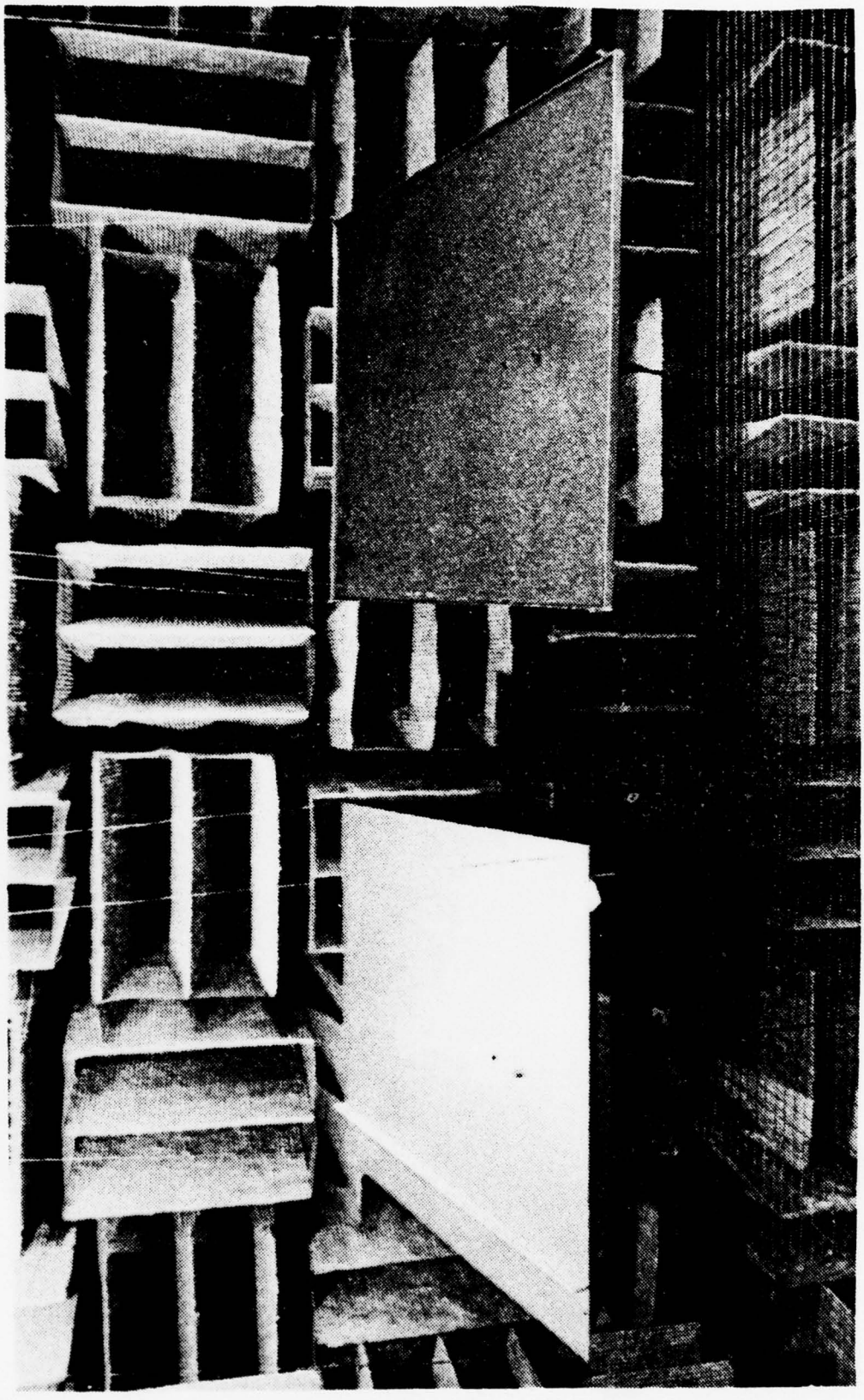

Figure 7. Experimental Plates In The Anechoic Chamber

microphone, a B&K Model 4136 (1/4 inch) condenser microphone, a B&K Model 4133 and a Model 4134 (½ inch) condenser microphone and a B&K Model 4145 (1 inch) condenser microphone.

With these piston-type sources embedded flush in the plate and by pulsing the sent signal, it was possible to produce acoustic pressures almost identical with those produced by a hemispherical radiating simple (point) source of equal strength, except for the presence of a directivity term. The directivity was investigated for various frequencies as a function of source radii (1/16, 1/8, 1/4, 1/2 inch). The 1/8 inch diameter B&K microphone most closely approximated a point source, however the maximum acoustic pressure generated was lower than for larger sources. The B&K Model 4134 (1/2 inch) microphone was selected as the best compromise for large output with nearly omnidirectional radiation pattern. This microphone could be driven with a maximum of 250 volts DC and 35 volts (RMS) AC and approximated adequately a point source for the wave-lengths to be used.

Receiver selection, likewise, was a compromise based on the sensitivity of the receiver and its frequency response range. The B&K Model 4133, with an 8 centimeter probe tube of outer diameter 3.2 millimeters was selected as the receiver. With a frequency range from 3.9 Hertz to 40 kilohertz and a noise floor at -38 dB re 1 Pa, this receiver provided the very best sensitivity and lowest noise available. A compatible B&K Model 2804 DC microphone power supply was

used in conjunction with a B&K Model 2619 preamplifier for this 1/2 inch condenser microphone. This power supply was electrically quieter and, of prime importance, did not drive the microphone heating element, thus reducing thermally induced signal fluctuations.

C. DATA COLLECTION PROCEDURES

The experiment, in general, involved the positioning of a source and receiver alternately on the smooth and the rough surface plates and recording the received signal for subsequent computer evaluation. As can be seen from figures 2 and 5, the source and receiver could be located in any of nine sites on either plate. These positions as shown in figure 2, will be referred to in the remainder of the text by their x_n designator. These source and receiver points were located at ten centimeter intervals, center to center.

With the source and receiver positioned, a 2.5 kHz pulsed sawtooth was sent by the Wavetek Model 144 through a wide-band pulse transformer with a 4 to 1 step-up voltage. An example of the sent signal can be seen in the top trace of figure 12. The slight distortion in the sawtooth was a result of the transformer response to this relatively low frequency signal. However a flat response was not essential to the experiment. The output AC voltage was maintained at a constant 35 volts RMS. A 250 volt DC polarizing voltage was then superimposed for a total of 300 volts peak applied

to the B&K Model 4134 source. These voltages and the source frequency were continually monitored for stability using a Donner Frequency Counter, a Fluke True RMS Voltmeter, a Fluke Digital Multimeter and a Hewlett-Packard Dual Trace Oscilloscope (see Figures 10 and 11).

The receiver signal (see second trace of Figure 12) from the B&K Model 4133 microphone, with its associated 2619 Preamplifier and 2804 Power Supply, was then fed through a PAR 133 PreAmp with a gain of 10. It then passed through two cascaded Krohn-Hite Model 3550 Filters, high passing above 1 kHz and low passing below 100 kHz. The filtered signal was then amplified by another PAR 113 PreAmp with a gain of 200.

The received analog signal was then sent into the adjoining Ocean Acoustics Laboratory to a Phoenix Analog to Digital Converter and digitized. Generally 1000 blocks of this pulsed signal were then averaged before being Fast Fourier Transformed by standard FFT algorithms. The results were then stored on magnetic discs.

In the Ocean Acoustics Laboratory, an Interface Technology Model RS648 Timing Simulator was used as the master timer for the sawtooth generator, the sampling frequency generator and the actual sampling duration of the Interdata 70 Computer. Using available channels on the timing simulator it was possible to trigger the sent signal, the sampling frequency and the proper sampling aperture from the master

clock within 100 nanosecond accuracy to sample any analog signal of interest. (See Figures 8 and 9.)

With a pulse duration of 0.4 milliseconds, there was a frequency resolution of 2.5 kilohertz. The sampling frequency, was in general, 320 kilohertz which provided 128 samples in each block. One thousand blocks, each containing 128 digitized samples were time averaged and these values printed out and/or stored in preparation for the FFT.

D. COMPUTER PROGRAM PROCESSES

Theoretical values were calculated from equation (5) for ranges from 10 centimeters to 50 centimeters and for frequencies from 10 kilohertz to 30 kilohertz. (See Figure 24, Appendix A.) Plotting these values, as a function of frequency or range for a specific frequency, provided the Tolstoy theoretical curves.

The processing of the experimental data for comparison with theory was accomplished in the following manner. Signals from the smooth plate and rough surface plate for equivalent distances were taken, Fourier transformed and stored on magnetic discs. These same data were also printed out at the terminal for real-time monitoring for consistency and stability. The data were printed out for frequencies from 2.5 kilohertz to 60 kilohertz in individual columns titled amplitude, phase angle, A (real part) and jB (imaginary part) of the complex form. (See Figures 25 and 26, Appendix A for an example of the data format).

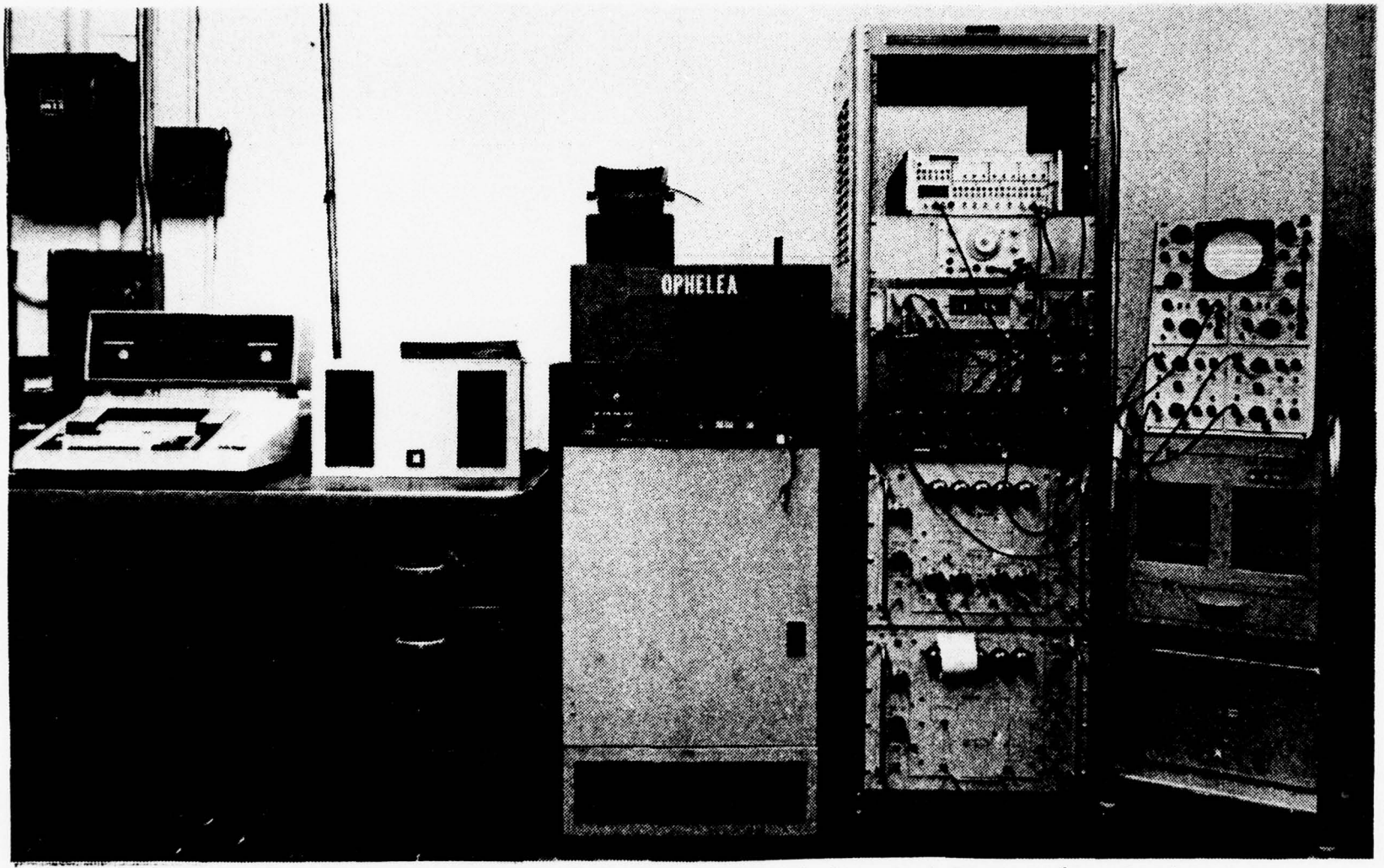

Figure 8. Ocean Acoustics Laboratory Receiving And Processing System

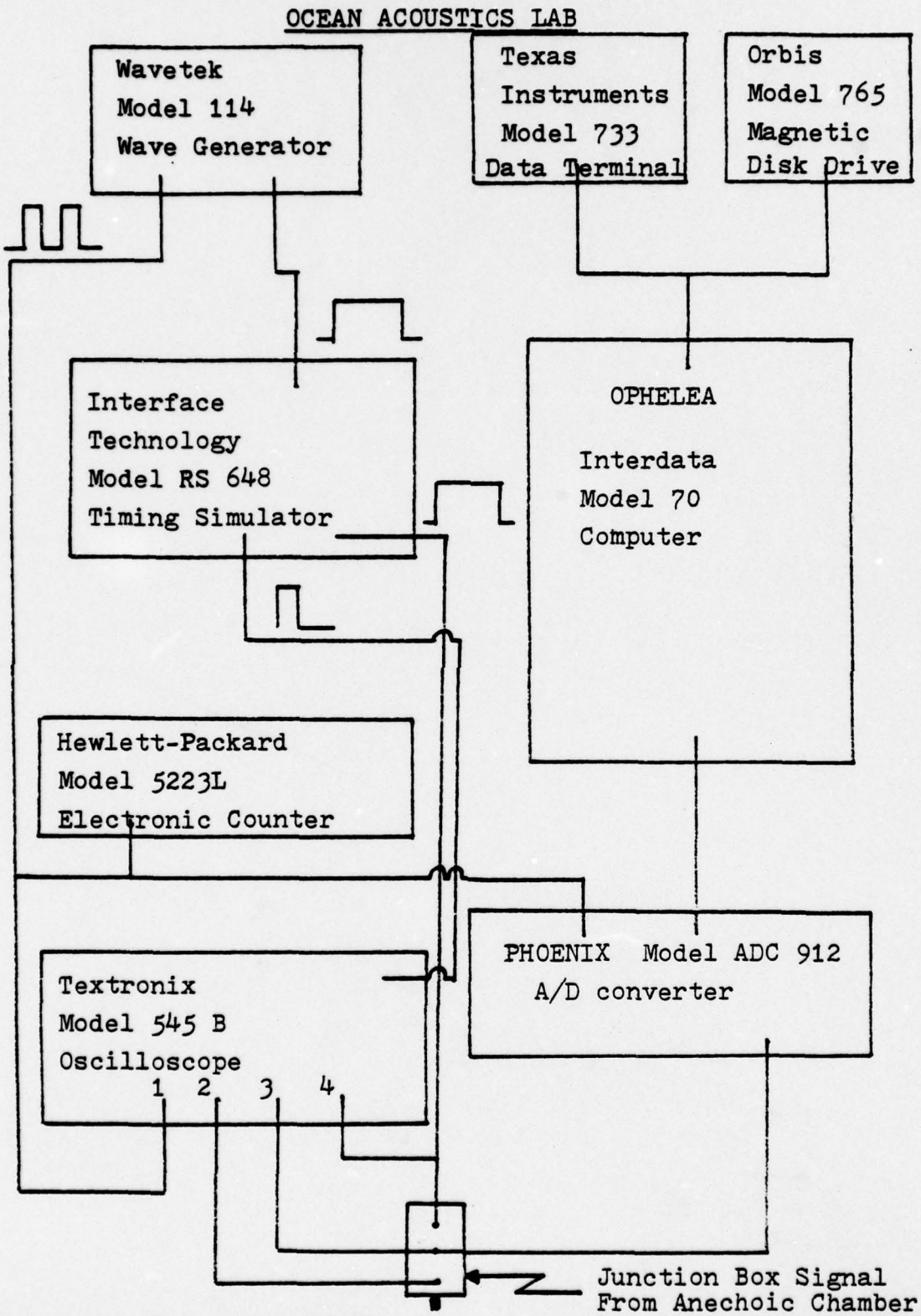

Figure 9. Schematic Of The Ocean Acoustics Laboratory Equipment

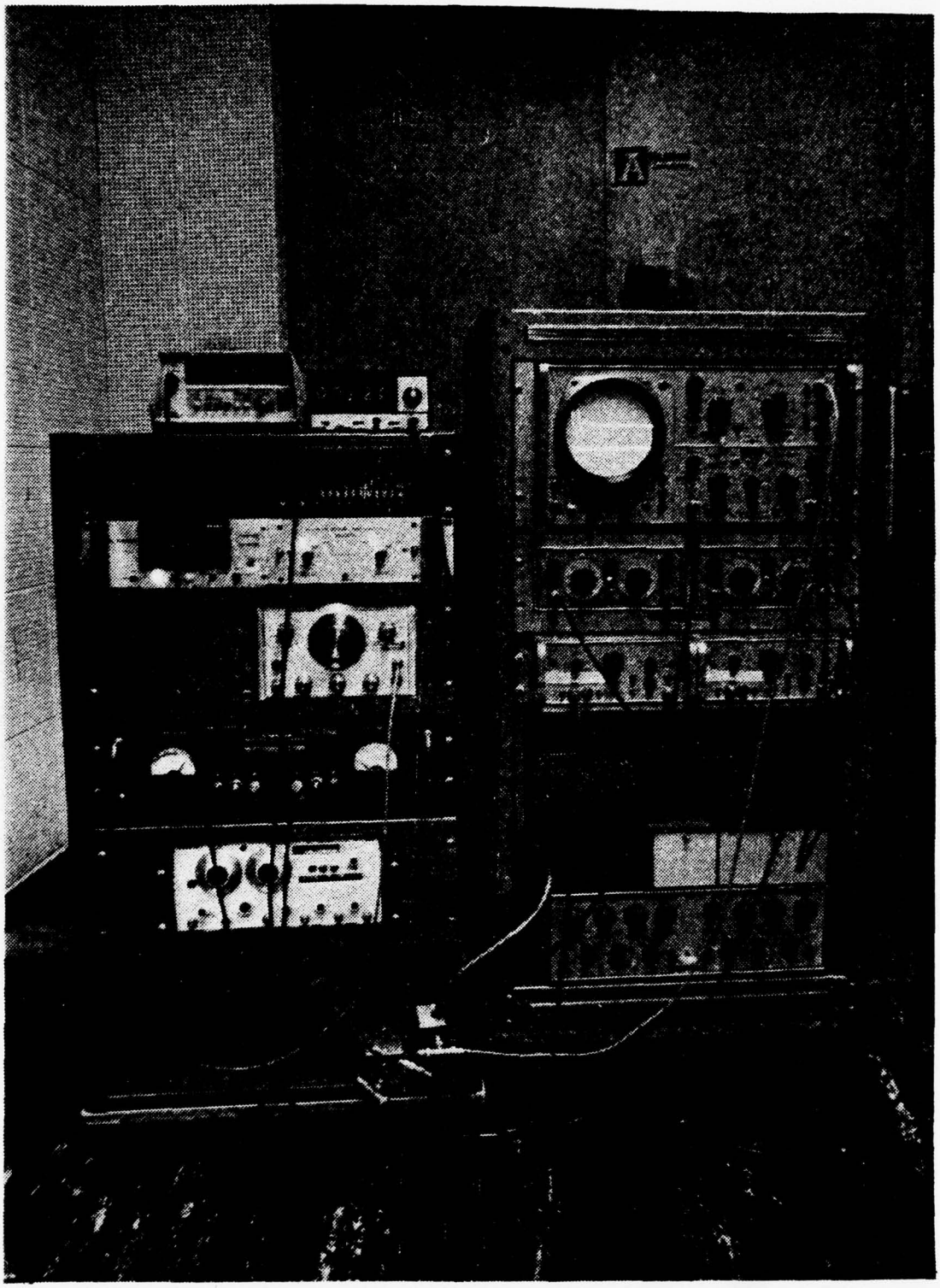

Figure 10. Transmitting And Receiving Equipment In The Anechoic Chamber

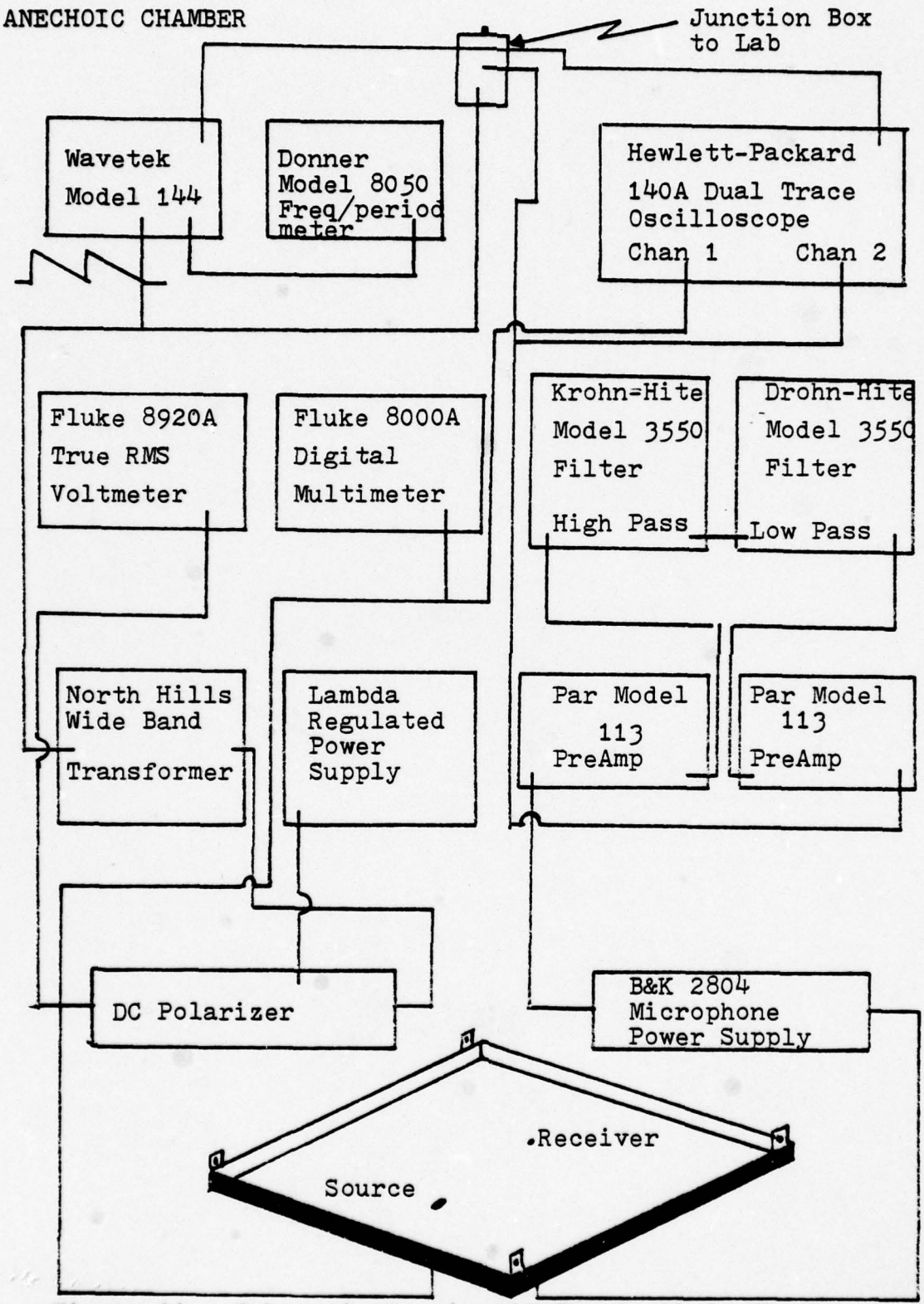

Figure 11. Schematic Drawing Of The Anechoic Chamber Equipment

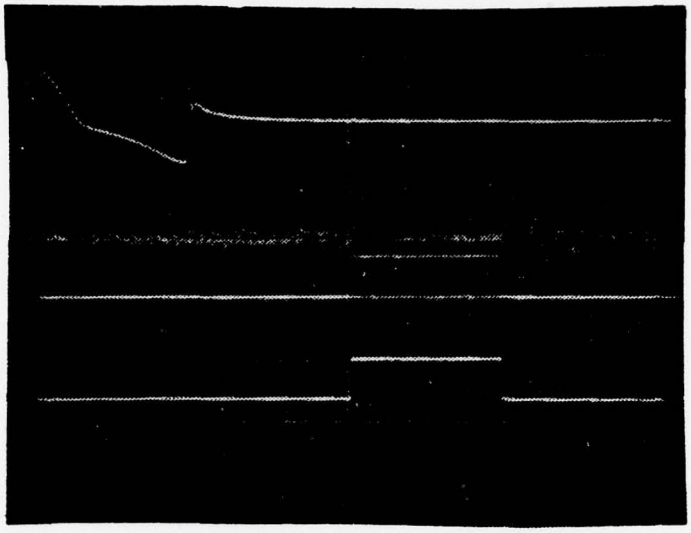

Figure 12. One Cycle Of The 2.5 Kilohertz Sawtooth Pulse (Top Trace). Received Pulse (Trace Two). The Sampling Pulse (Trace Three). Sampling Aperture Pulse (Trace Four).

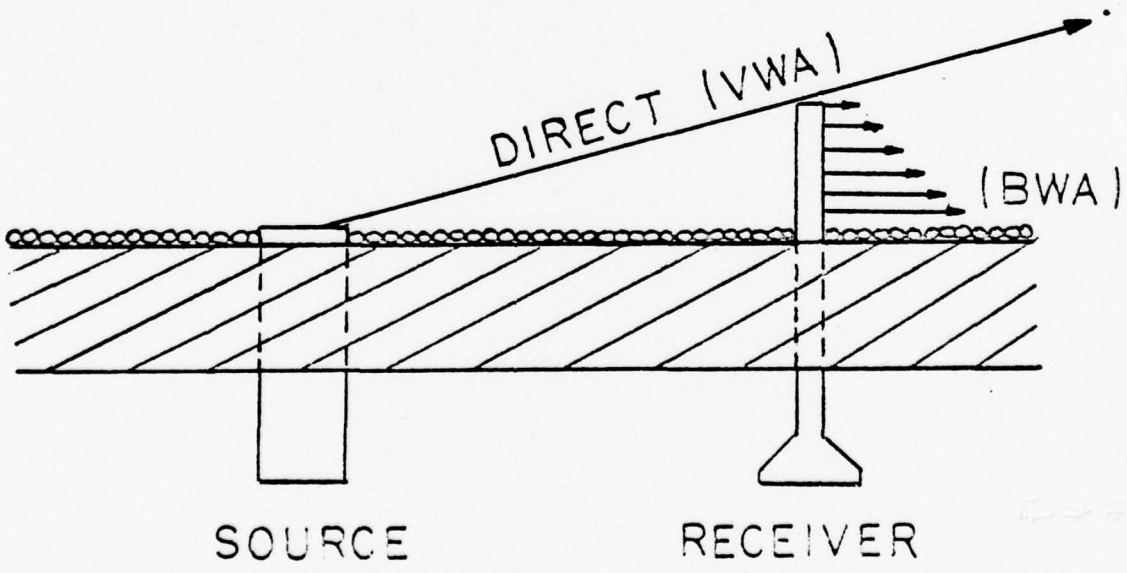

Figure 13. Cross-Sectional Drawing Of The Rough Surface Model.

With the transformed data stored for various distances, a computer program was written to form the required normalized ratio of the boundary wave amplitude to the volume wave amplitude, BWA/VWA. The program first subtracted the complex spectral amplitudes for the smooth plate (VWA) from the data for the rough surface plate; for the source and receiver on the surface the difference was the complex spectral amplitude of the boundary wave. The real and the imaginary components of these complex boundary wave values were then squared and the square root taken with the result being the boundary wave amplitude, BWA. The boundary wave amplitude for specific frequencies was then divided by the volume wave amplitude (smooth surface amplitude) for corresponding frequencies and their ratio, BWA/VWA, plotted versus frequency and range. These data plots were then compared to the theoretical curves calculated from eg. 5. (See Section V for results and analysis.)

For the vertical pressure evaluations (P_s/P_δ), the data were calculated using the same program as for the preceding process. However, equation (2) was now evaluated using incremental vertical values (z) for a specific horizontal distance. Data were then collected by positioning the receiver probe at the equivalent required vertical positions. The experimental P_s was determined by subtracting the smooth surface complex spectral amplitude from the rough surface

complex spectral amplitude and dividing this amplitude by the smooth surface amplitude.

The theoretical curve of P_s/P_δ was determined by dividing equation (2) by the spectral amplitude for an impulse in half space (eq. 4).

V. EXPERIMENTAL RESULTS AND ANALYSIS

A. SOURCE AND RECEIVER ON SURFACE

The first rough surface model (Plate 1) was constructed with a source/receiver hold drilled in the center of the plate and three equally spaced holes on either side, as described in Section IV, A. The source was positioned in hole x_1 (20 cm. from the end, see Figure 2) and the receiver was then moved form x_2 to x_3 and finally to x_4. For these initial runs two cycles of the 2.5 kilohertz sawtooth were sent and a sampling rate of 256 kilohertz was used. The B&K 4133 receiver was positioned flush (z=0) in the plates without the microphone grid installed. A run was made at 10 centimeters and every fourth point was printed out giving the desired 2500 Hertz multiples for evaluation. This data was compared favorably with previous recorded data and showed excellent consistency up to approximately 25 kilohertz.

In hopes of improving higher frequency stability ($\sim$25 kilohertz and above), a B&K 0.32 centimeter outer diameter probe tube was attached to the receiver. All subsequent runs were made with tube installed, primarily to protect the exposed diaphragm, since very little enhancement was observed at the frequencies of interest.

These data showed, in general, excellent agreement with theory. (See Figures 27 through 30, Appendix A).

Next, two runs were made reversing the B&K 4133 and 4134 microphones. The data collection procedures were modified by taking a data set at a given distance on a given plate and then after several minutes, another data set was taken before the source and receiver were changed to the next position. The first smooth data set was then processed with the first rough data set and then with the second rough data set. This procedure was also used for the second smooth data set. The results were then plotted. (See Figures 31 through 33, Appendix A). The excellent agreement with the theoretical curves of these data, would appear to have ruled out any adverse temporal effects on the experiment.

The BWA/VWA of these same data were then plotted for specific frequencies (10 kHz, 20 kHz, and 30 kHz) as a function of range. (See Figures 34 through 36, Appendix A.) These preliminary data also showed excellent agreement with theory to their limit of 30 centimeters. However, further evaluation was required at greater source to receiver ranges.

Before continuing further, it was decided to try and determine if any significant spatially induced data fluctuations were generated by the frequent positioning and subsequent adjustments of the source and receiver in the plates. To check this, the source was removed and replaced. Data were collected and compared for each individual run. (See Figures 37 and 38, Appendix A for multiple data

consistency.) From this test it was concluded that the positioning of the source and receiver at z=0 could be accomplished to within approximately a millimeter, and thus that the positioning could be considered equivalent for all runs.

Due to the fact that the source/receiver positioning holes were one-half inch in diameter, it was necessary to fill in with dry bosses each time the receiver was repositioned in the rough surface model. To investigate the sensitivity of this parameter on the experiment, five consecutive packings were accomplished without any significant fluctuations in the transformed data. Thus it was concluded that the repacking required for each positioning of the receiver could also be considered constant. (See Figure 39, Appendix A for data.)

Source/receiver positioning holes x_0 and x_8 were drilled in both plates to extend measurement capabilities to maximum range available. However aluminum shavings adhered to the surface of the rough plate and a new surface had to be constructed (Plate 2). It was also decided to try a dilute polyurethane as the adhesive/filler vice the rubber cement. Two data runs were made with the source positioned at x_0 and the receiver progressively positioned at x_1 through x_5. The plotted data showed considerable variation when compared to the previous results for Plate 1. (See Figures 40 through 47, Appendix A.)

Further investigation revealed that the wavelength of the two cycles of the sawtooth, coupled with the minimal 20 centimeters travel between the source and edge of the plate was inducing coherent/incoherent signal interference. In addition microscopic inspection of this surface revealed that the bosses, in fact, were covered to a greater depth than their equatorial planes and that there were air spaces under the equatorial plane. However, these data still showed fair agreement with theory.

A third rough surface (Plate 3) was constructed with rubber cement as the adhesive/filler. One cycle of the 2.5 kilohertz sawtooth signal was sent with the source positioned at x_1 to insure that the previously stated problems would be avoided completely. These data once again showed excellent agreement with the Tolstoy theoretical curves up to the 27.5 to 30 kilohertz region.

These data were also plotted as a function of range for specific frequencies and compared with previous data runs. They also showed excellent agreement with theory at frequencies up to about 15 kilohertz for all tested ranges. However, as the frequency increased these data diverged with range relative to the theoretical curves. (See Figures 48 through 60, Appendix A.) It was felt that attenuation effects were the primary reason for this divergence, as these effects are not considered in the theory.

Since this was the third separate experimental rough surface and since the results were consistent with theory to approximately 30 kilohertz, it was decided to attempt to intentionally smooth the rough surface and thus change the roughness parameter (ϵ). Lightweight lubricating oil was poured over the bosses until only 20-25 percent of the surface area of individual shot remained exposed. A data run was made and the results plotted on Figures 61 through 64, Appendix A, as a function of frequency.

Because the roughness had been decreased (smaller ϵ), as expected these data were displaced well below the previous data for the hemispherical packing density. A set of smooth data was substituted as rough surface data and processed to evaluate what happened experimentally as the difference between the smooth (control) plate and the rough surface was decreased (i.e. roughness parameter reduced). These results showed the curve displaced well below the theoretical curve for the hemispherical bosses. In fact, the ratio BWA/VWA differed from zero only because of noise in the signal processing. This procedure was undertaken simply as a sidelight to investigate the relative sensitivity of the experiment and theory to the surface roughness.

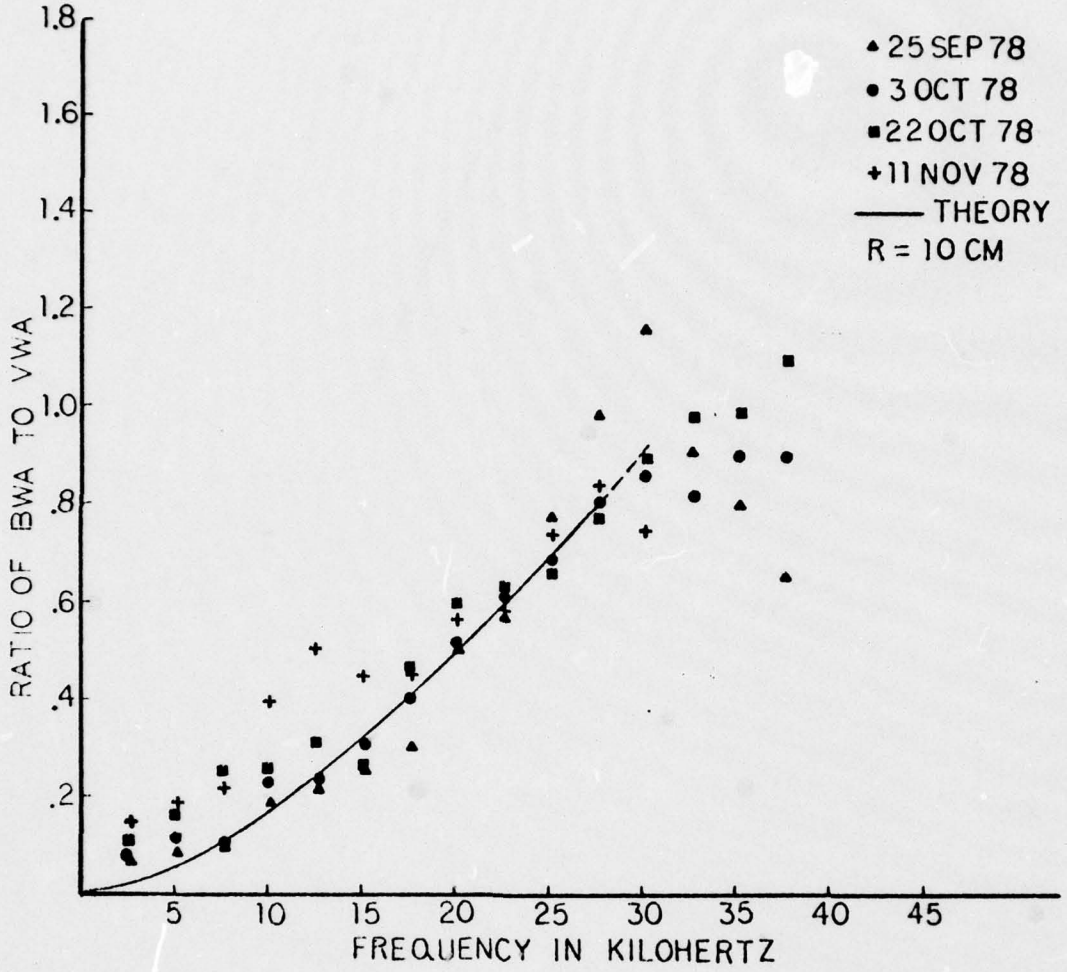

Figure 14. Composite Plot (Ratio of BWA to VWA vs. Frequency) 10 cm.

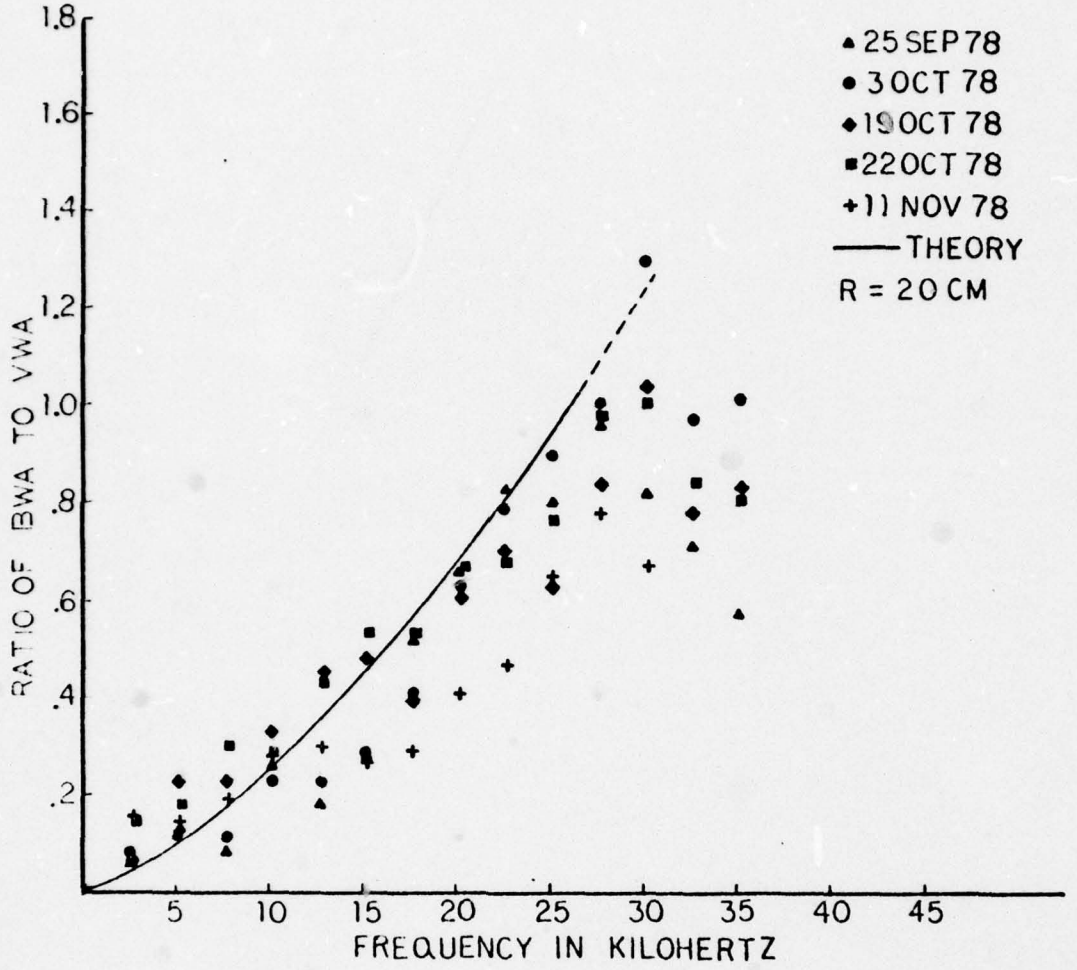

Figure 15. Composite Plot (Ratio of BWA to VWA v. Frequency) 20 cm.

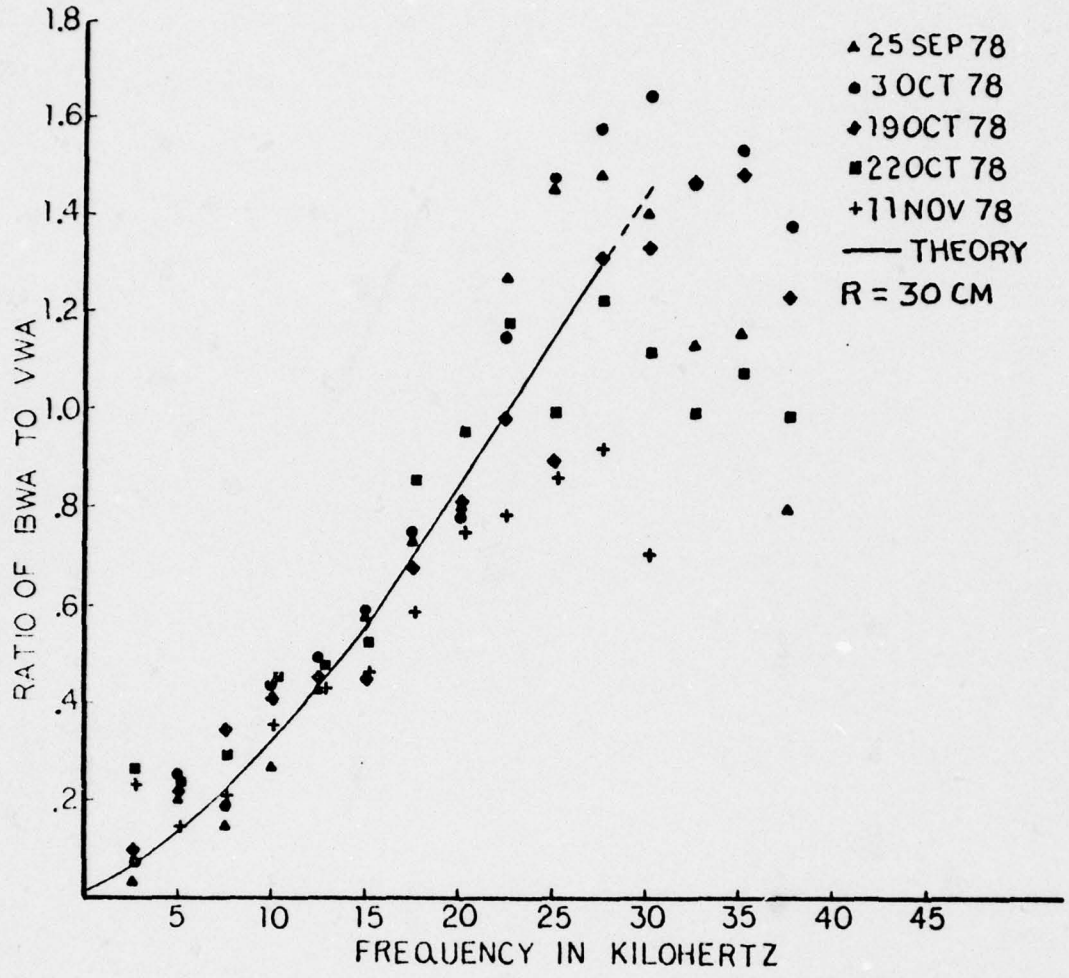

Figure 16. Composite Plot (Ratio of BWA to VWA vs. Frequency) 30 cm.

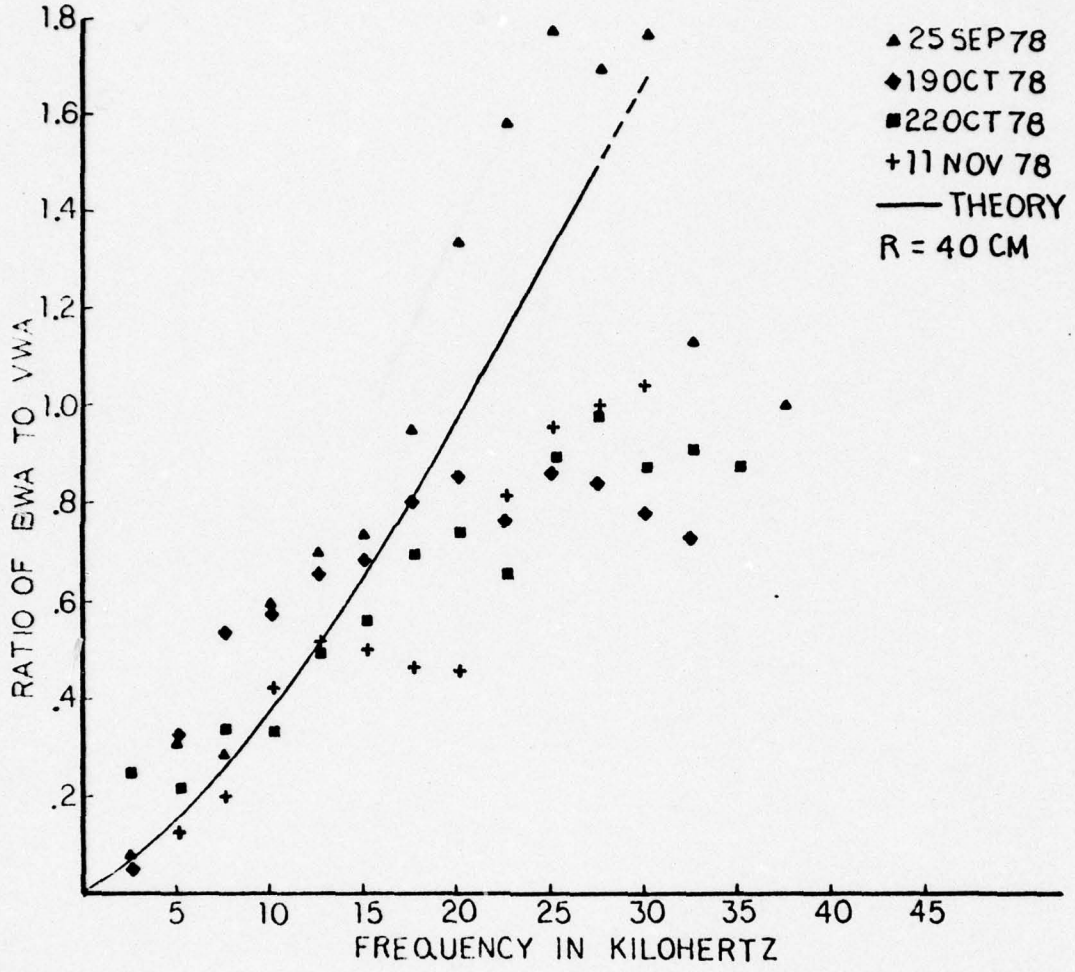

Figure 17. Composite Plot (Ratio of BWA to VWA vs. Frequency) 40 cm.

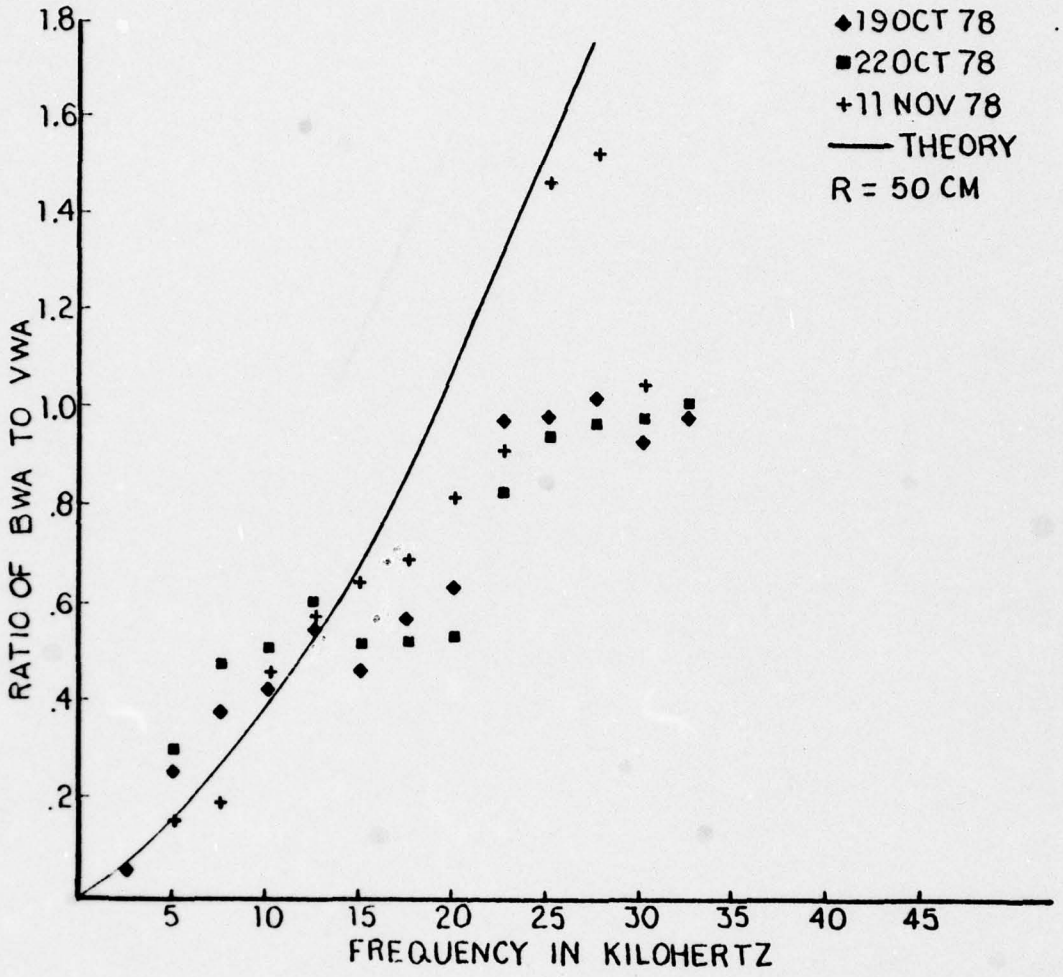

Figure 18. Composite Plot (Ratio of BWA to VWA vs.Frequency) 50 cm.

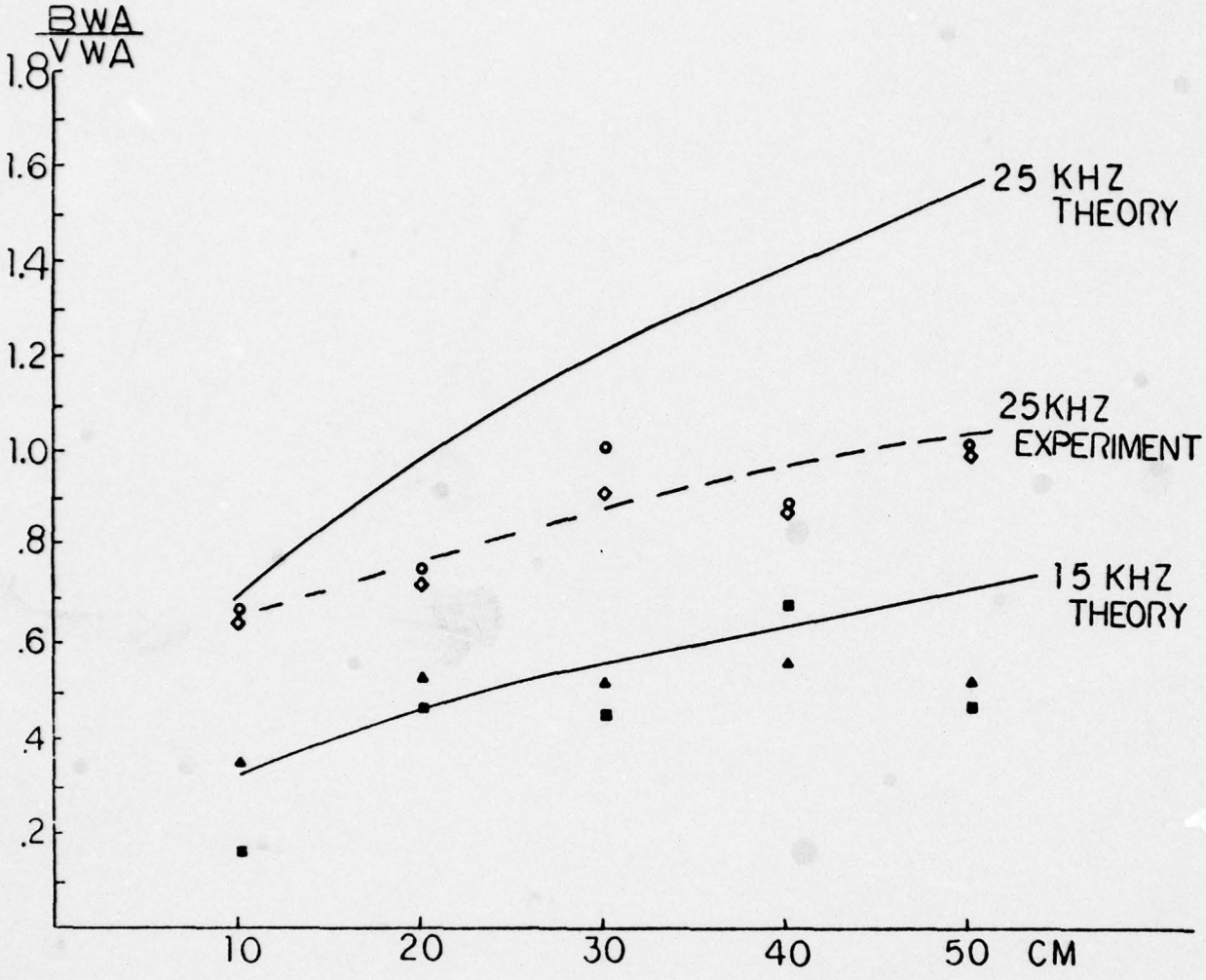

Figure 19. BWA/VWA vs. Range Composite Plot

A fourth plate was only partially constructed and never used. Plate 5 was the final rough surface model constructed. A final data run was made to a range of 50 centimeters and these data plotted. (See Figures 65 through 77, Appendix A.) Once again they showed agreement with theory except that at increasing range the ratio BWA/VWA drops away from the theoretical curve. This appears to happen at $kr \simeq 100$ and is presumably due to attenuation. The composite Figures 14 through 19 summarize the experimental work for source and receiver on surface.

B. SOURCE ON SURFACE; RECEIVER ABOVE SURFACE

The source and receiver were positioned twenty centimeters apart and data sets were taken for individual runs by moving the receiver probe above the plates in one centimeter increments to five centimeters. These processed data were then plotted. (See Figures 20 and 21.) This entire run showed much divergence when compared with theory, due to the fact that at twenty centimeters horizontal distance and for vertical distances above two centimeters the angle of inclination was excessive to compare with theory.

The same experiment was repeated with data sets being collected at one quarter centimeter intervals to a maximum height of two centimeters. These data were processed and plotted. The ratio, P_s to P_g, was plotted against range for specific frequencies. The results were then compared to calculated theoretical values. Fair agreement with

theory was observed from five to fifteen kilohertz. However, the results diverged from theory at frequencies above 15 kilohertz. (See Figures 22 and 23.)

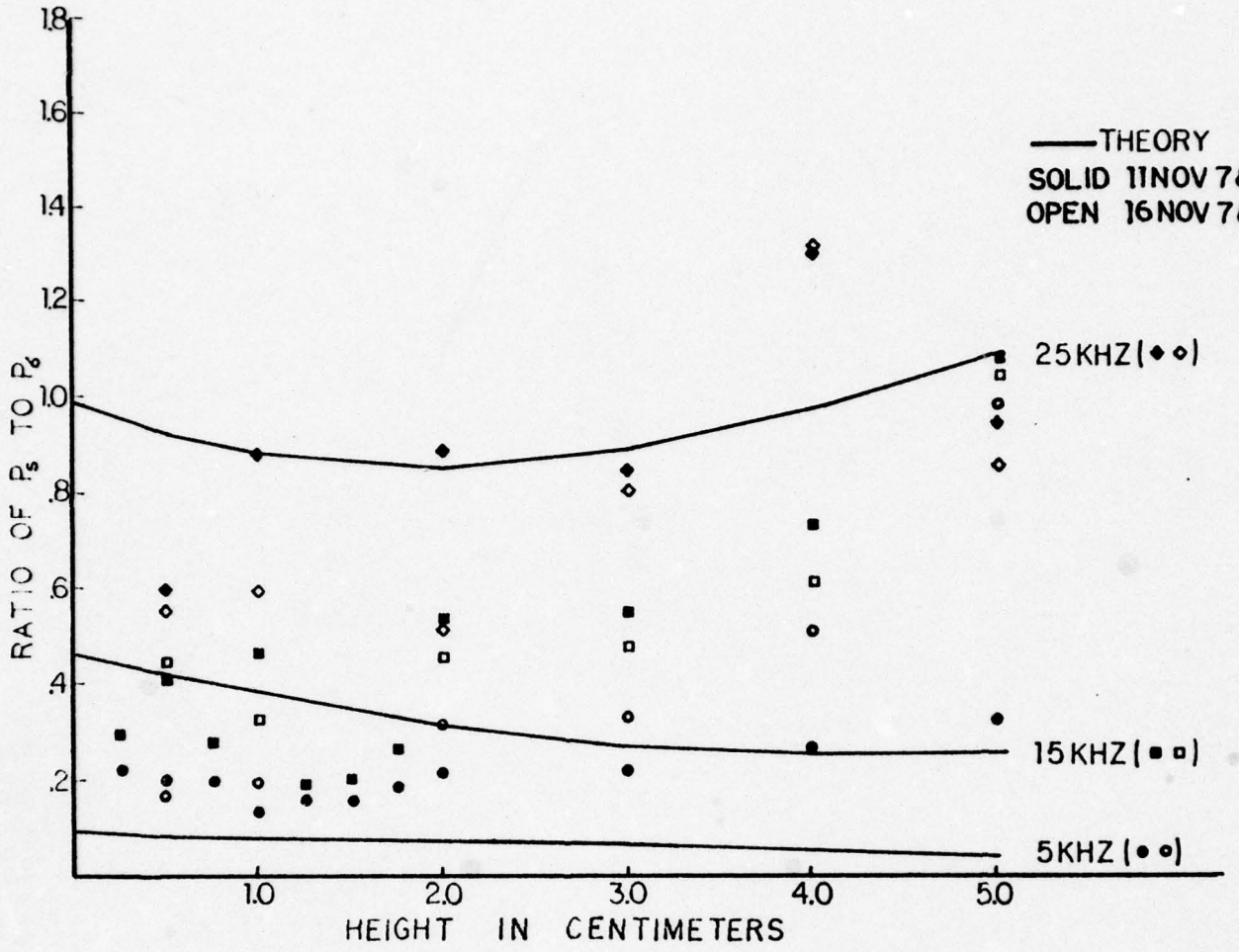

Figure 20. Ratio Of P_s To P_6 vs. Height of Receiver (20 cm. Separation Source To Receiver)

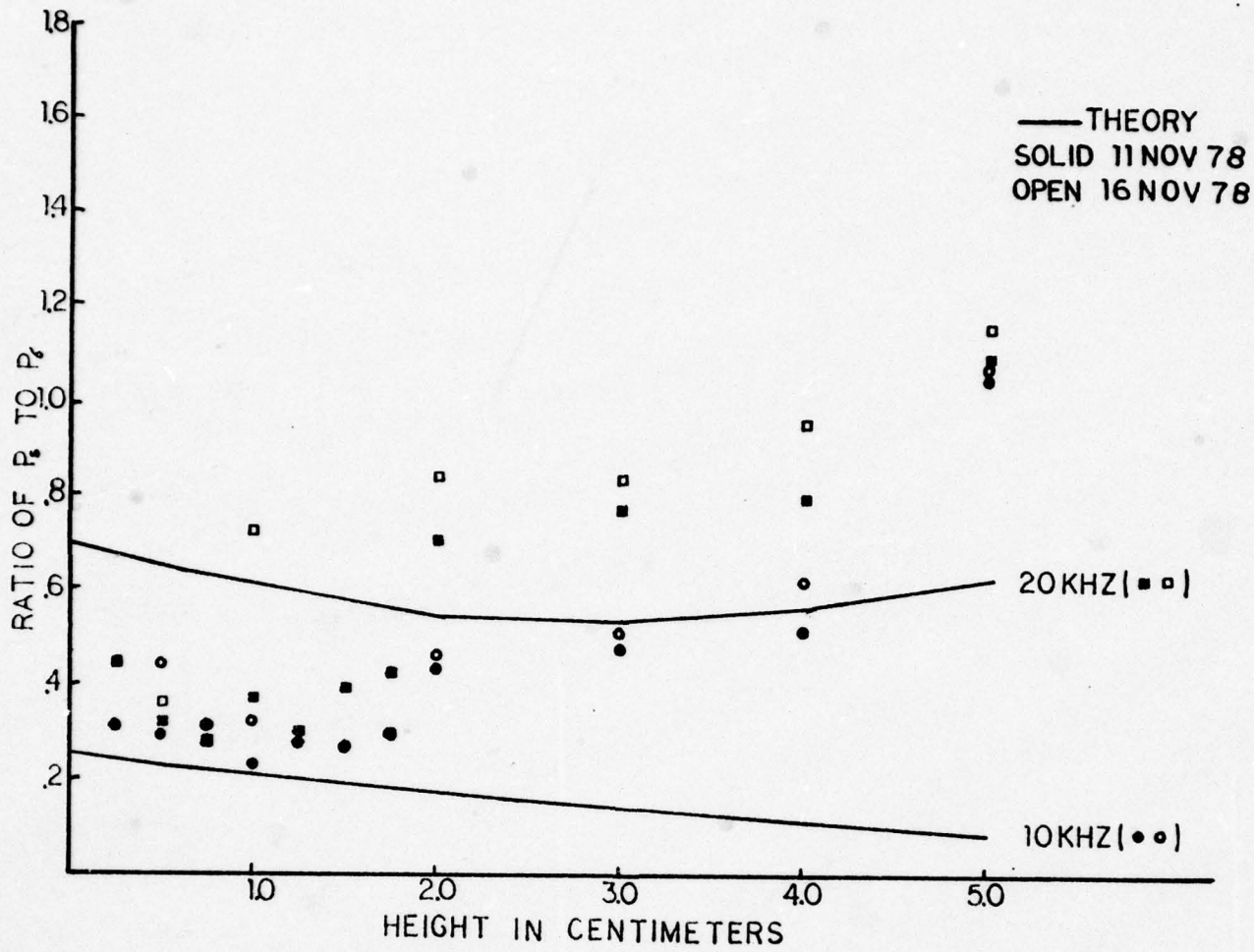

Figure 21. Ratio of P_s To P_δ vs. Height of Receiver (20 cm. Separation Source To Receiver)

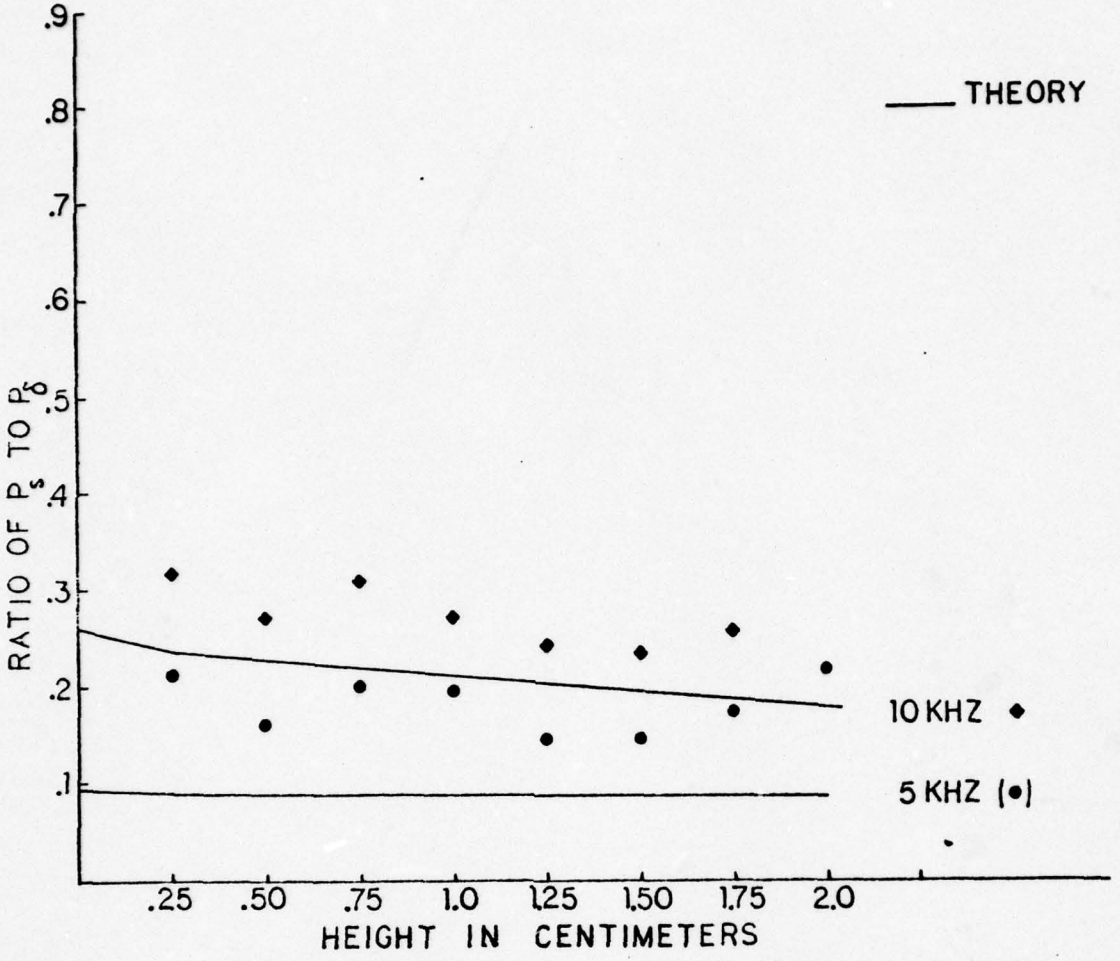

Figure 22. Ratio Of P_s To P_o vs. Height of Receiver (20 cm. Source Receiver Separation)

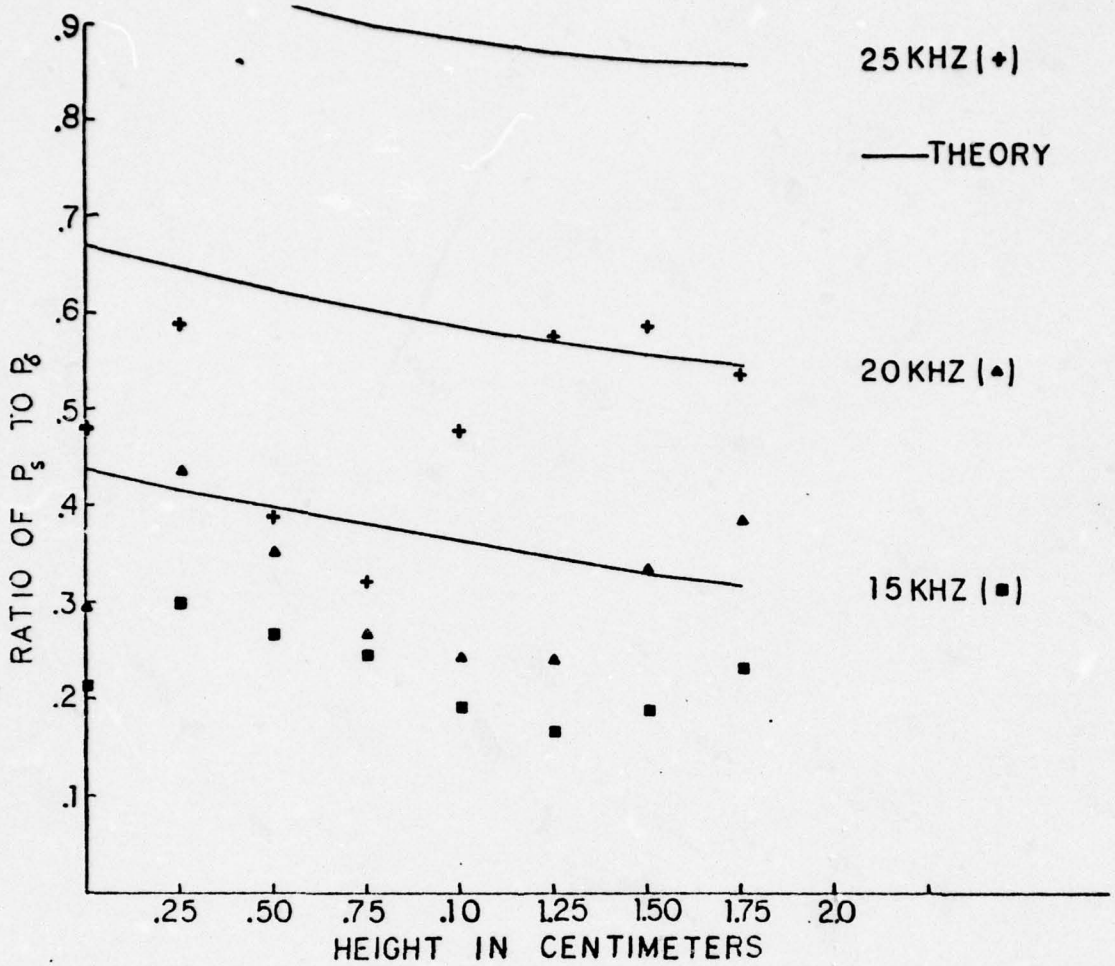

Figure 23. Ratio Of P_s To P_6 vs. Height.

VI. CONCLUSIONS

Using the experimental rough surface models, it has been shown that for $kh<1$ and for ranges less than $kr \simeq 100$, when source and receiver are on the surface the near-grazing incidence scattering is in excellent agreement with the Tolstoy predictions for the boundary wave behavior. (See Figures 14 through 18.) As the range is increased beyond $kr \simeq 100$ the experimental data diverges from theory. (See Figure 19.) This divergence is due presumably to boundary wave attenuation processes which the theory does not include.

For the receiver above the surface the experimental values of the scattered sound show some agreement with the theoretical predictions: for example the dependence on receiver height is approximately parallel to theory.

APPENDIX A

$$P_s/P_\sigma = BWA/VWA = (2\pi r)^{\frac{1}{2}} k^{3/2}$$

Frequency (Hz)	r=10	r=20	r=30	r=40	r=50
1.0×10^4	.176	.25	.305	.35	.394
1.25×10^4	.250	.354	.433	.498	.558
1.5×10^4	.323	.457	.560	.646	.722
1.75×10^4	.411	.579	.712	.823	.921
2.0×10^4	.498	.7	.863	1.00	1.12
2.25×10^4	.597	.842	1.04	1.20	1.34
2.5×10^4	.696	.984	1.21	1.39	1.56
2.75×10^4	.806	1.14	1.40	1.61	1.81
3.0×10^4	.916	1.29	1.59	1.83	2.05

Figure 24. Biot-Tolstoy Theoretical Values ($Z_o = Z = 0$)
(r = range in centimeters)

PERFORMING FFT.

FREQ	AMPLITUDE	PHASE ANGLE	A	JB
0.	0.306E-01	0.314E 01	-0.306E-01	0.000E 00
2500.	0.546E 00	0.243E 01	-0.414E 00	0.356E 00
5000.	0.108E 01	0.511E 00	0.940E 00	0.527E 00
7500.	0.817E 00	0.279E 00	0.786E 00	0.225E 00
10000.	0.114E 01	-0.137E 00	0.113E 01	-0.155E 00
12500.	0.149E 01	-0.828E 00	0.101E 01	-0.110E 01
15000.	0.152E 01	-0.173E 01	-0.235E 00	-0.151E 01
17500.	0.103E 01	-0.263E 01	-0.899E 00	-0.502E 00
20000.	0.562E 00	-0.313E 01	-0.562E 00	-0.889E-02
22500.	0.363E 00	0.274E 01	-0.335E 00	0.140E 00
25000.	0.236E 00	0.261E 01	-0.203E 00	0.120E 00
27500.	0.200E 00	0.240E 01	-0.148E 00	0.134E 00
30000.	0.170E 00	0.212E 01	-0.881E-01	0.146E 00
32500.	0.138E 00	0.186E 01	-0.397E-01	0.132E 00
35000.	0.113E 00	0.161E 01	-0.498E-02	0.113E 00
37500.	0.906E-01	0.141E 01	0.148E-01	0.893E-01
40000.	0.703E-01	0.115E 01	0.288E-01	0.642E-01
42500.	0.452E-01	0.951E 00	0.263E-01	0.368E-01
45000.	0.223E-01	0.110E 01	0.101E-01	0.198E-01
47500.	0.212E-01	0.158E 01	-0.273E-03	0.212E-01
50000.	0.275E-01	0.188E 01	-0.841E-02	0.261E-01
52500.	0.261E-01	0.185E 01	-0.706E-02	0.251E-01
55000.	0.242E-01	0.170E 01	-0.305E-02	0.240E-01
57500.	0.238E-01	0.202E 01	-0.104E-01	0.215E-01
000.	0.233E-01	0.190E 01	-0.750E-02	0.221E-01

25 POINTS HAVE BEEN WRITTEN ONTO FLOPPY.

PERFORMING FFT.

FREQ	AMPLITUDE	PHASE ANGLE	A	JB
0.	0.135E 00	0.314E 01	-0.135E 00	0.000E 00
2500.	0.407E 00	0.251E 01	-0.329E 00	0.240E 00
5000.	0.102E 01	0.371E 00	0.947E 00	0.368E 00
7500.	0.786E 00	0.834E-01	0.783E 00	0.655E-01
10000.	0.115E 01	-0.486E 00	0.102E 01	-0.537E 00
12500.	0.143E 01	-0.128E 01	0.403E 00	-0.137E 01
15000.	0.147E 01	-0.218E 01	-0.842E 00	-0.120E 01
17500.	0.116E 01	0.309E 01	-0.116E 01	0.560E-01
20000.	0.659E 00	0.247E 01	-0.515E 00	0.412E 00
22500.	0.394E 00	0.197E 01	-0.154E 00	0.362E 00
25000.	0.258E 00	0.175E 01	-0.457E-01	0.254E 00
27500.	0.190E 00	0.141E 01	0.308E-01	0.188E 00
30000.	0.135E 00	0.133E 01	0.325E-01	0.131E 00
32500.	0.113E 00	0.108E 01	0.536E-01	0.100E 00
35000.	0.877E-01	0.552E 00	0.747E-01	0.460E-01
37500.	0.555E-01	0.202E 00	0.544E-01	0.111E-01
40000.	0.300E-01	-0.184E 00	0.295E-01	-0.549E-02
42500.	0.110E-01	-0.957E 00	0.634E-02	-0.899E-02
45000.	0.107E-01	0.289E 01	-0.104E-01	0.272E-02
47500.	0.156E-01	0.210E 01	-0.788E-02	0.135E-01
50000.	0.115E-01	0.191E 01	-0.386E-02	0.108E-01
52500.	0.855E-02	0.179E 01	-0.184E-02	0.835E-02
55000.	0.100E-01	0.186E 01	-0.286E-02	0.963E-02
57500.	0.122E-01	0.232E 01	-0.830E-02	0.888E-02
000.	0.976E-02	0.219E 01	-0.570E-02	0.792E-02

25 POINTS HAVE BEEN WRITTEN ONTO FLOPPY.

Figure 25. Fast Fourier Transform Data Format.

BOUNDARY WAVE

FREQ	REAL	IMAG	AMP	PHI ANG	BWA-VWA	BWP-VW
0.	-0.104E 00	0.000E 00	0.104E 00	0.314E 01	0.340E 01	0.00E 00
2500.	0.851E-01	-0.116E 00	0.144E 00	-0.939E 00	0.264E 00	-0.34E 01
5000.	0.725E-02	-0.159E 00	0.159E 00	-0.153E 01	0.148E 00	-0.20E 01
7500.	-0.286E-02	-0.160E 00	0.160E 00	-0.159E 01	0.196E 00	-0.19E 01
10000.	-0.114E 00	-0.382E 00	0.398E 00	-0.186E 01	0.350E 00	-0.17E 01
12500.	-0.604E 00	-0.273E 00	0.663E 00	-0.272E 01	0.445E 00	-0.19E 01
15000.	-0.607E 00	0.303E 00	0.678E 00	0.268E 01	0.445E 00	0.44E 01
17500.	-0.263E 00	0.558E 00	0.616E 00	0.201E 01	0.599E 00	0.46E 01
20000.	0.471E-01	0.421E 00	0.423E 00	0.146E 01	0.753E 00	0.46E 01
22500.	0.181E 00	0.222E 00	0.286E 00	0.887E 00	0.787E 00	-0.19E 01
25000.	0.158E 00	0.134E 00	0.207E 00	0.705E 00	0.876E 00	-0.19E 01
27500.	0.179E 00	0.536E-01	0.186E 00	0.291E 00	0.934E 00	-0.21E 01
30000.	0.121E 00	-0.142E-01	0.121E 00	-0.117E 00	0.714E 00	-0.22E 01
32500.	0.933E-01	-0.323E-01	0.987E-01	-0.333E 00	0.715E 00	-0.22E 01
35000.	0.797E-01	-0.670E-01	0.104E 00	-0.700E 00	0.920E 00	-0.23E 01
37500.	0.395E-01	-0.782E-01	0.876E-01	-0.110E 01	0.968E 00	-0.25E 01
40000.	0.741E-03	-0.696E-01	0.696E-01	-0.156E 01	0.990E 00	-0.27E 01
42500.	-0.199E-01	-0.458E-01	0.499E-01	-0.198E 01	0.110E 01	-0.29E 01
45000.	-0.205E-01	-0.171E-01	0.267E-01	-0.245E 01	0.120E 01	-0.35E 01
47500.	-0.761E-02	-0.775E-02	0.109E-01	-0.235E 01	0.511E 00	-0.39E 01
50000.	0.455E-02	-0.153E-01	0.160E-01	-0.128E 01	0.582E 00	-0.32E 01
52500.	0.522E-02	-0.167E-01	0.175E-01	-0.127E 01	0.673E 00	-0.31E 01
55000.	0.190E-03	-0.144E-01	0.144E-01	-0.156E 01	0.594E 00	-0.33E 01
57500.	0.207E-02	-0.126E-01	0.127E-01	-0.141E 01	0.535E 00	-0.34E 01
60000.	0.180E-02	-0.142E-01	0.143E-01	-0.144E 01	0.612E 00	-0.33E 01

NORMALIZATION

FREQ	NBWA	
0.	0.180E-01	
2500.	0.140E-02	+
5000.	0.784E-03	+
7500.	0.104E-02	+
10000.	0.185E-02	
12500.	0.236E-02	+
15000.	0.236E-02	+
17500.	0.318E-02	
20000.	0.400E-02	
22500.	0.418E-02	
25000.	0.465E-02	
27500.	0.495E-02	+
30000.	0.379E-02	+
32500.	0.379E-02	+
35000.	0.488E-02	+
37500.	0.513E-02	+
40000.	0.525E-02	+
42500.	0.586E-02	+
45000.	0.636E-02	+
47500.	0.271E-02	+
50000.	0.309E-02	+
52500.	0.357E-02	+
55000.	0.315E-02	+
57500.	0.284E-02	+
60000.	0.325E-02	+

Figure 26. Computer Processed Data Format

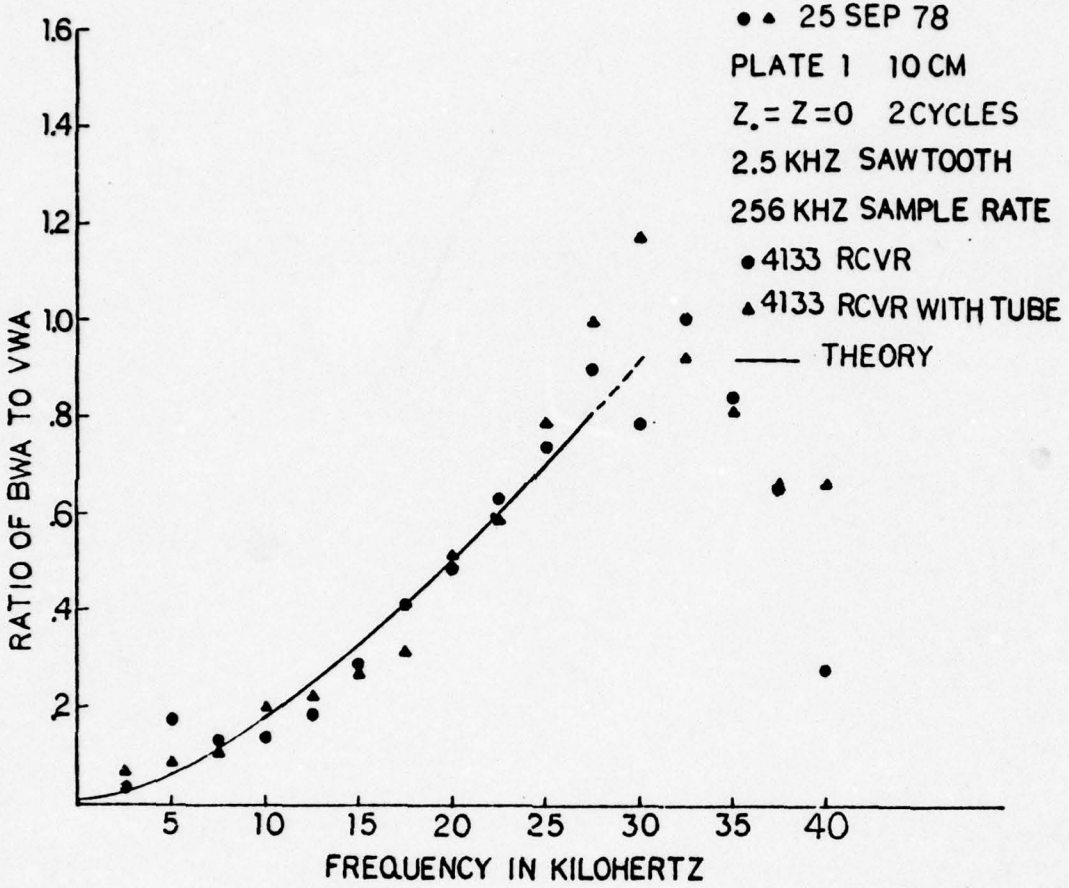

Figure 27. Ratio of BWA to VWA vs. Frequency (10 cm.)

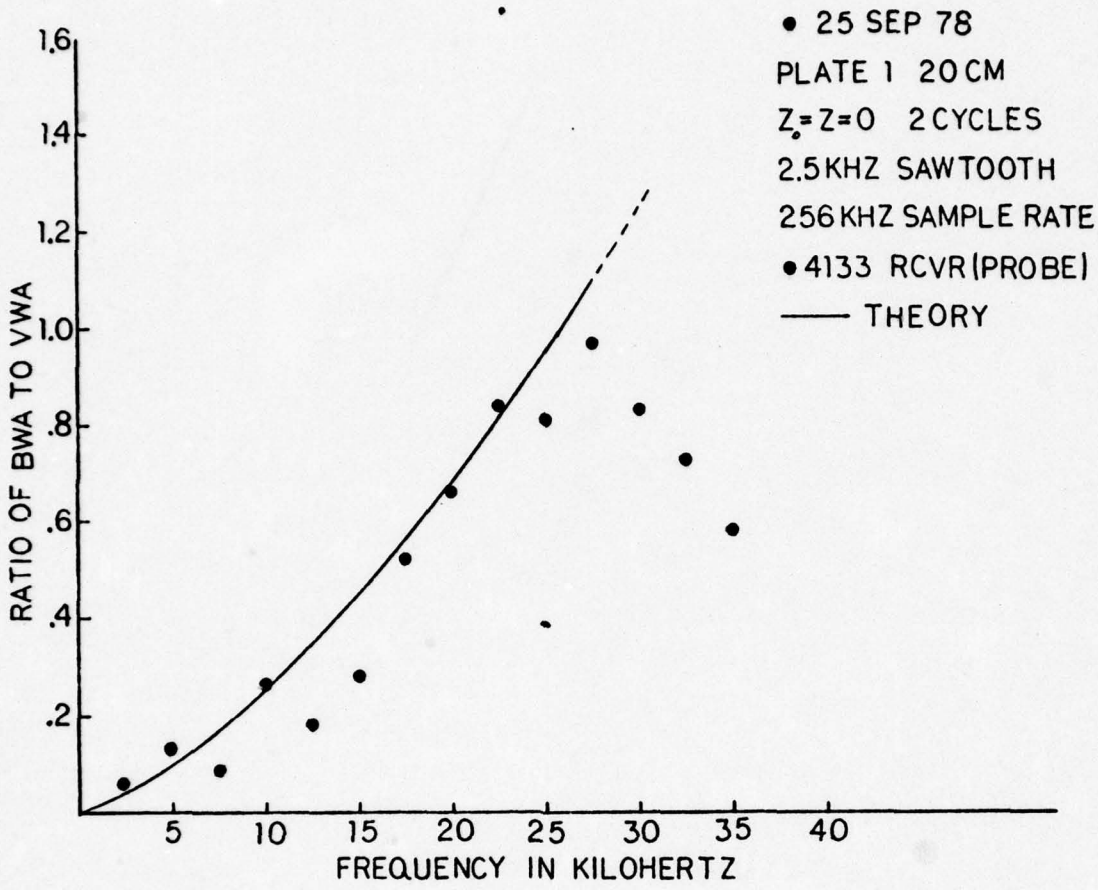

Figure 28. Ratio of BWA To VWA vs. Frequency (20 cm.)

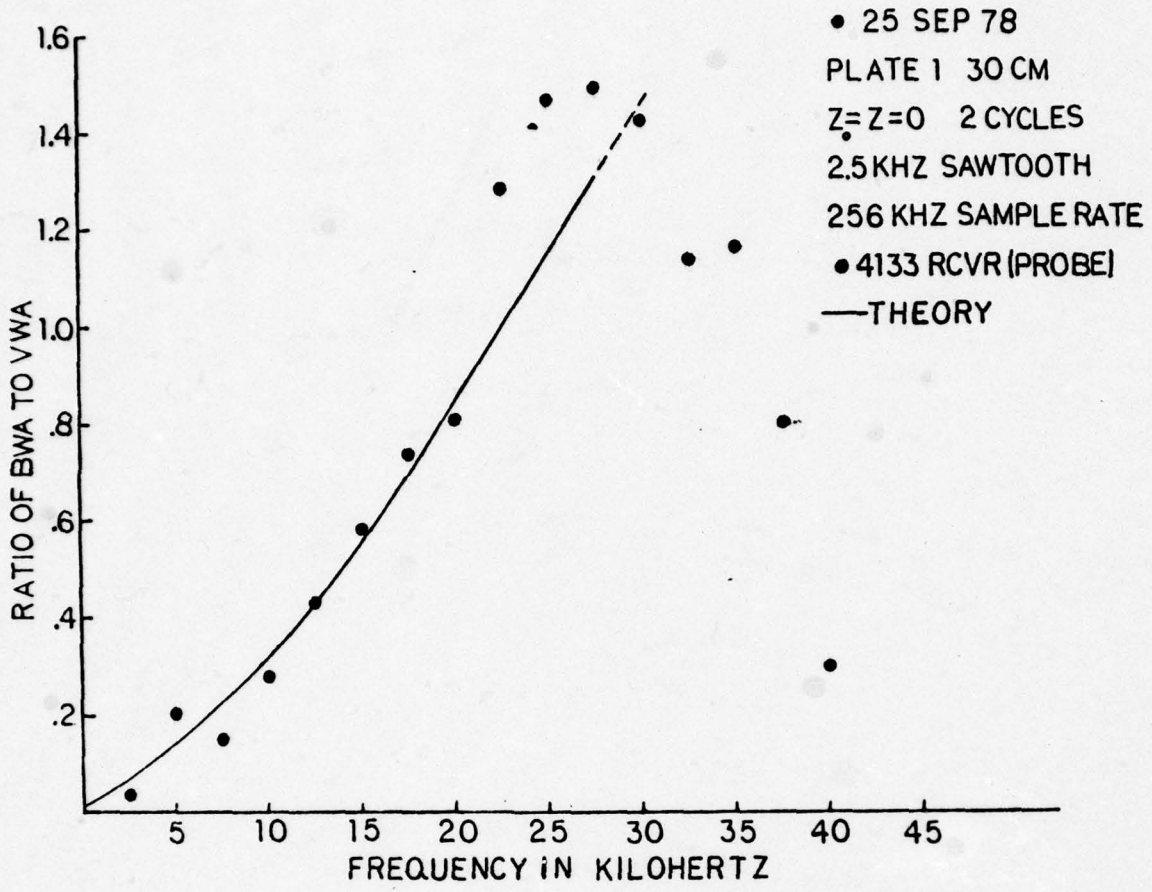

Figure 29. Ratio Of BWA To VWA vs. Frequency (30 cm.)

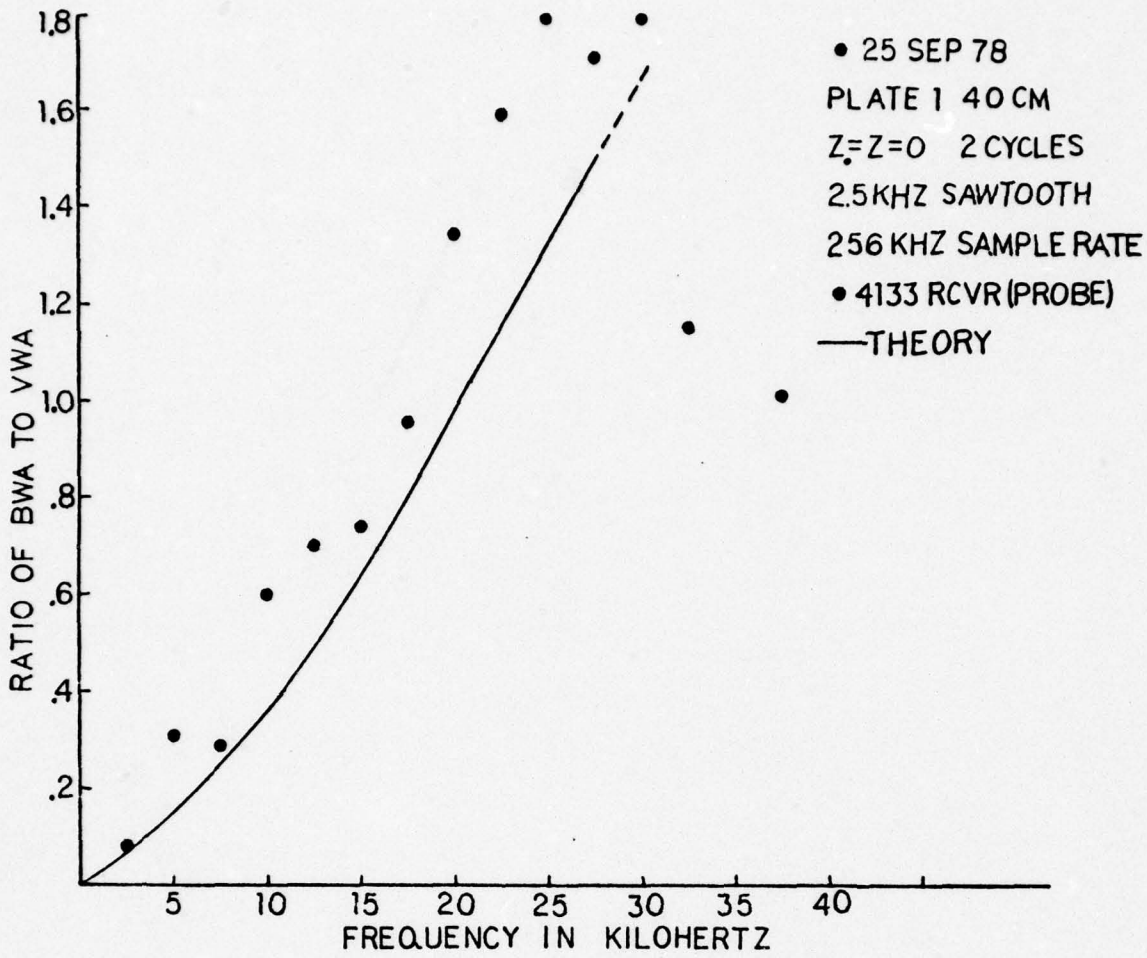

Figure 30. Ratio Of BWA To VWA vs. Frequency (40 cm.)

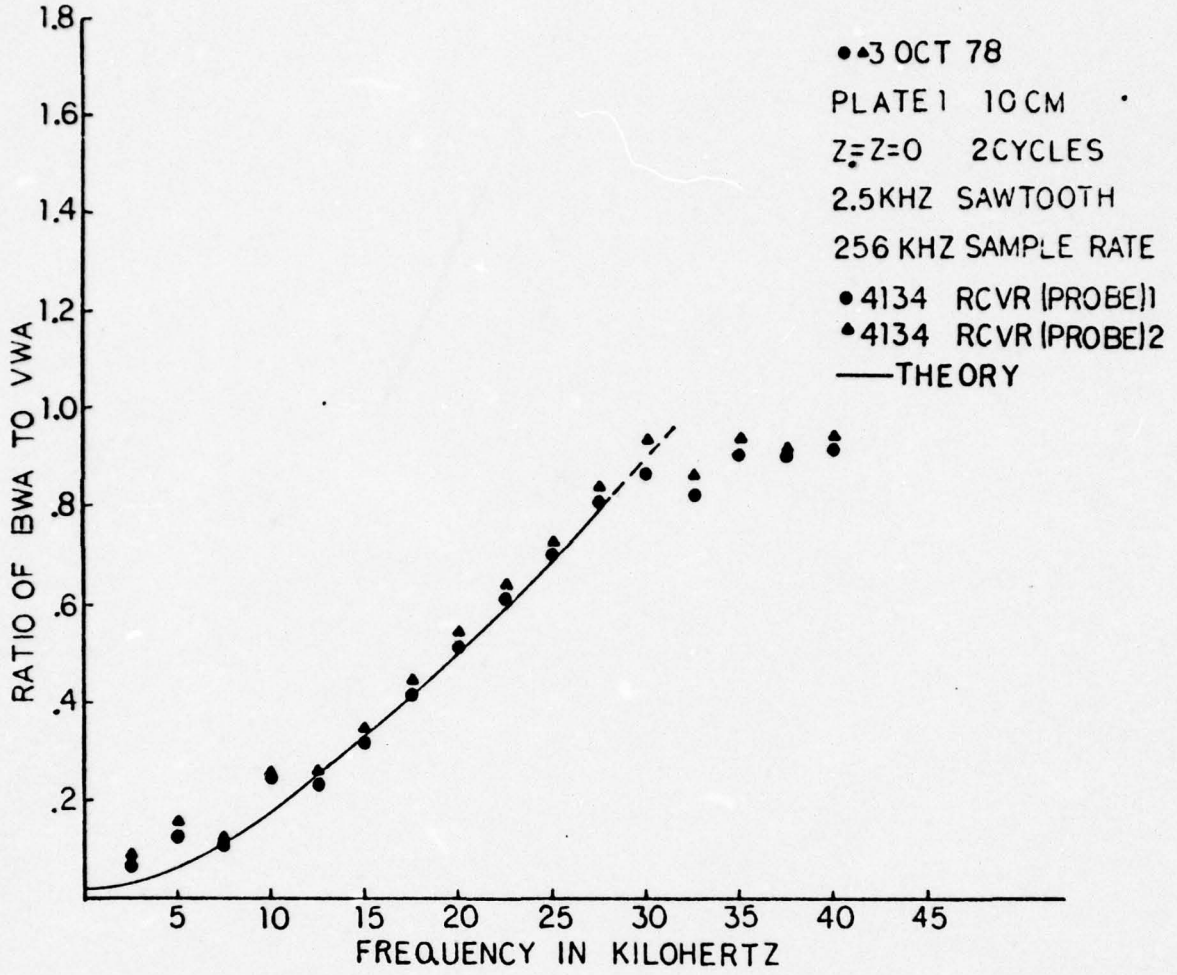

Figure 31. Ratio Of BWA To VWA vs. Frequency (10 cm.)

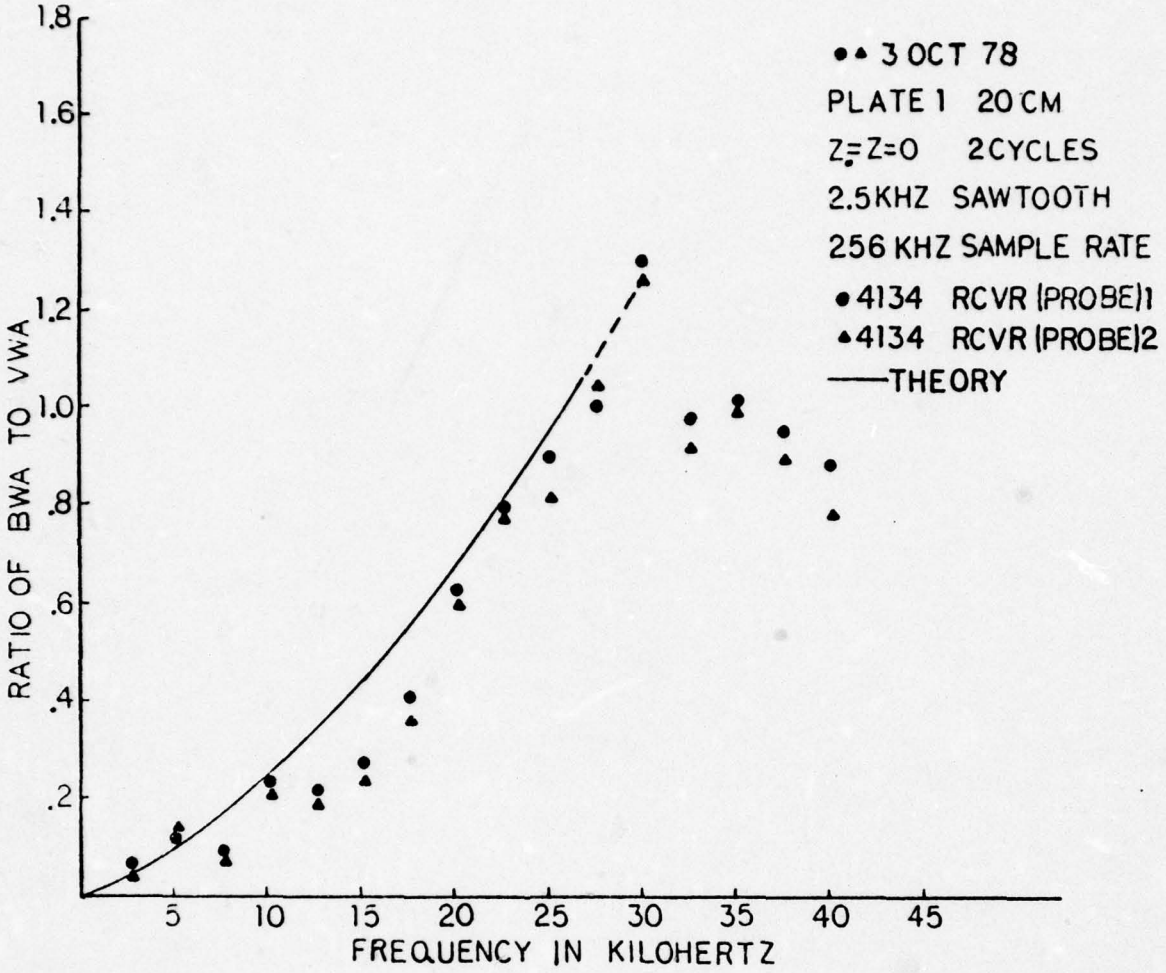

Figure 32. Ratio of BWA To VWA vs. Frequency (20 cm.)

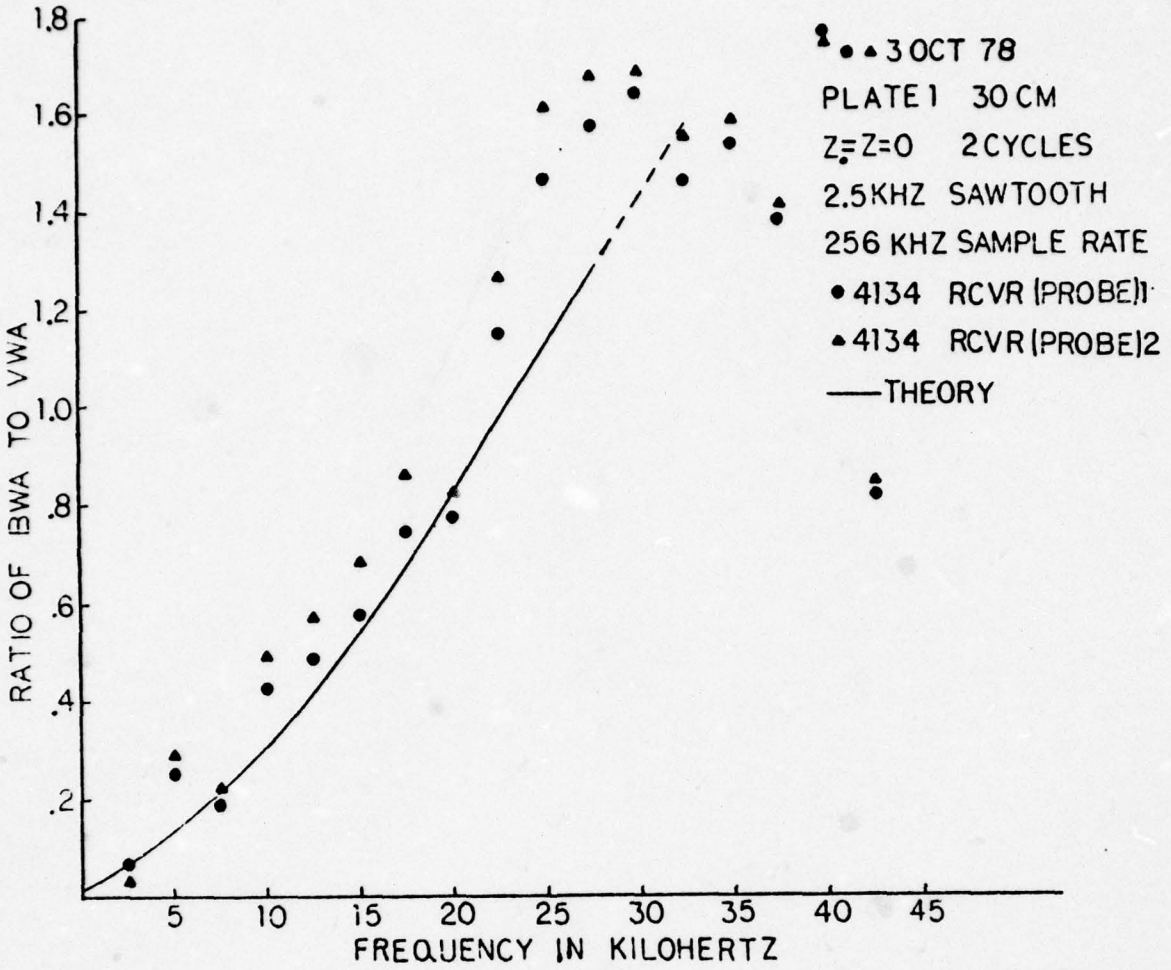

Figure 33. Ratio of BWA To VWA vs. Frequency (30 cm.)

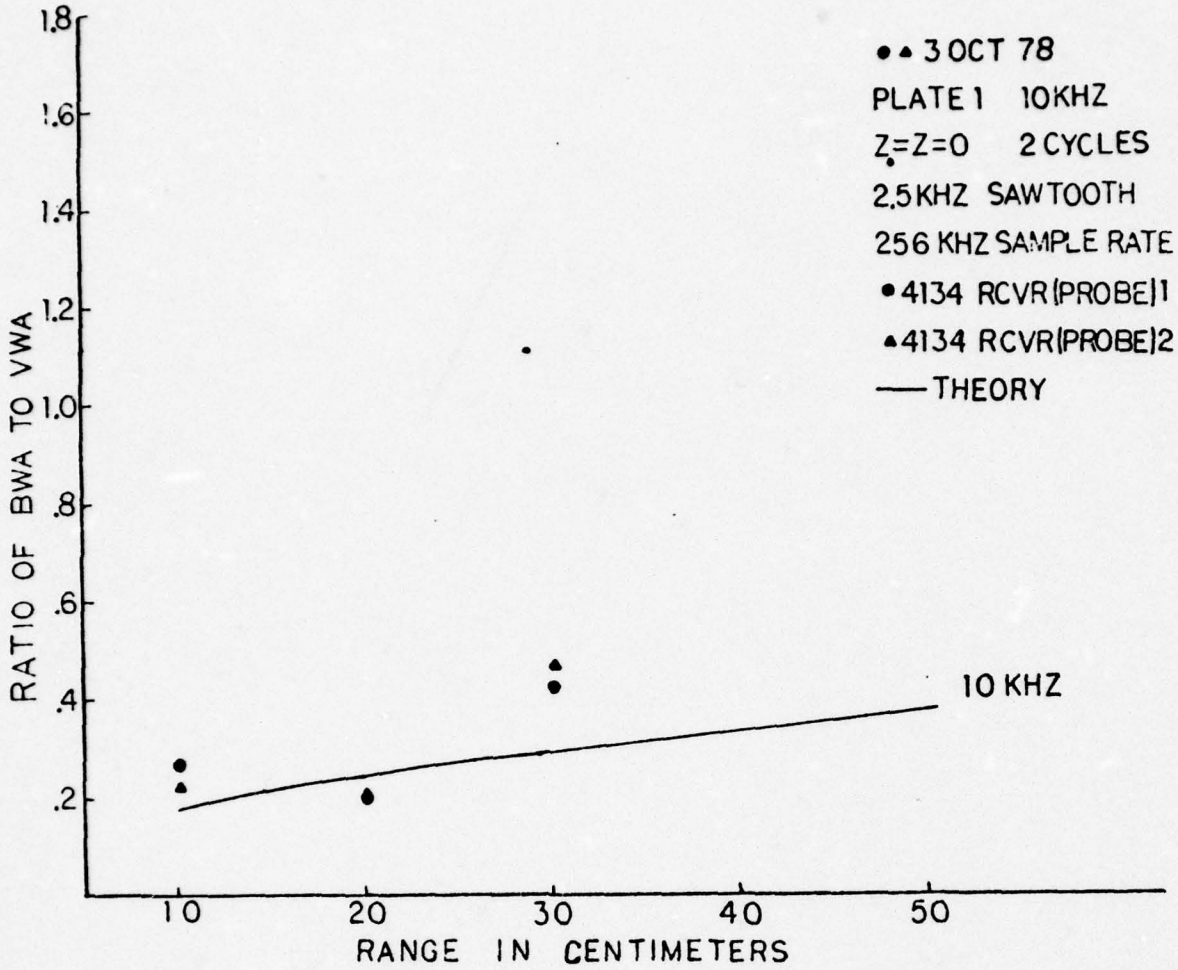

Figure 34. Ratio of BWA To VWA vs. Range (10 kHz)

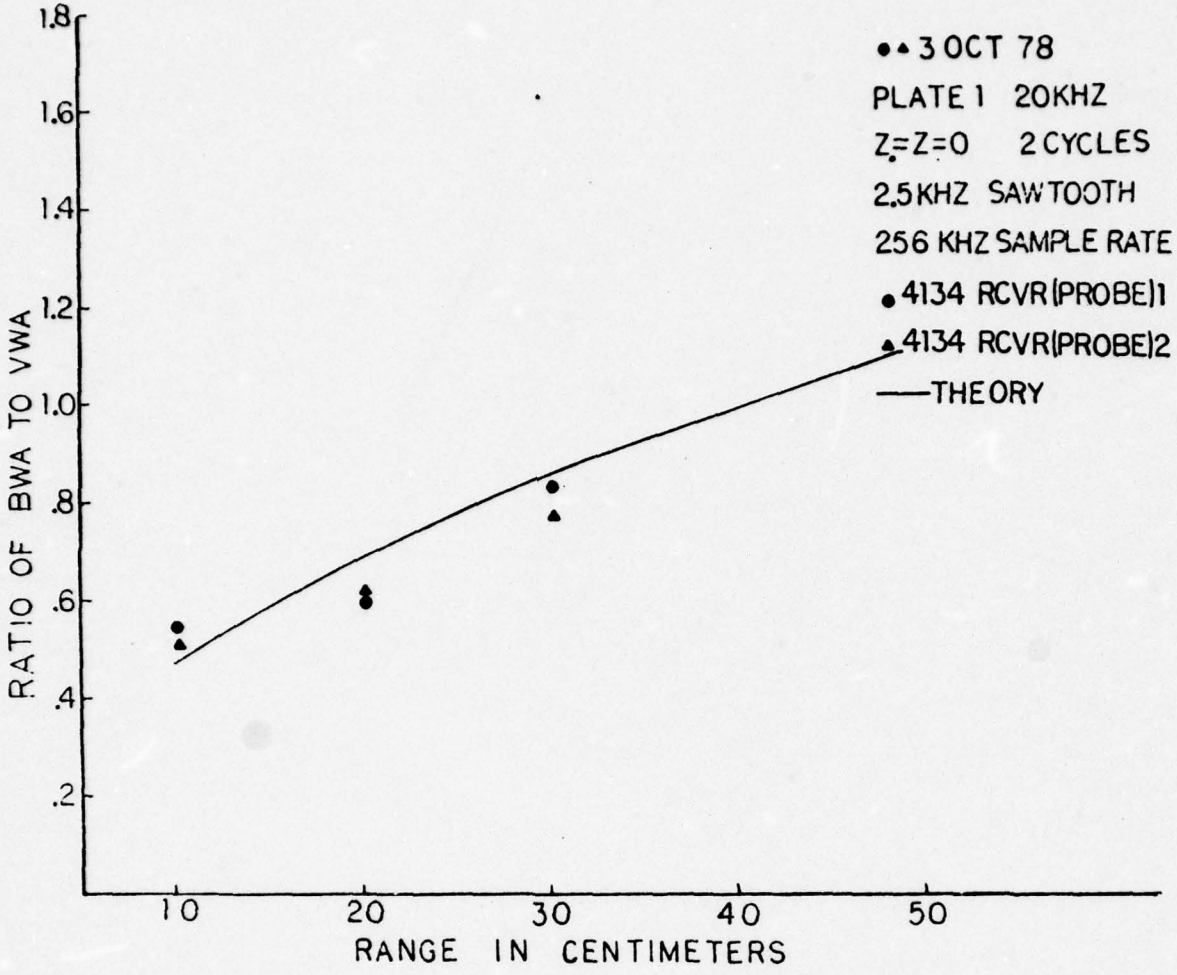

Figure 35. Ratio Of BWA To VWA vs. Range (20 kHz)

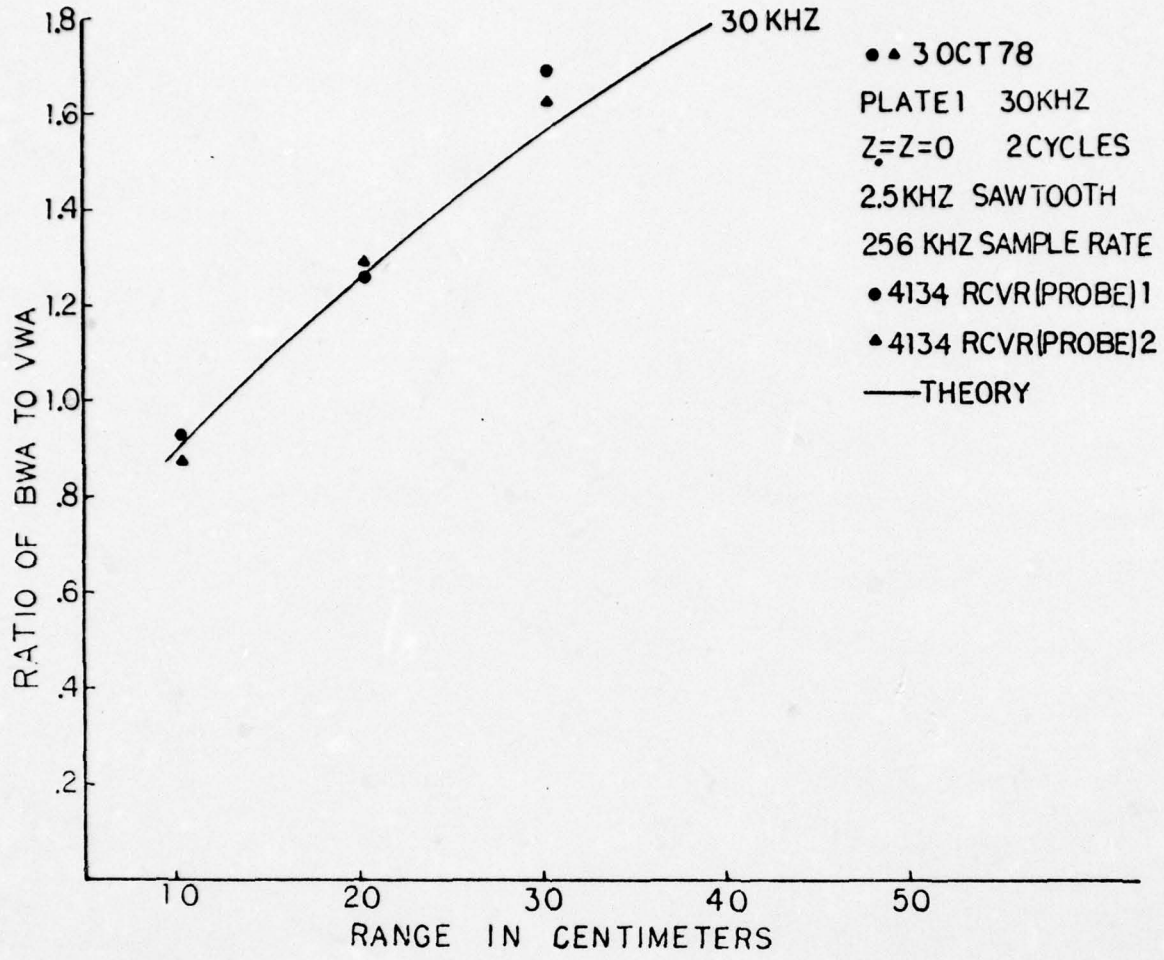

Figure 36. Ratio Of BWA To VWA vs. Range (30 kHz)

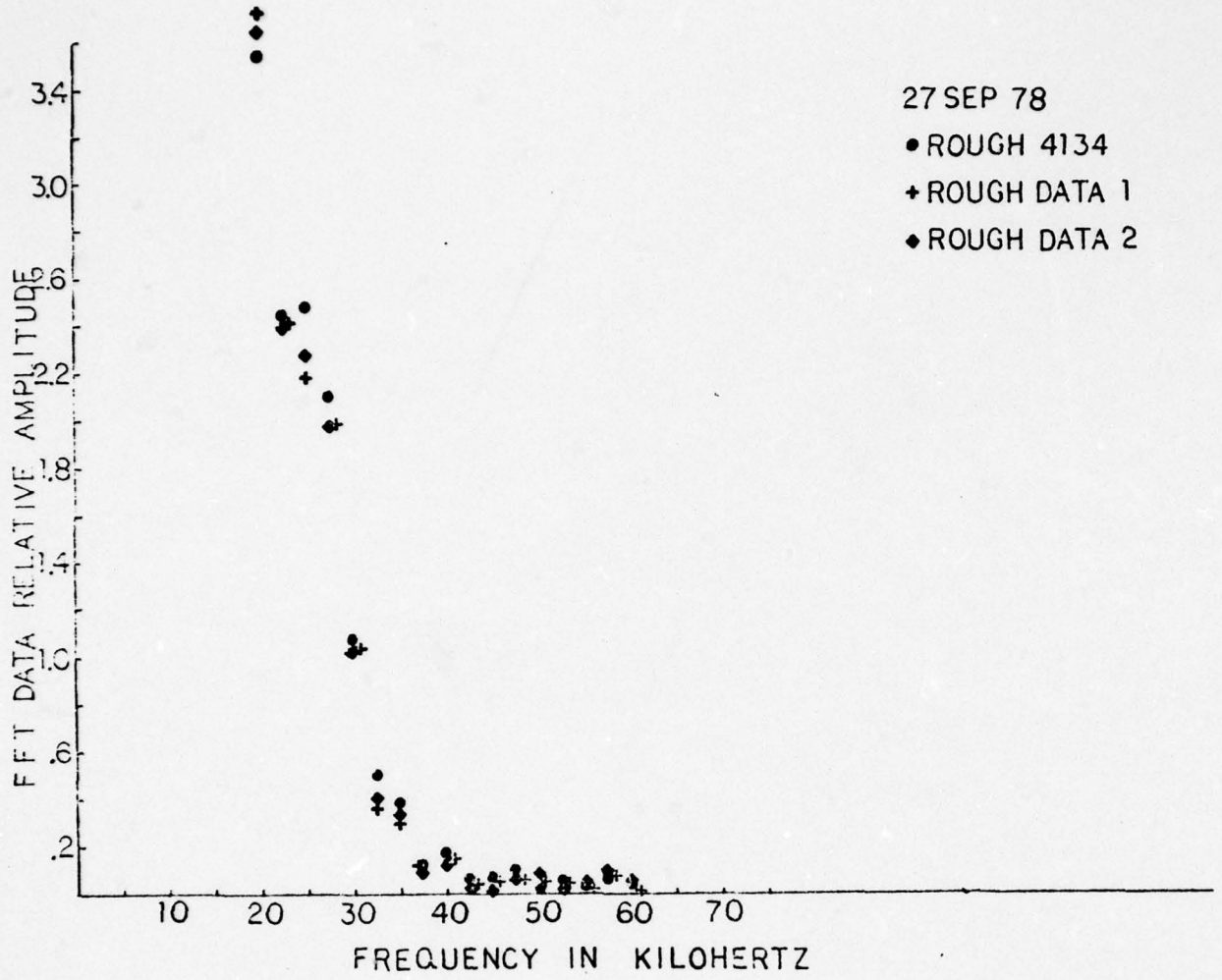

Figure 37. FFT Data Relative Amplitude vs. Frequency For Smooth Plate

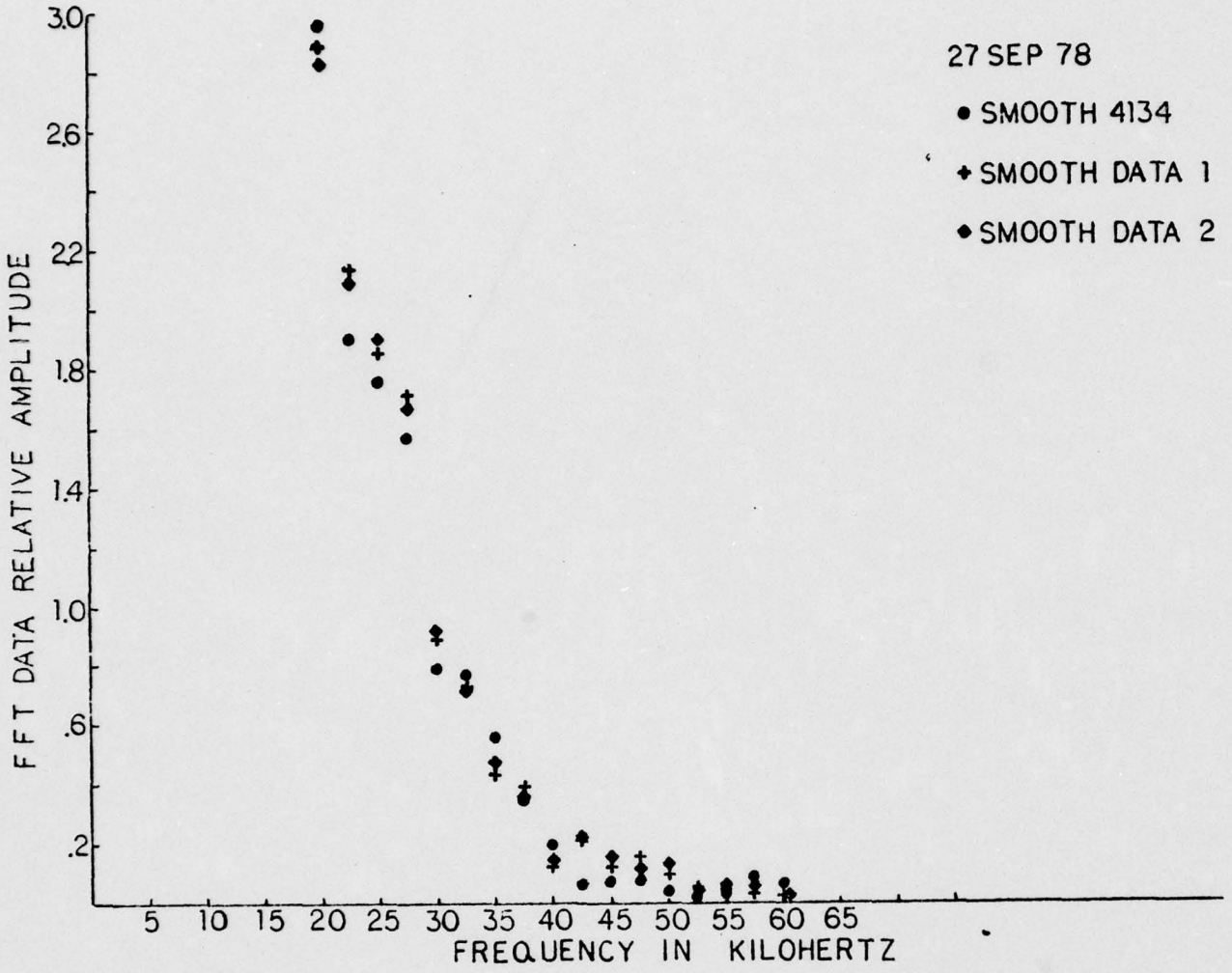

Figure 38. FFT Data Relative Amplitude vs. Frequency For Rough Plate

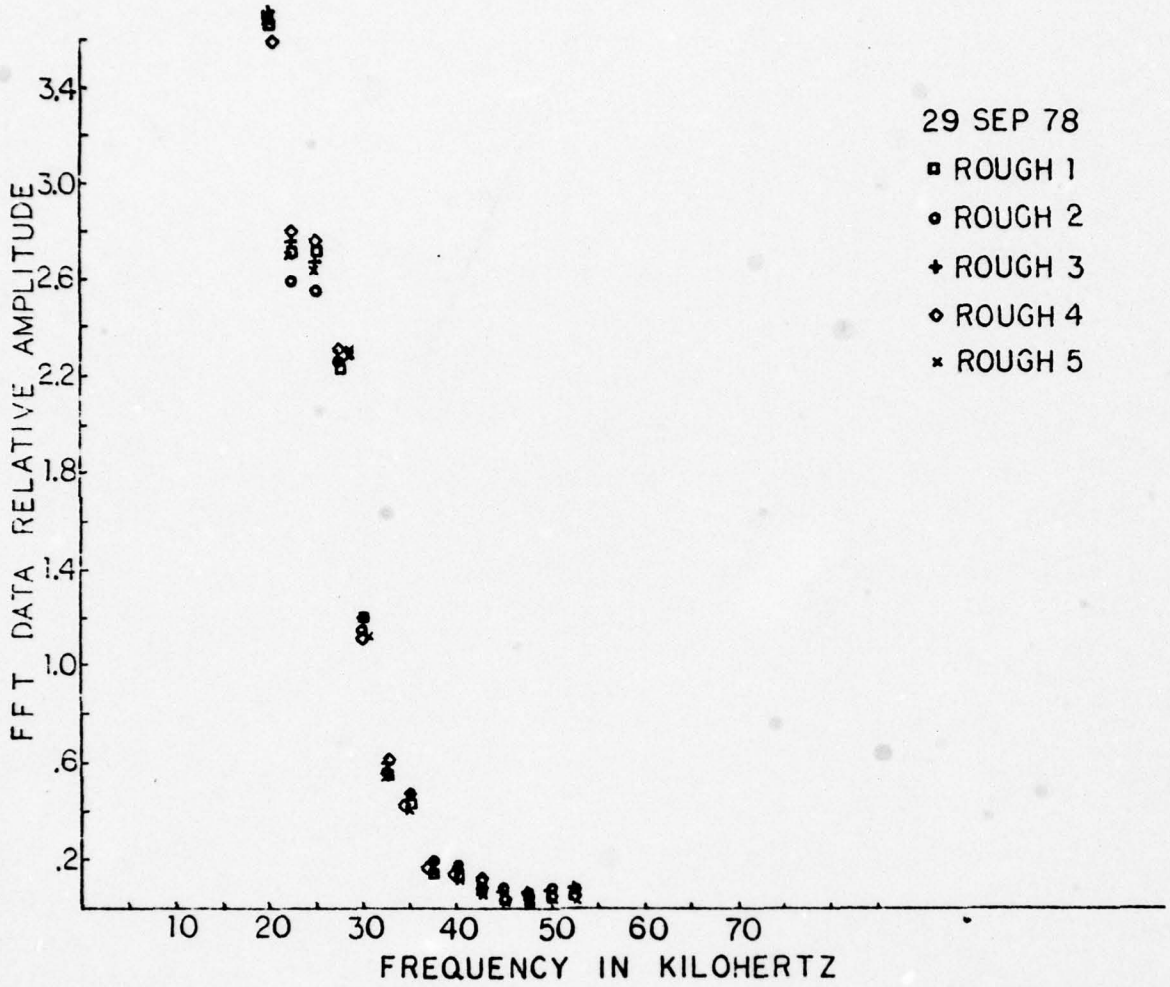

Figure 39. FFT Data Relative Amplitude vs. Frequency For Hemispherical Boss Repacks

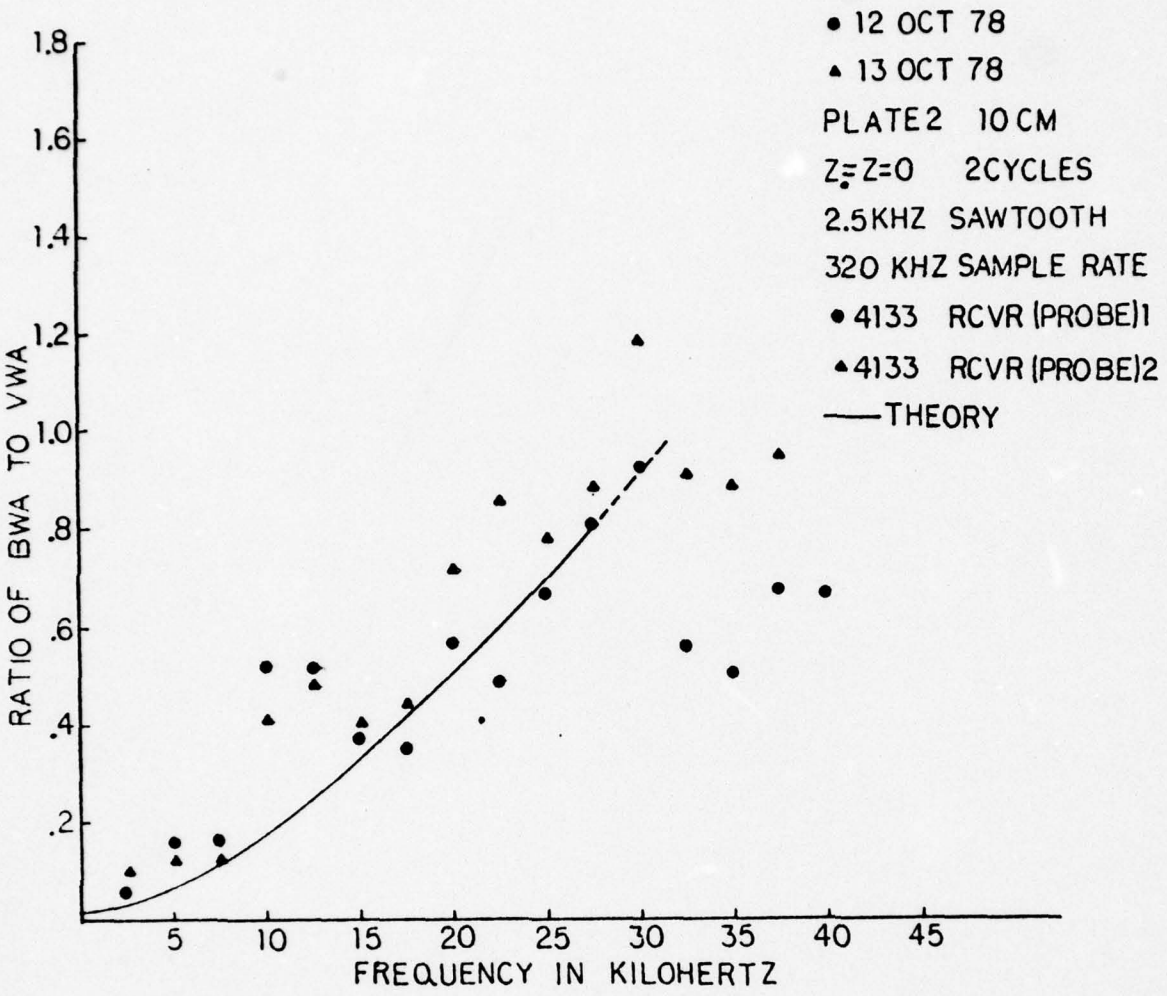

Figure 40. Ratio Of BWA To VWA vs. Frequency (10 cm.)

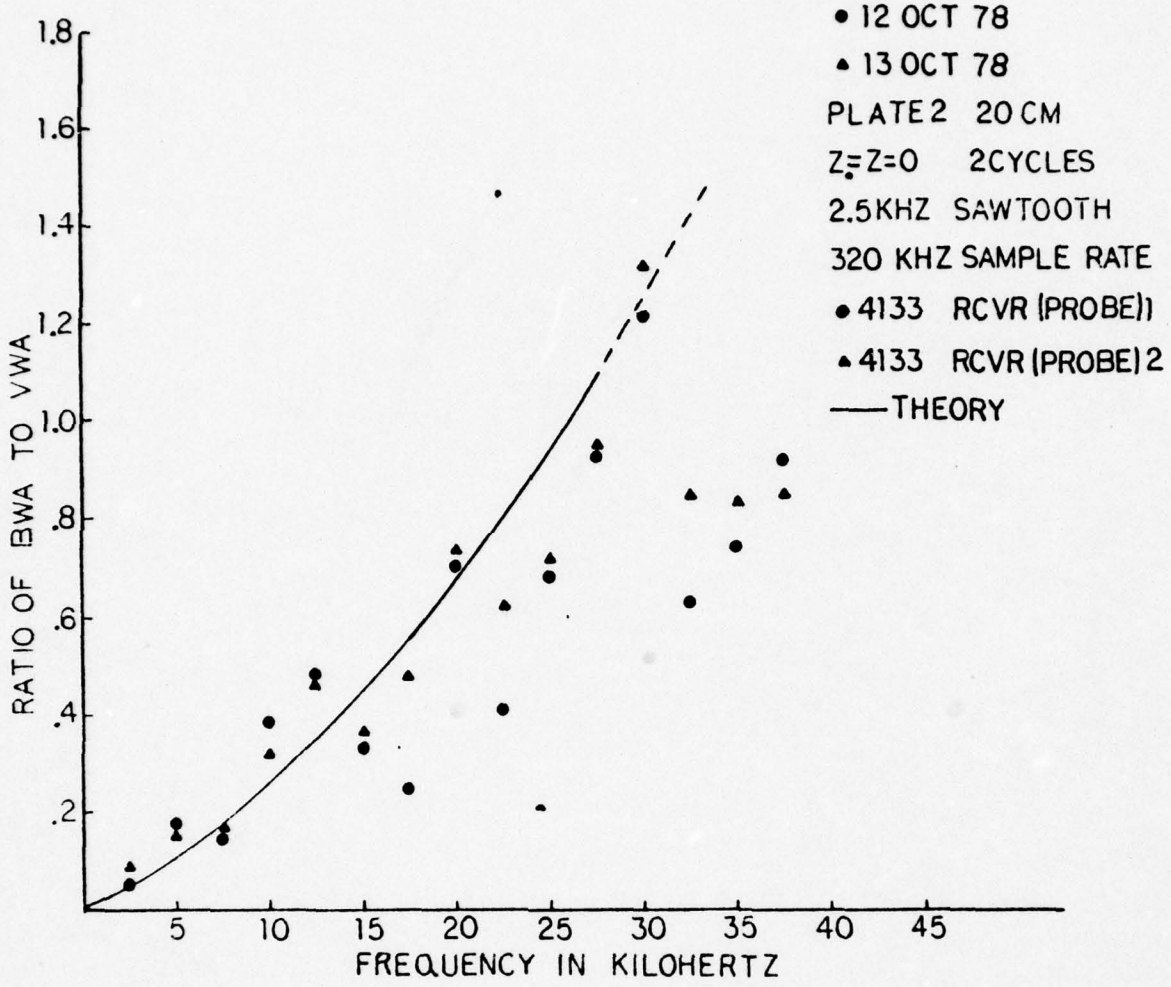

Figure 41. Ratio Of BWA To VWA vs. Frequency (20 cm.)

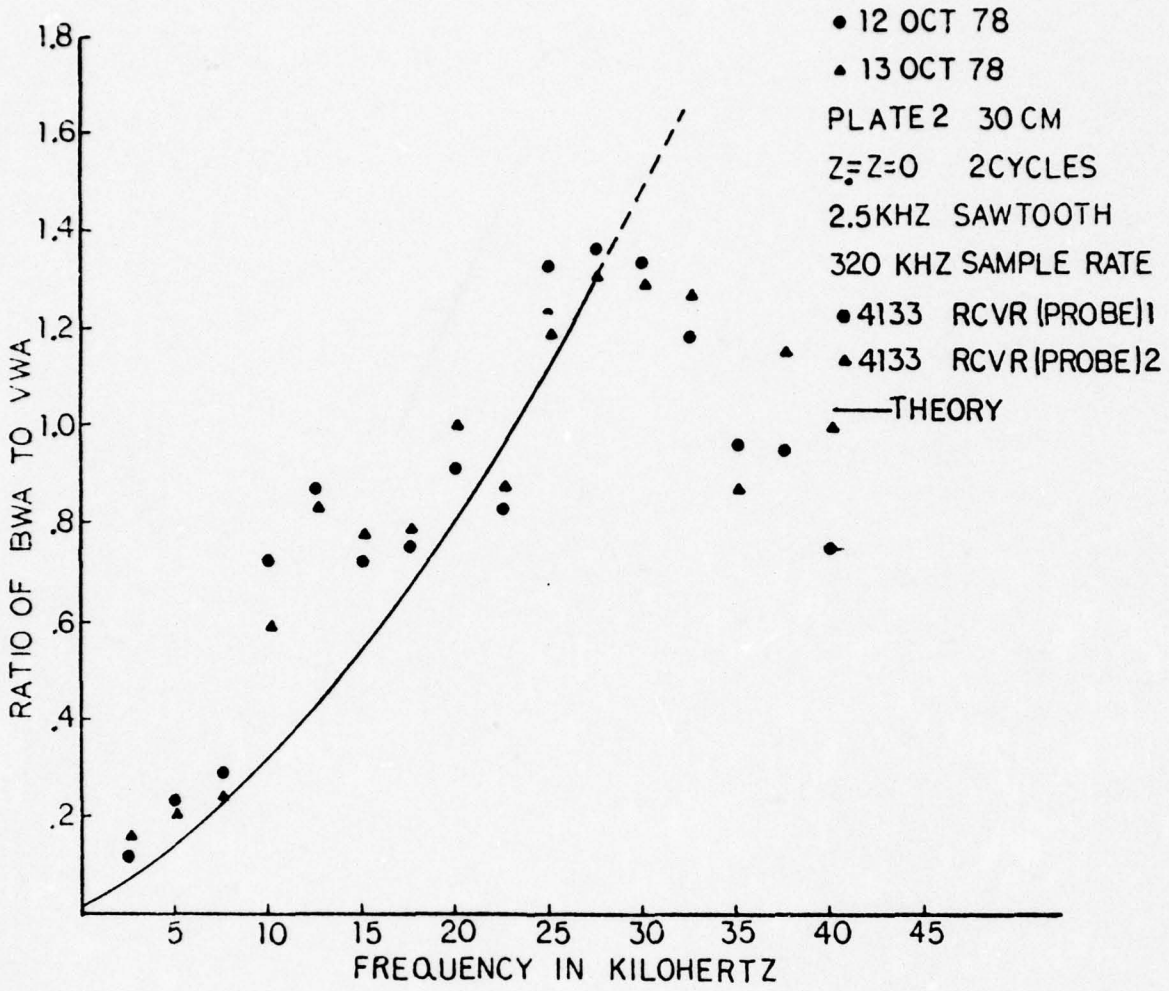

Figure 42. Ratio Of BWA To VWA vs. Frequency (30 cm.)

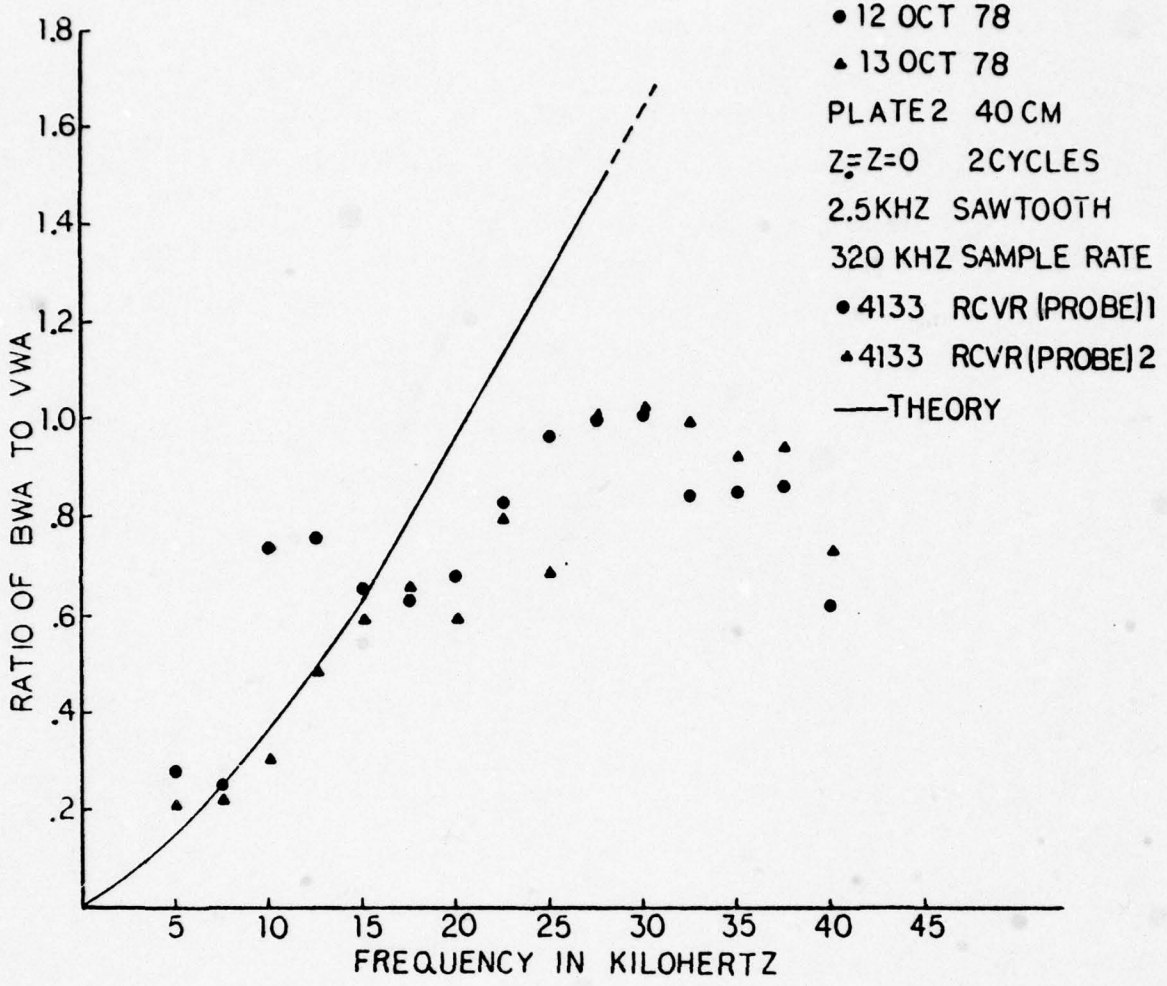

Figure 43. Ratio of BWA To VWA vs. Frequency (40 cm.)

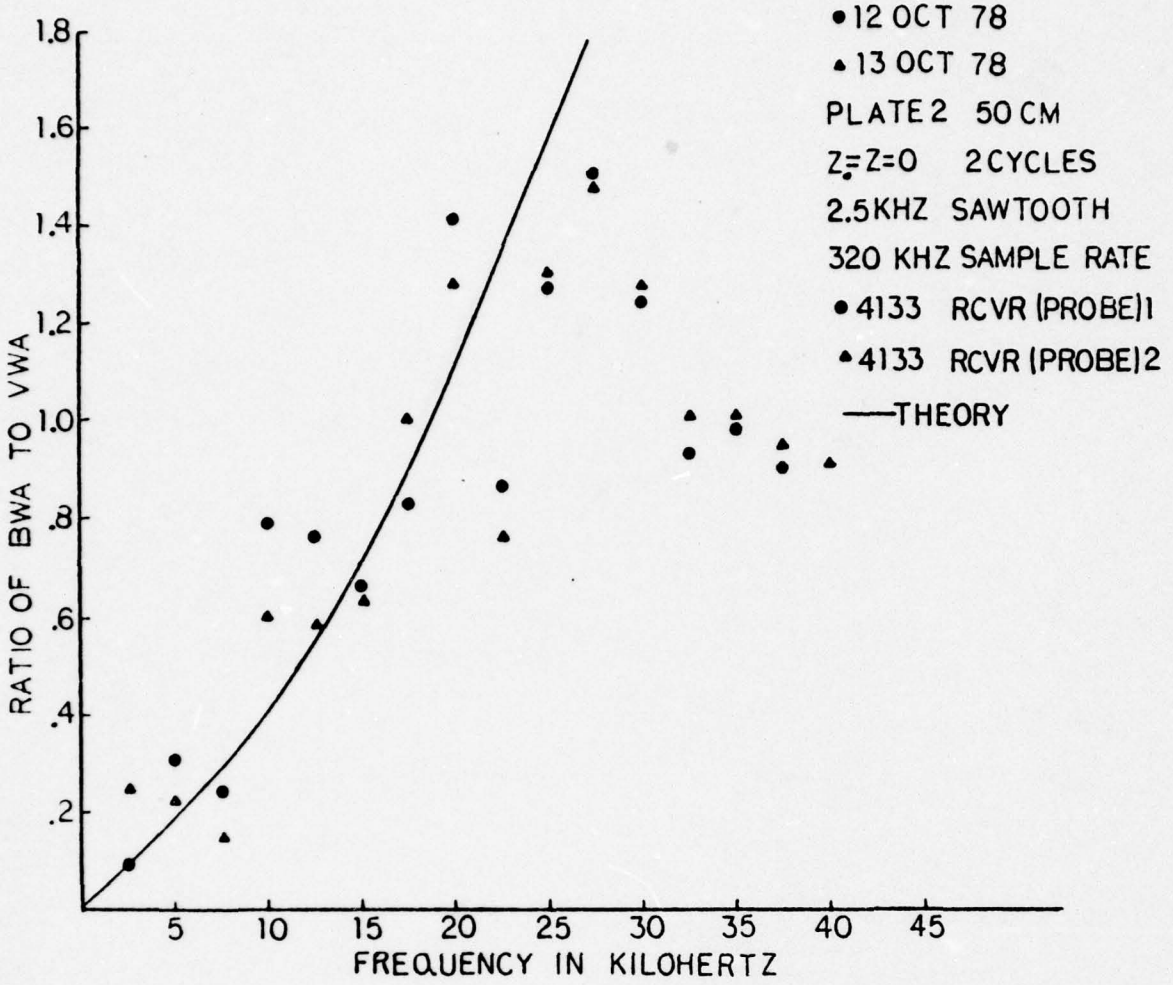

Figure 44. Ratio Of BWA To VWA vs. Frequency (50 cm.)

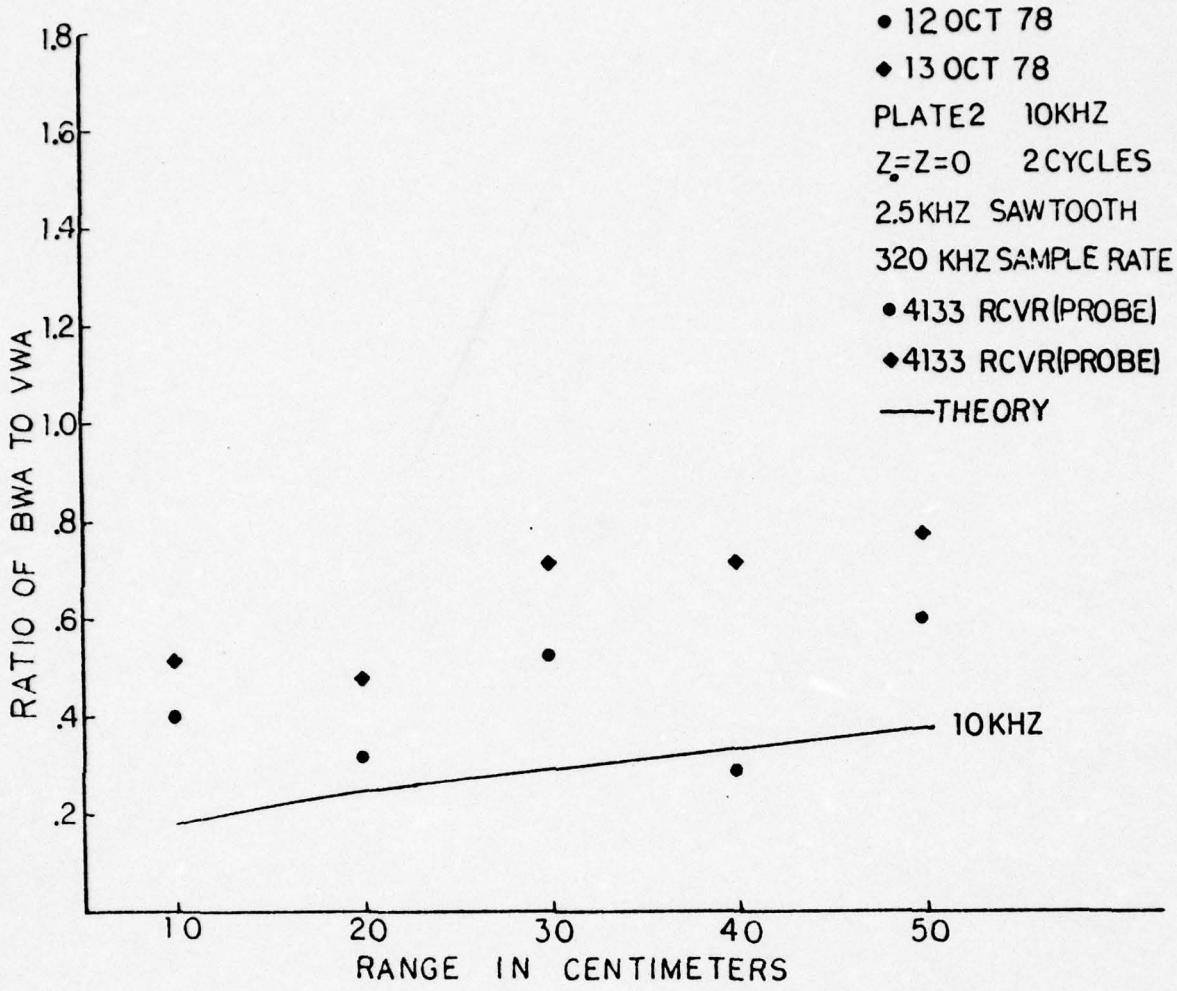

Figure 45. Ratio Of BWA To VWA vs. Range (10 kHz)

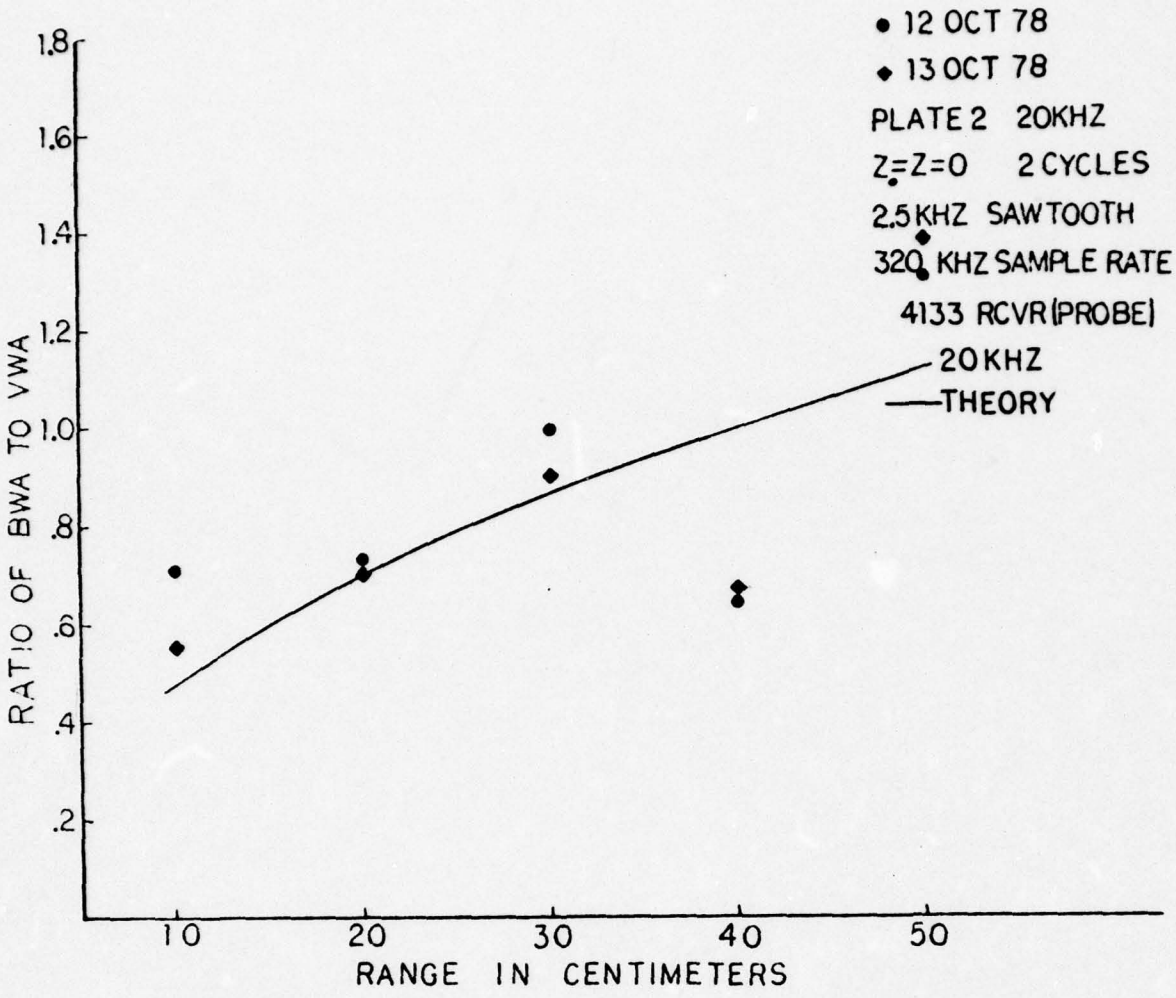

Figure 46. Ratio Of BWA To VWA vs. Range (20 kHz)

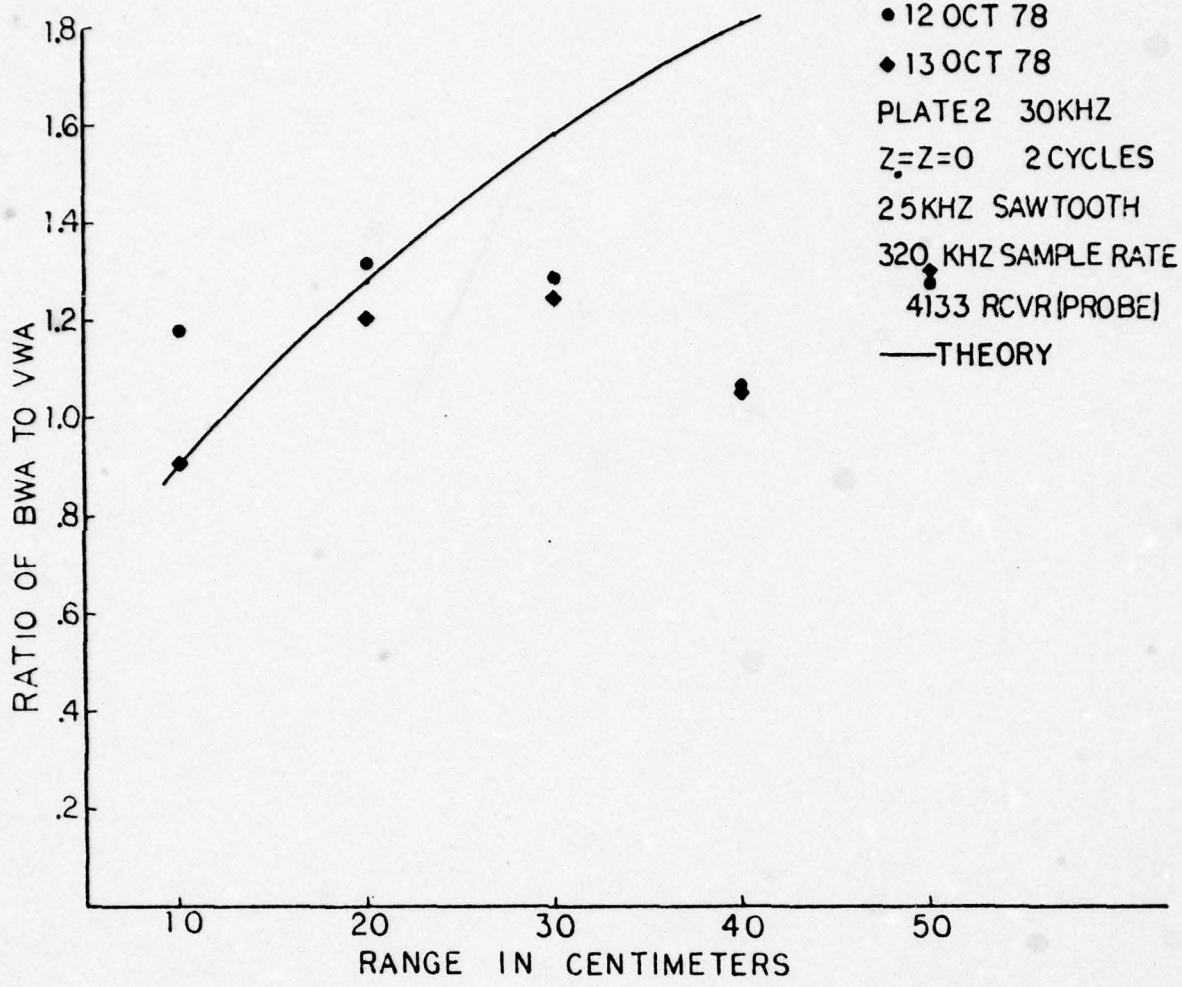

Figure 47. Ratio Of BWA To VWA vs. Range (30 kHz)

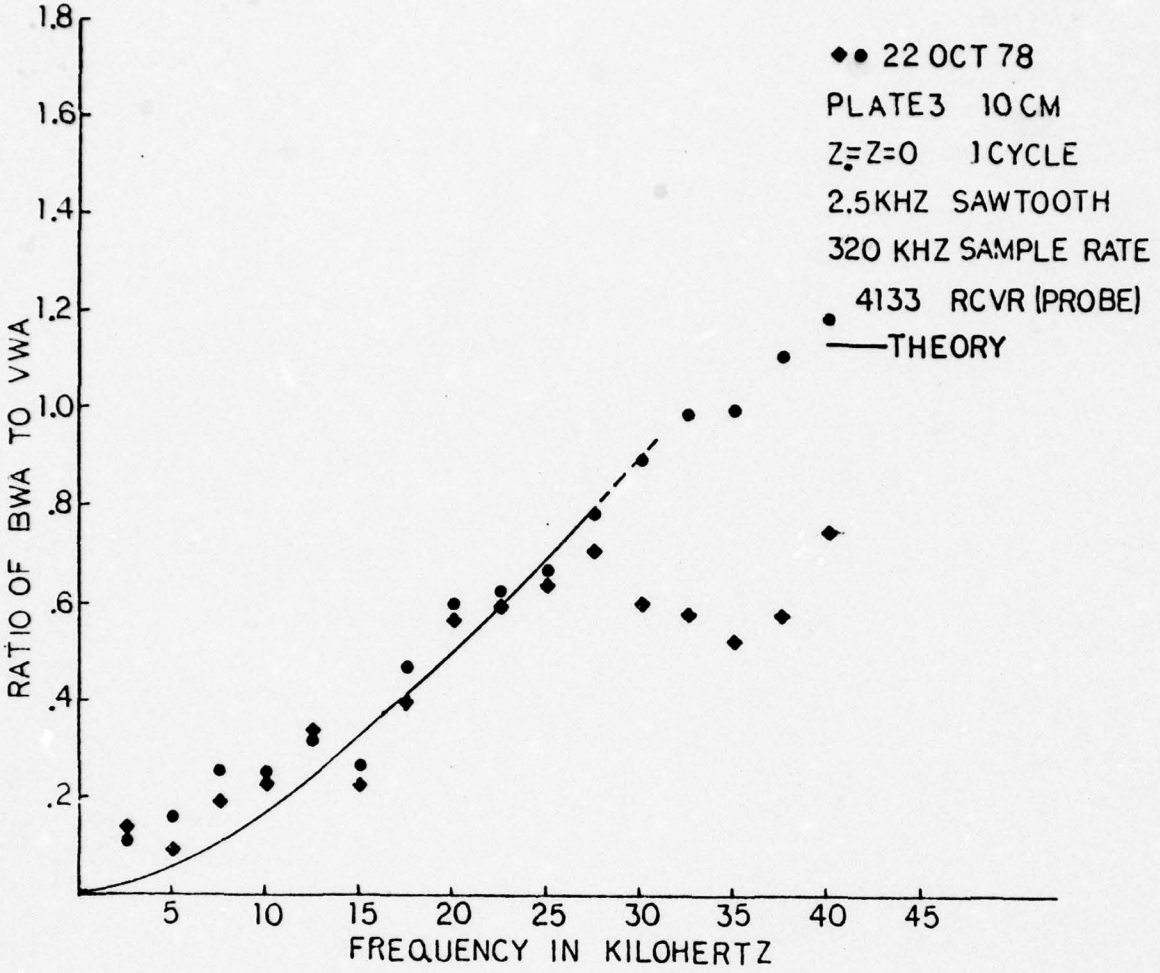

Figure 48. Ratio Of BWA To VWA vs. Frequency (10 cm.)

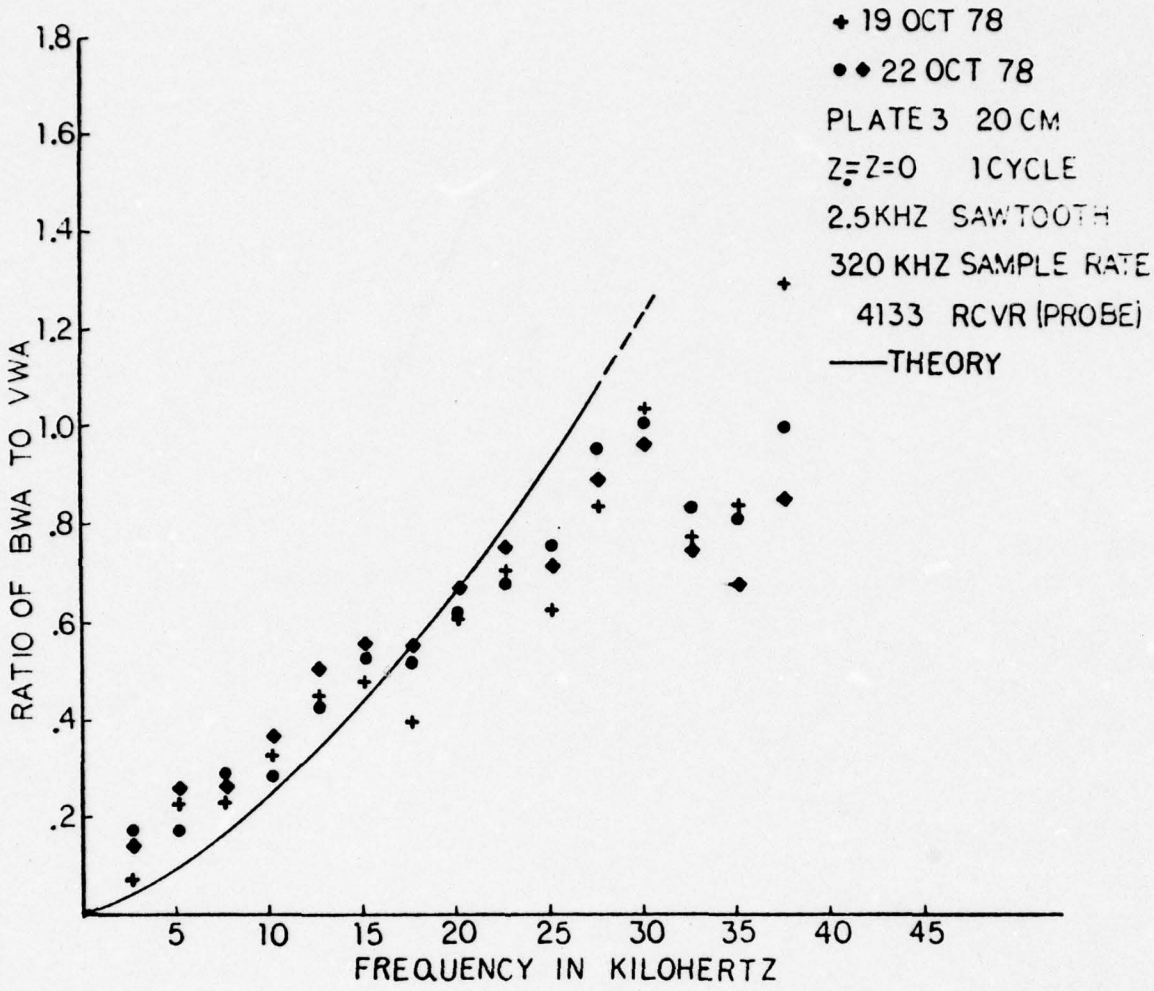

Figure 49. Ratio Of BWA To VWA vs. Frequency (20 cm.)

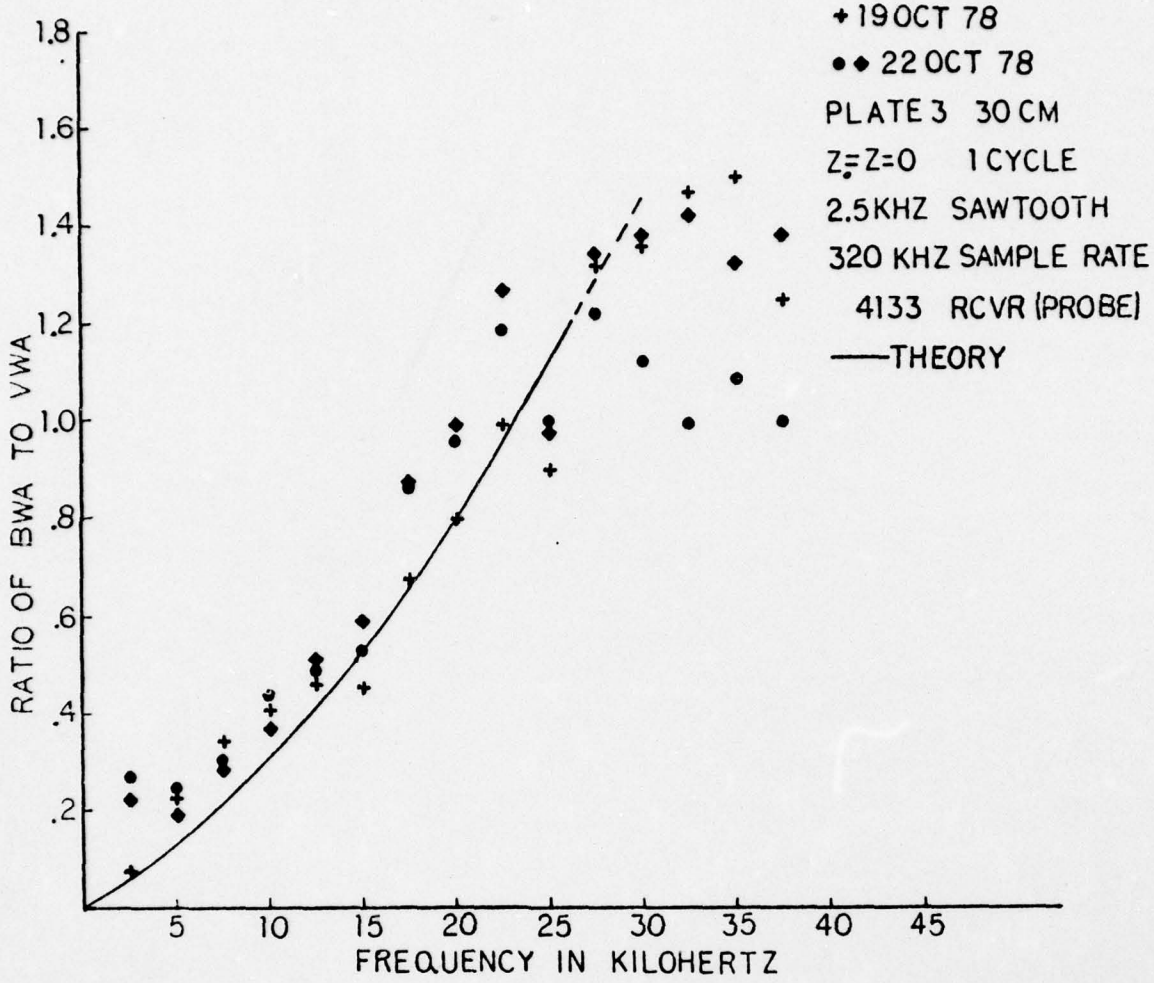

Figure 50. Ratio Of BWA to VWA vs. Frequency (30 cm.)

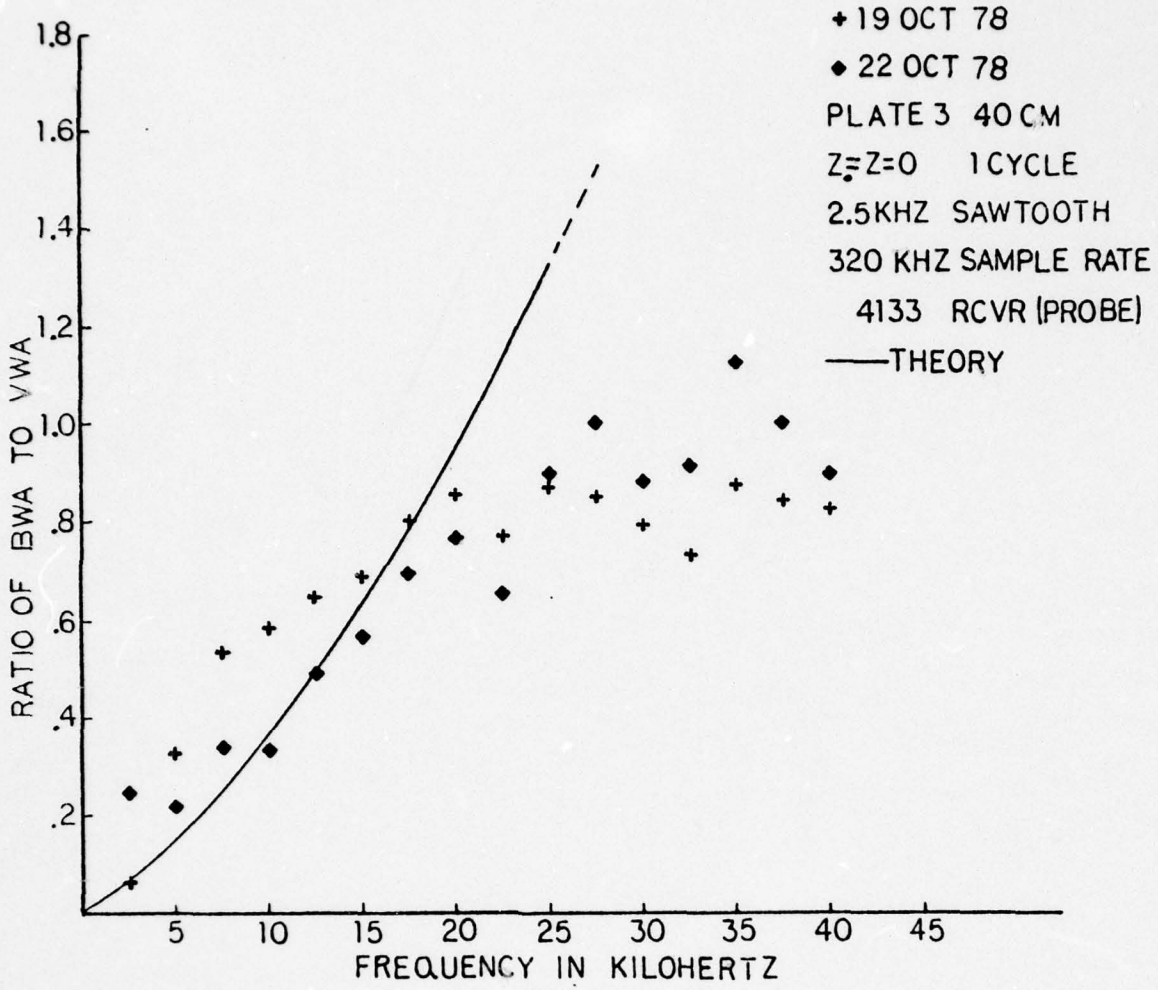

Figure 51. Ratio Of BWA To VWA vs. Frequency (40 cm.)

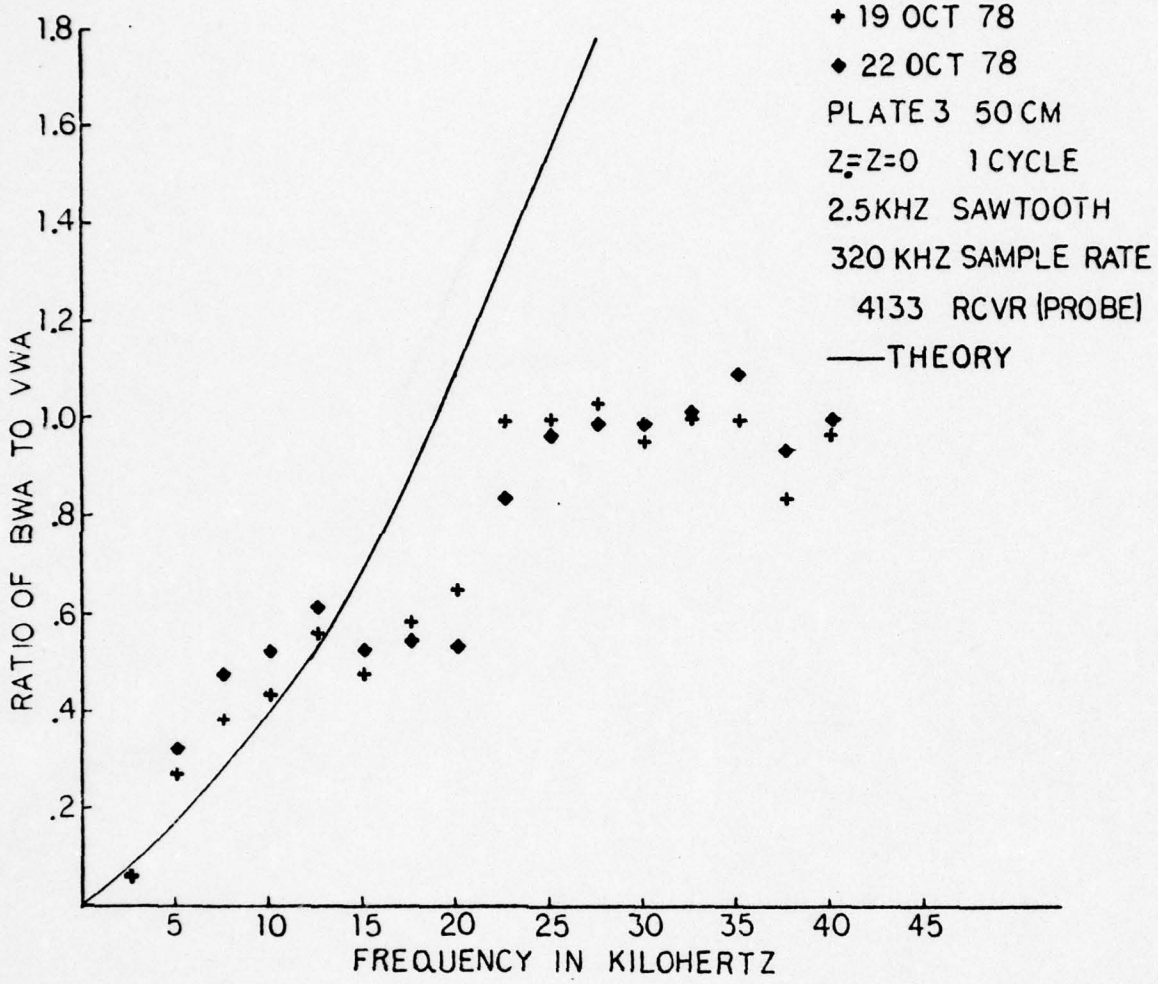

Figure 52. Ratio Of BWA To VWA vs. Frequency (50 cm.)

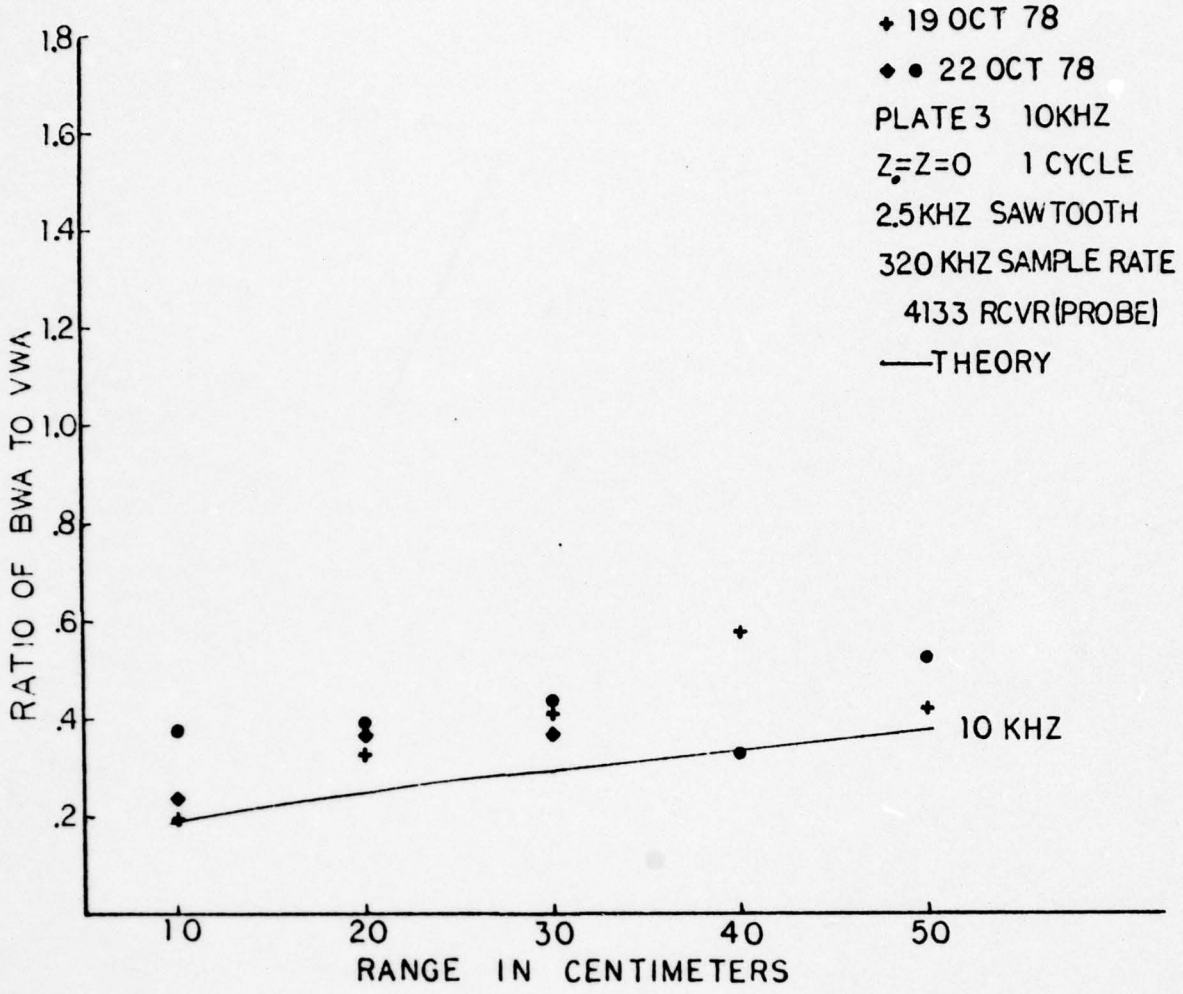

Figure 53. Ratio Of BWA To VWA vs. Range (10 kHz)

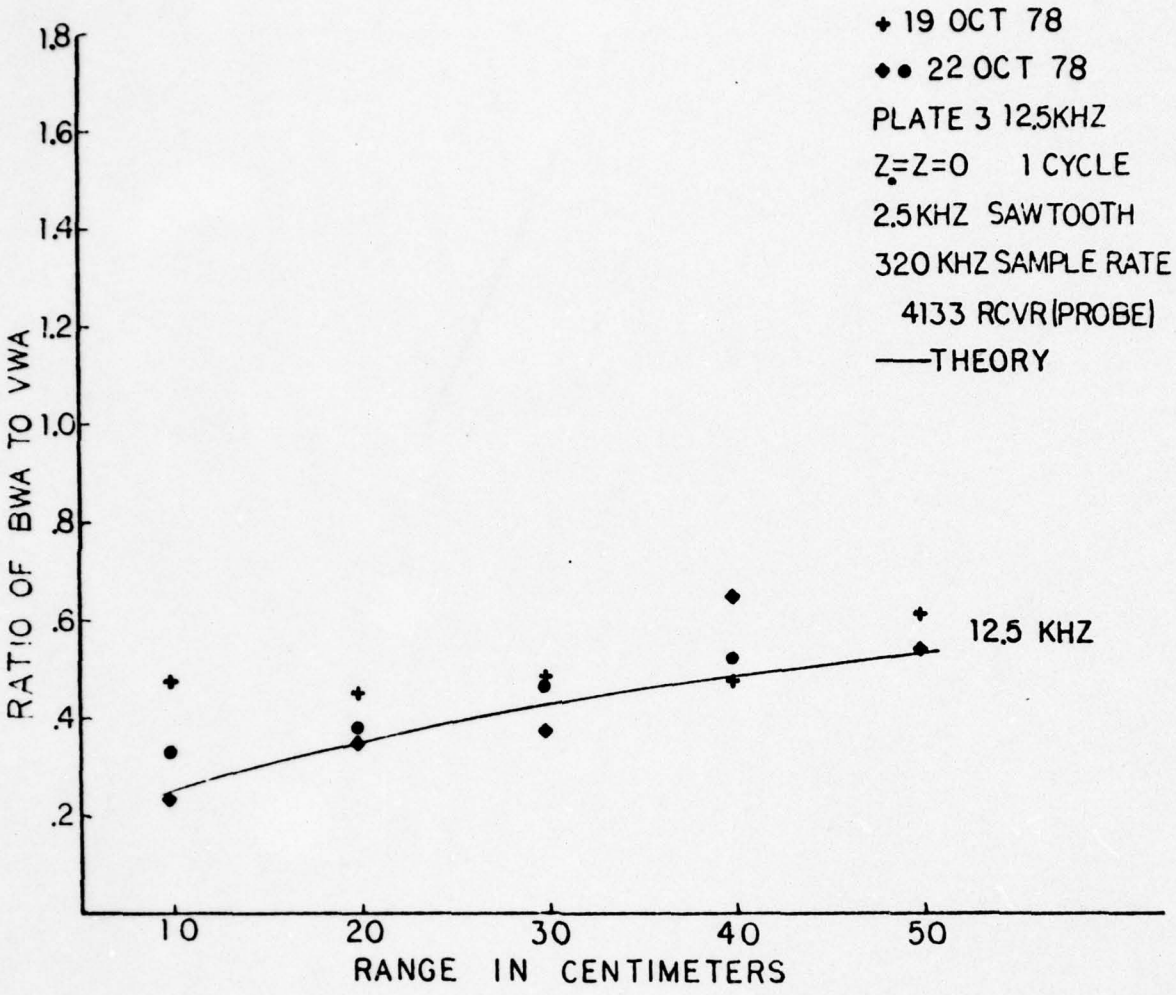

Figure 54. Ratio Of BWA To VWA vs. Range (12.5 kHz)

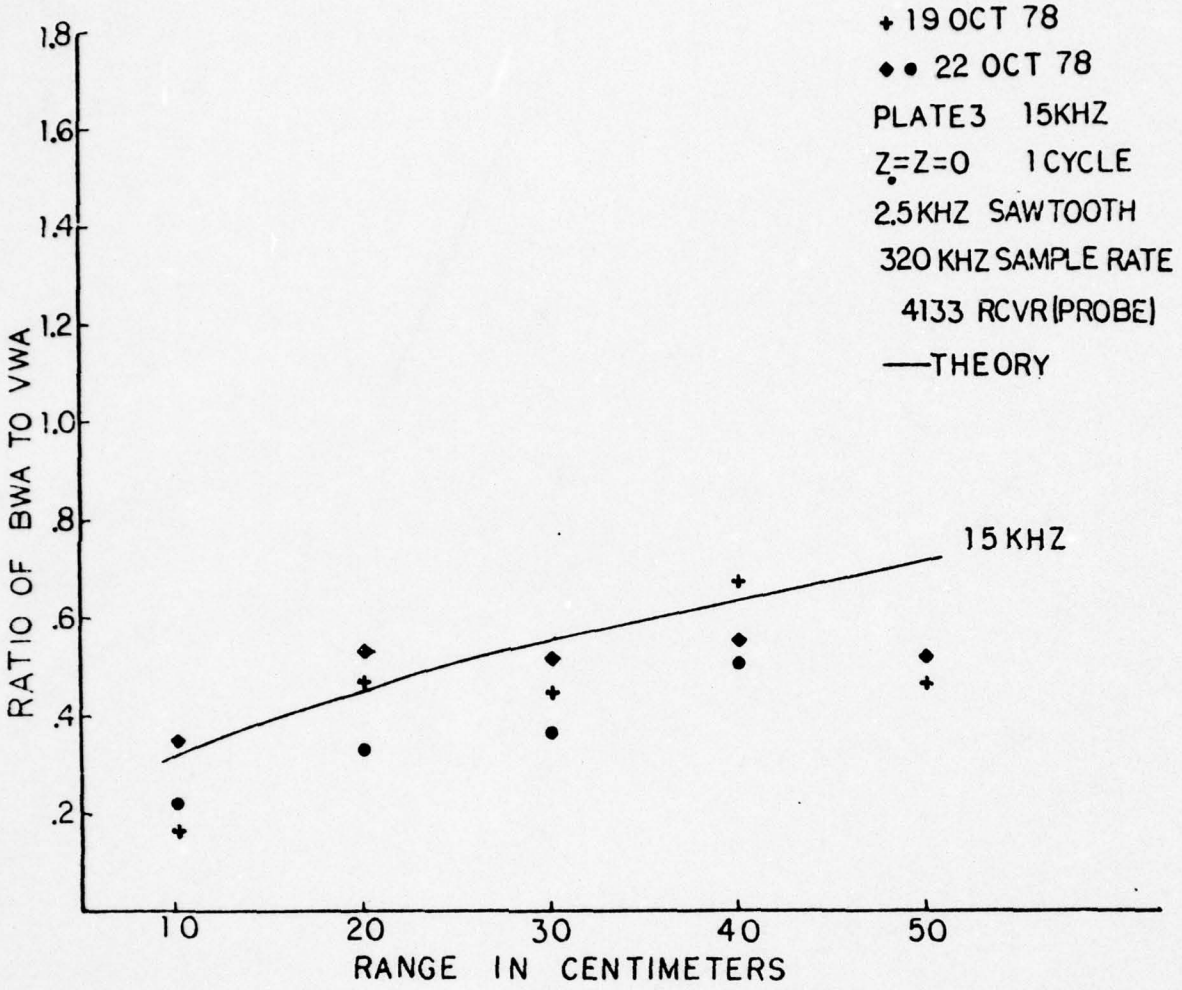

Figure 55. Ratio Of BWA To VWA vs. Range (15 kHz)

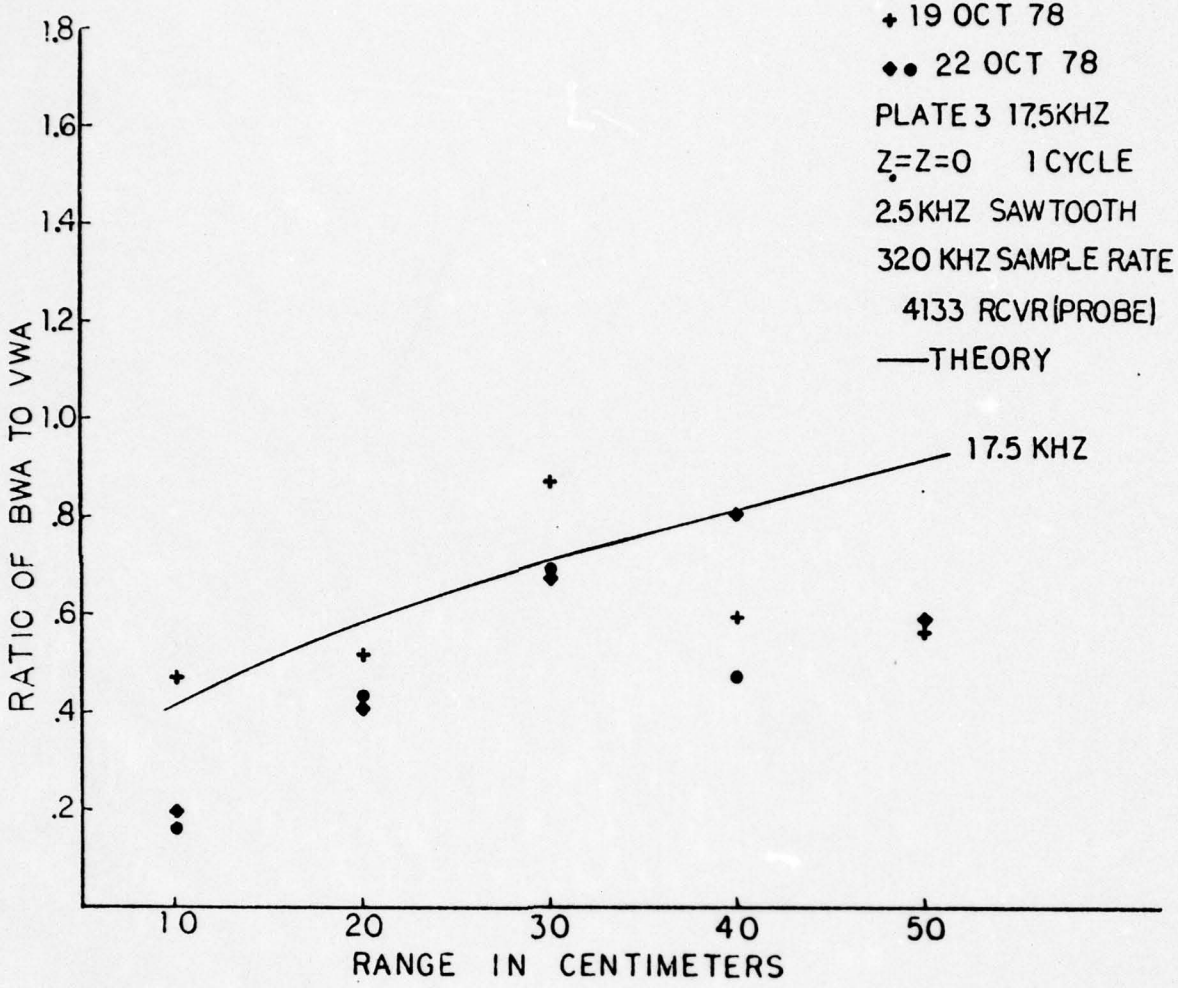

Figure 56. Ratio Of BWA To VWA vs. Range (17.5 kHz)

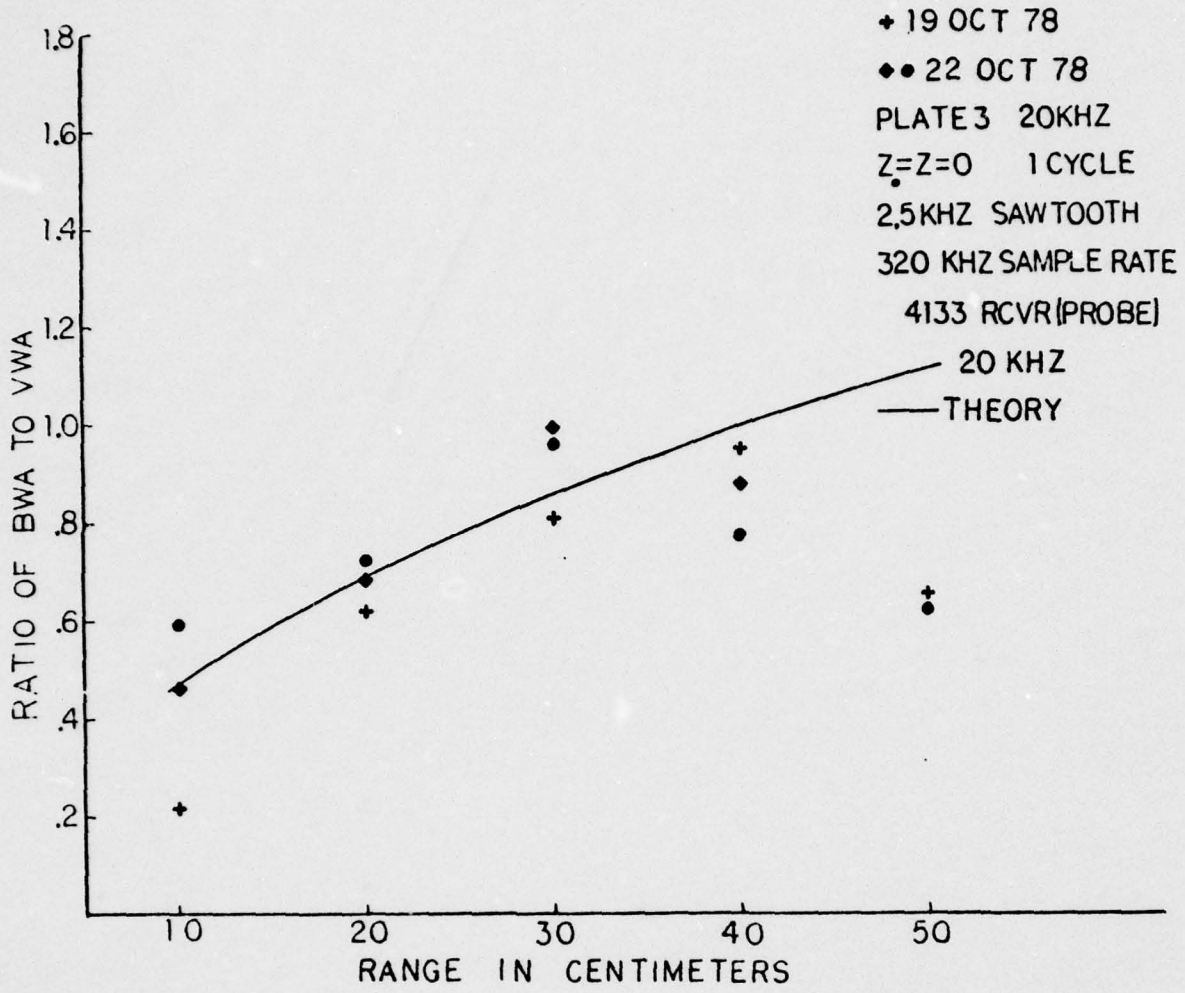

Figure 57. Ratio of BWA To VWA vs. Range (20 kHz)

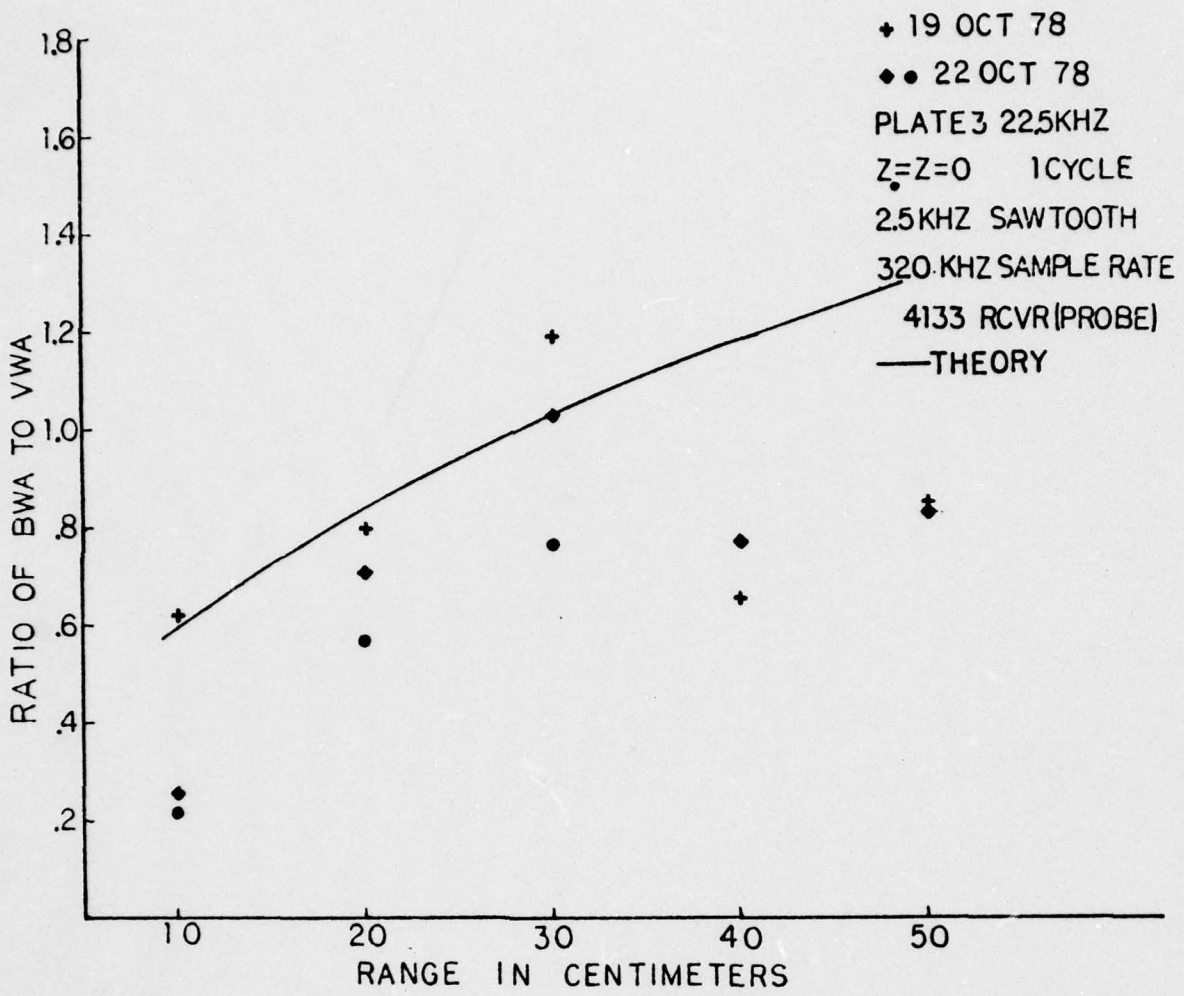

Figure 58. Ratio Of BWA To VWA vs. Range (22.5 kHz)

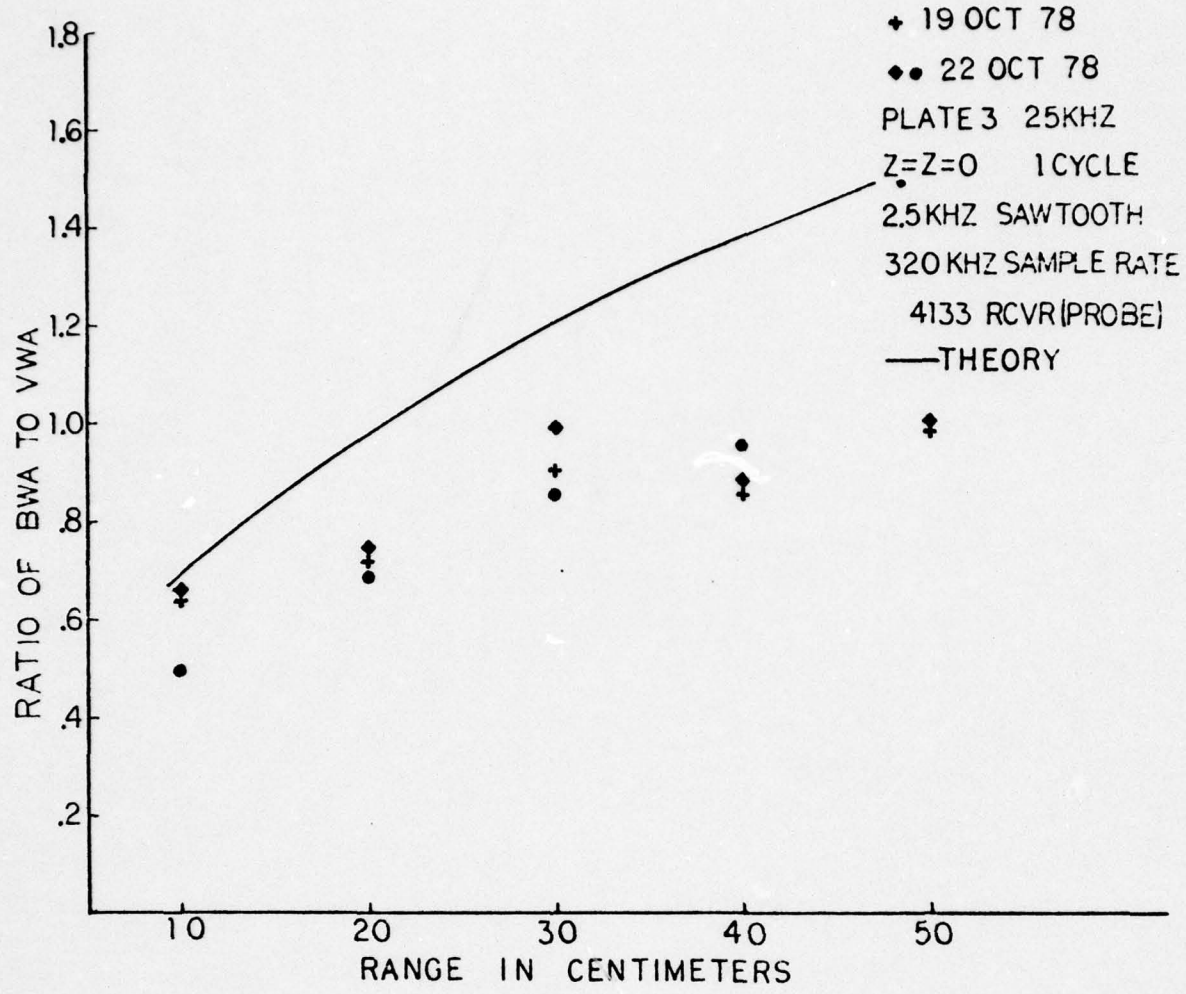

Figure 59. Ratio Of BWA To VWA vs. Range (25 kHz)

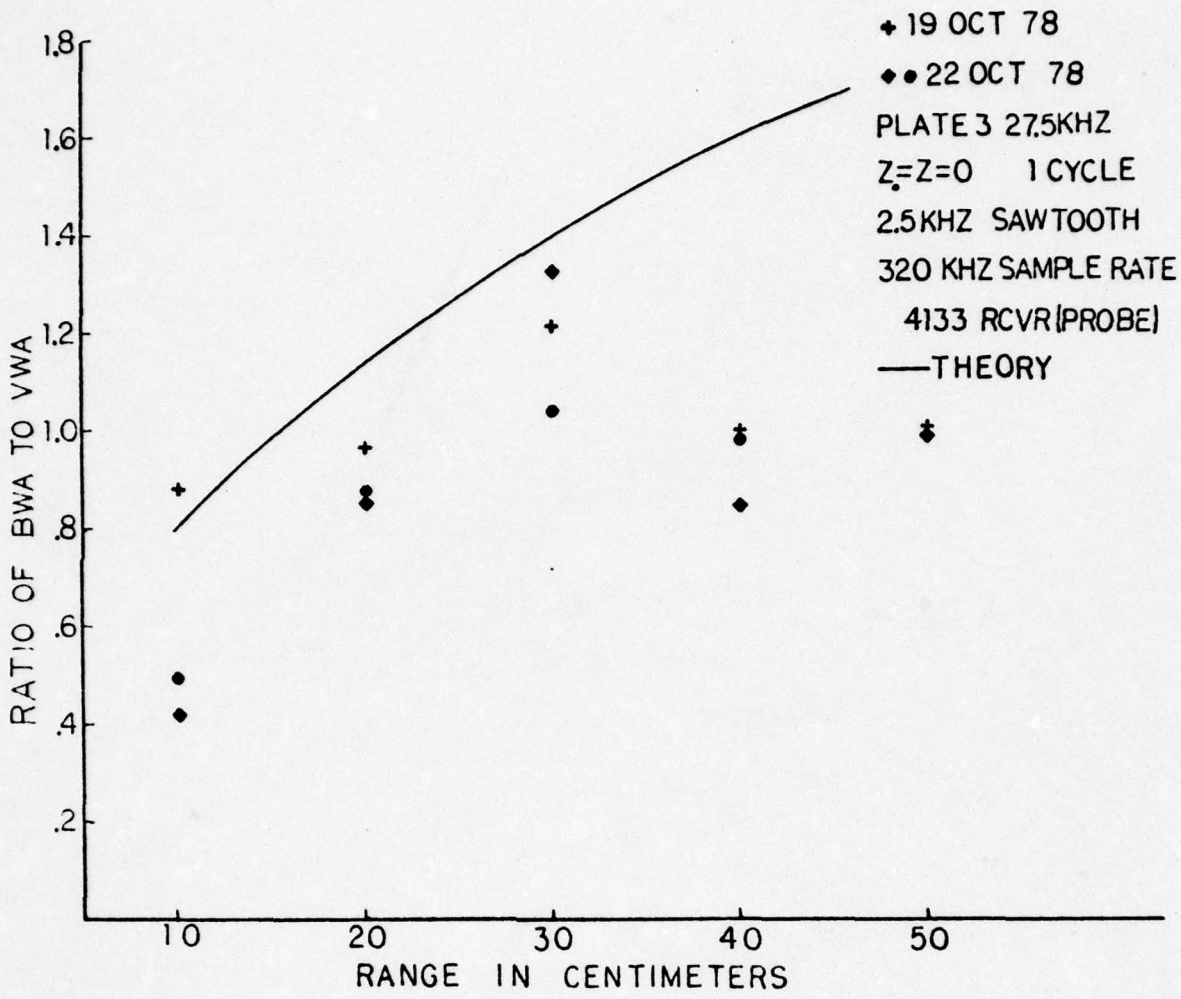

Figure 60. Ratio Of BWA To VWA vs. Range (27.5 kHz)

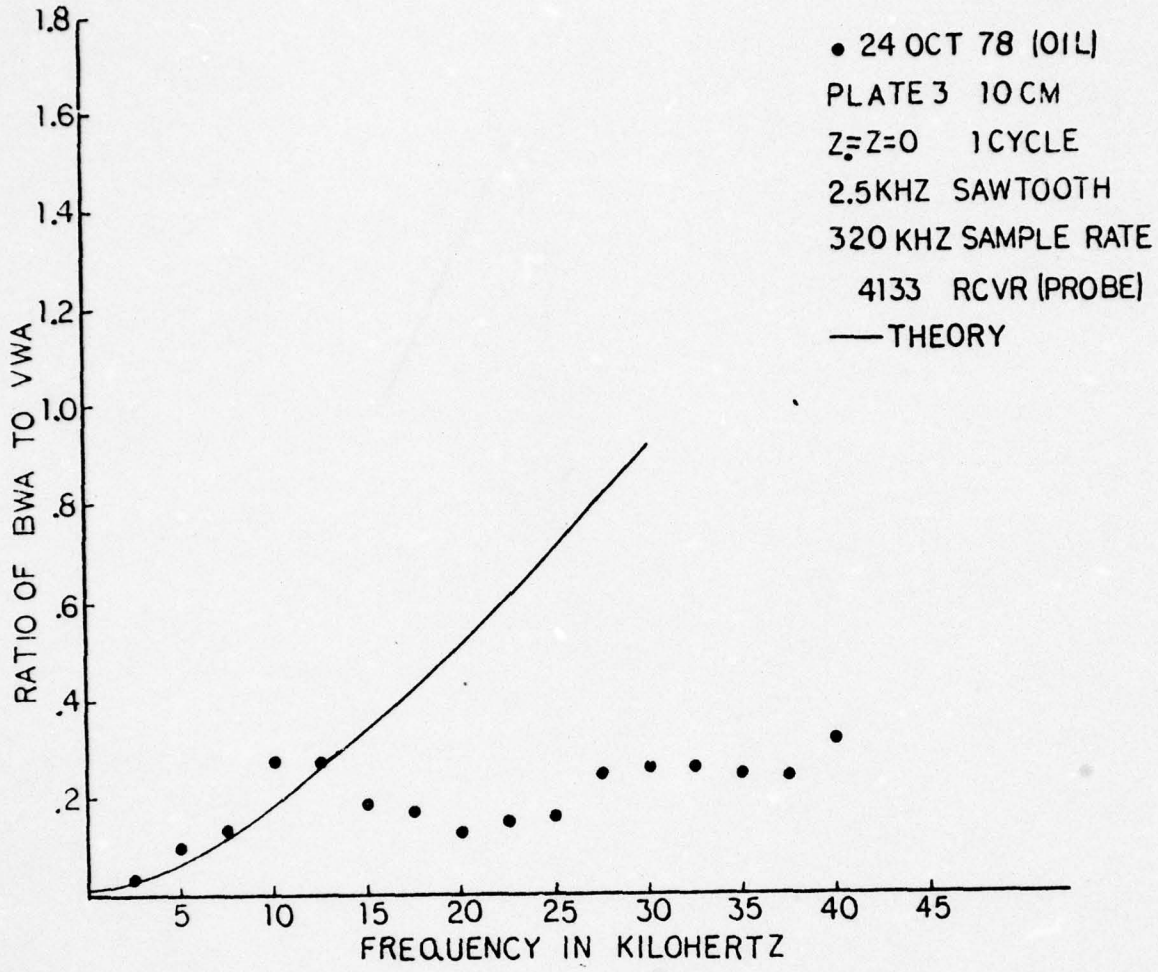

Figure 61. Ratio of BWA To VWA vs. Frequency (10 cm)

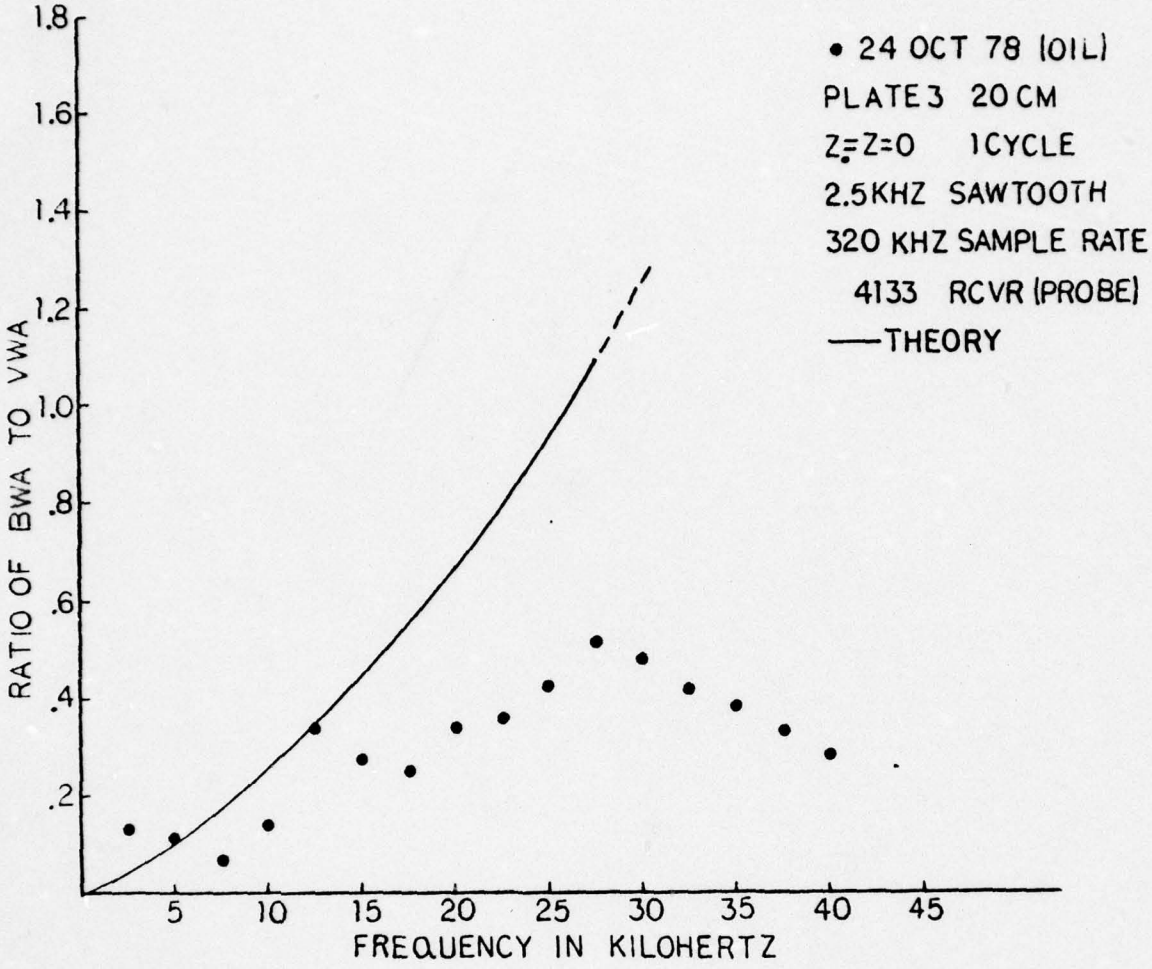

Figure 62. Ratio Of BWA To VWA vs. Frequency (20 cm.)

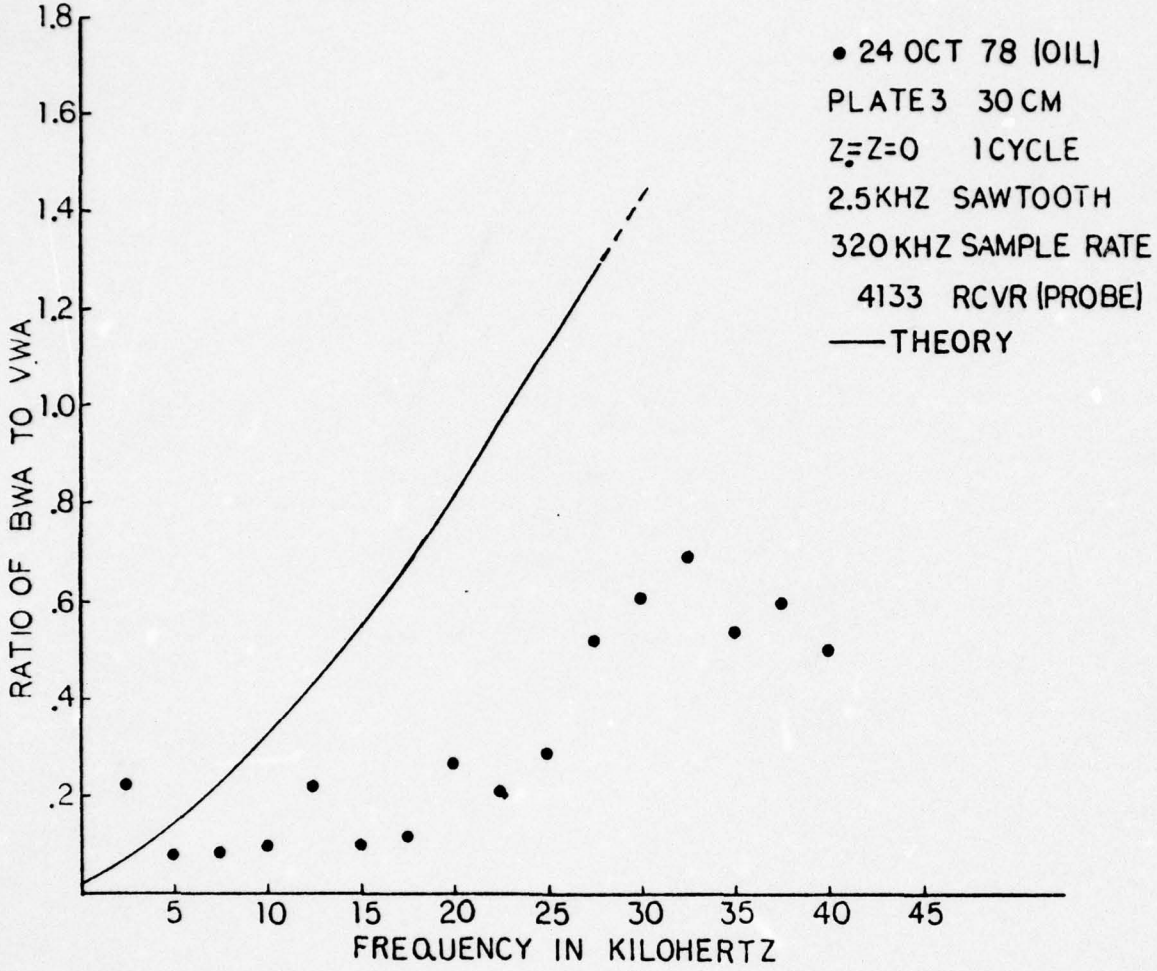

Figure 63. Ratio of BWA To VWA vs. Frequency (30 cm.)

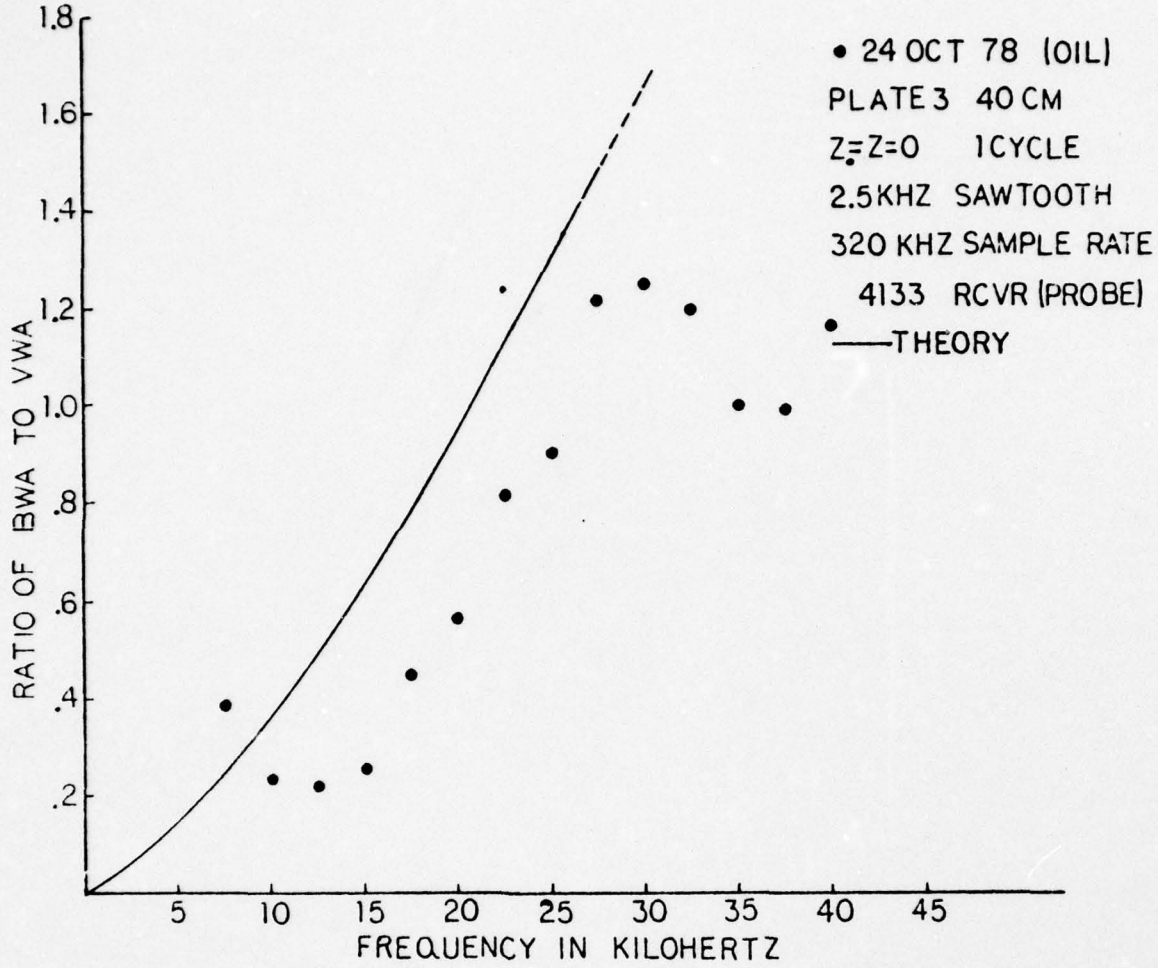

Figure 64. Ratio Of BWA To VWA vs. Frequency (40 cm.)

AD-A066 365 NAVAL POSTGRADUATE SCHOOL MONTEREY CALIF F/G 20/1
NEAR GRAZING SCATTERING BY SLIGHTLY ROUGH SURFACES.(U)
DEC 78 J M BAILIE

UNCLASSIFIED NL

2 OF 2
AD
A066365

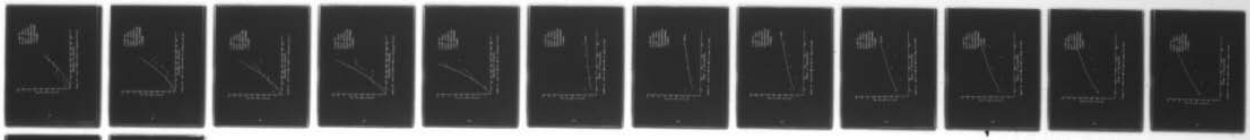

END
DATE
FILMED
5--79
DDC

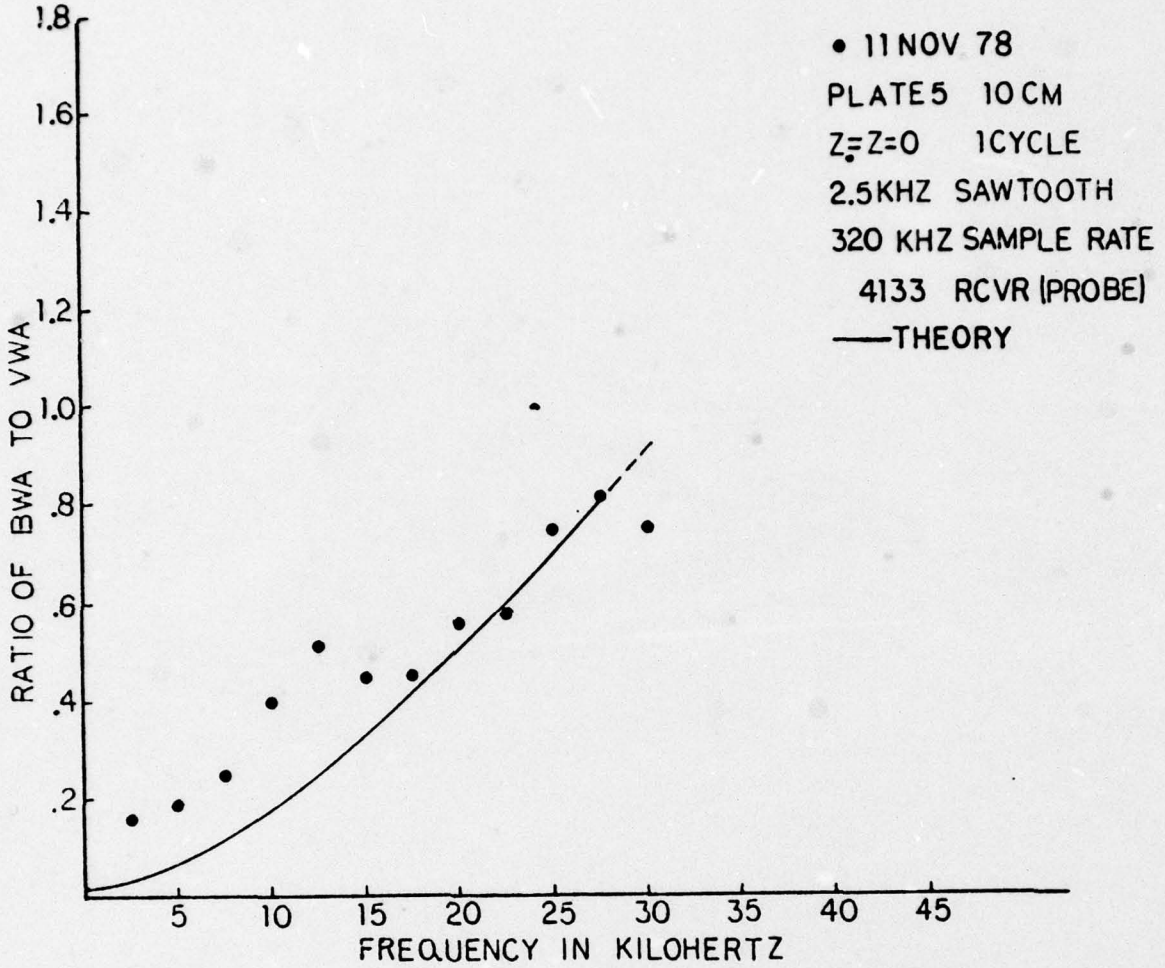

Figure 65. Ratio Of BWA To VWA vs. Frequency (10 cm.)

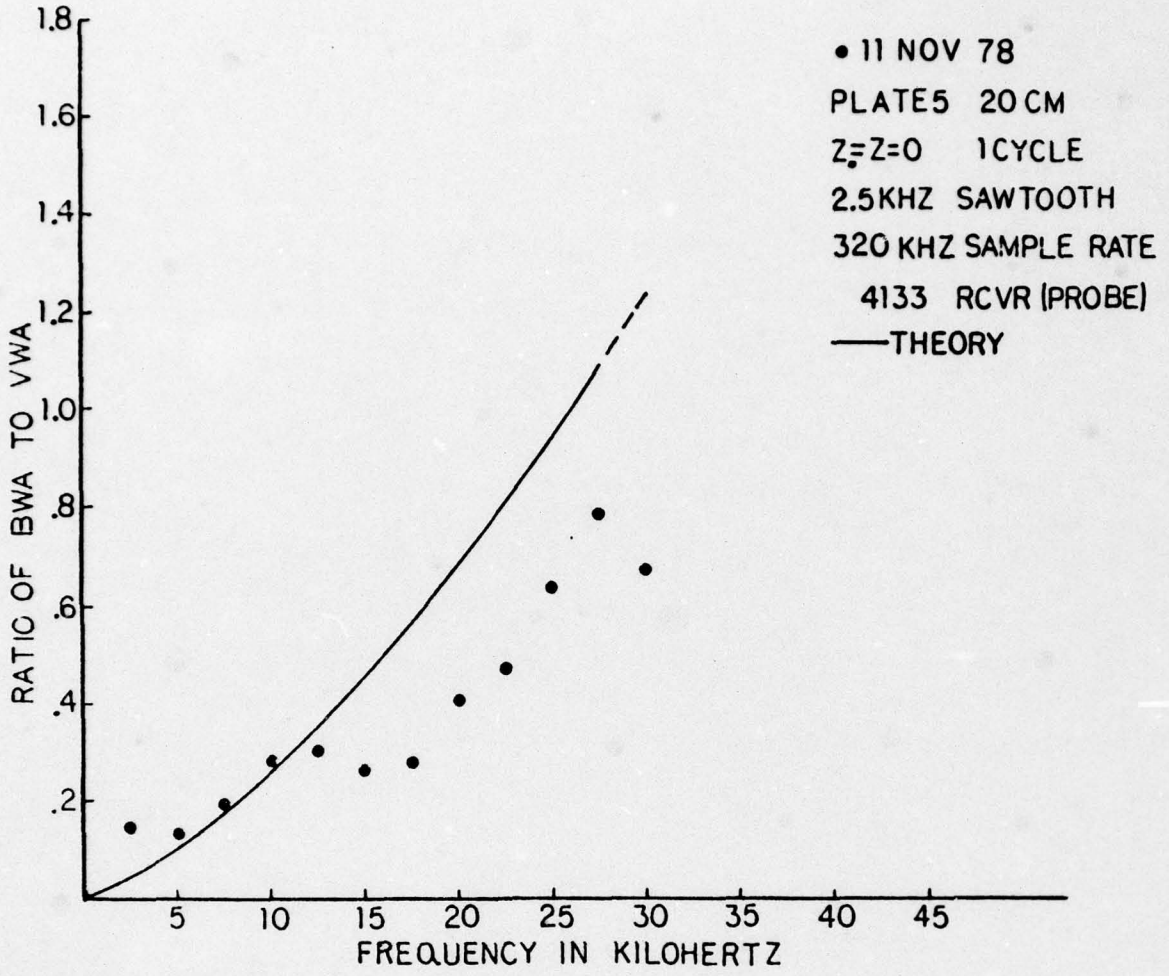

Figure 66. Ratio of BWA To VWA vs. Frequency (20 cm.)

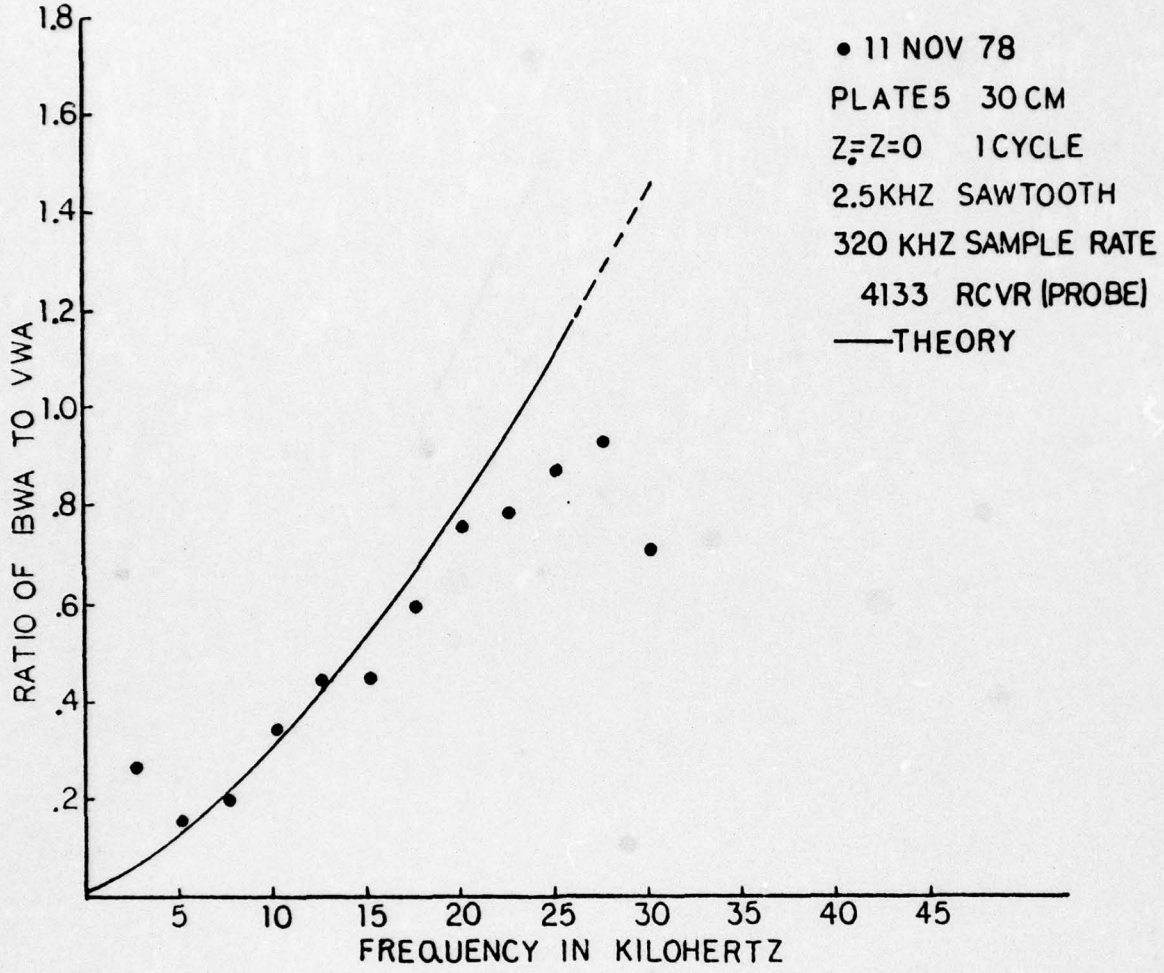

Figure 67. Ratio Of BWA To VWA vs. Frequency (30 cm.)

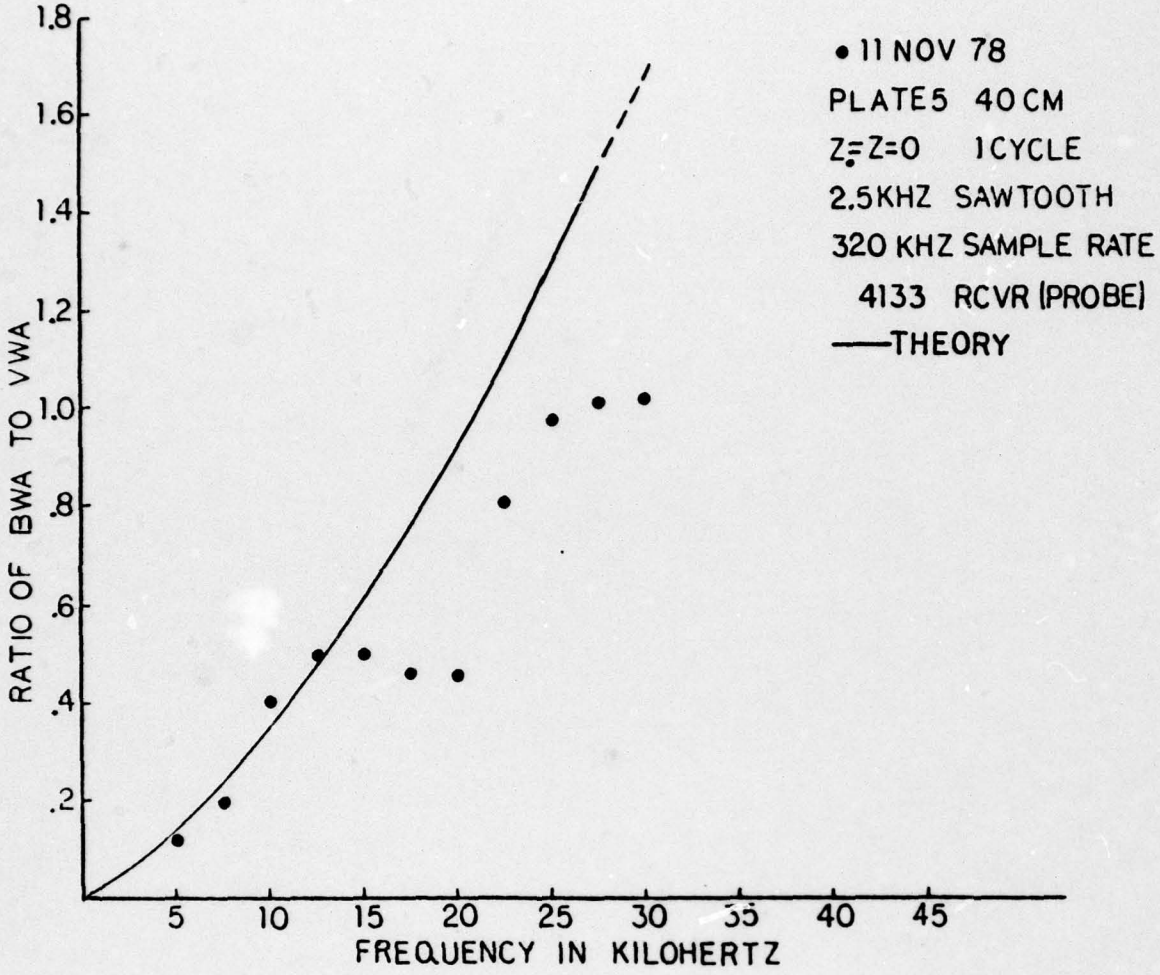

Figure 68. Ratio Of BWA To VWA vs. Frequency (40 cm.)

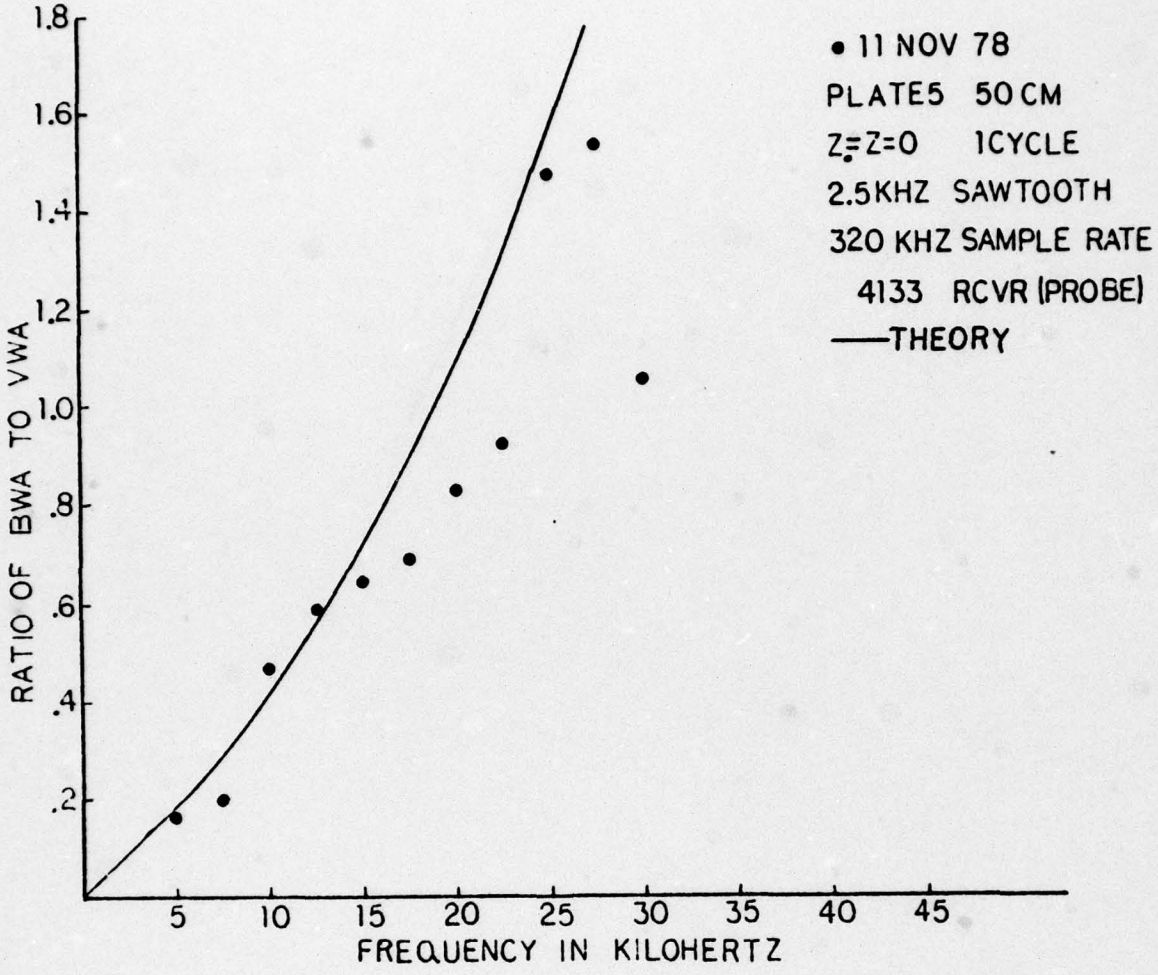

Figure 69. Ratio of BWA To VWA vs. Frequency (50 cm.)

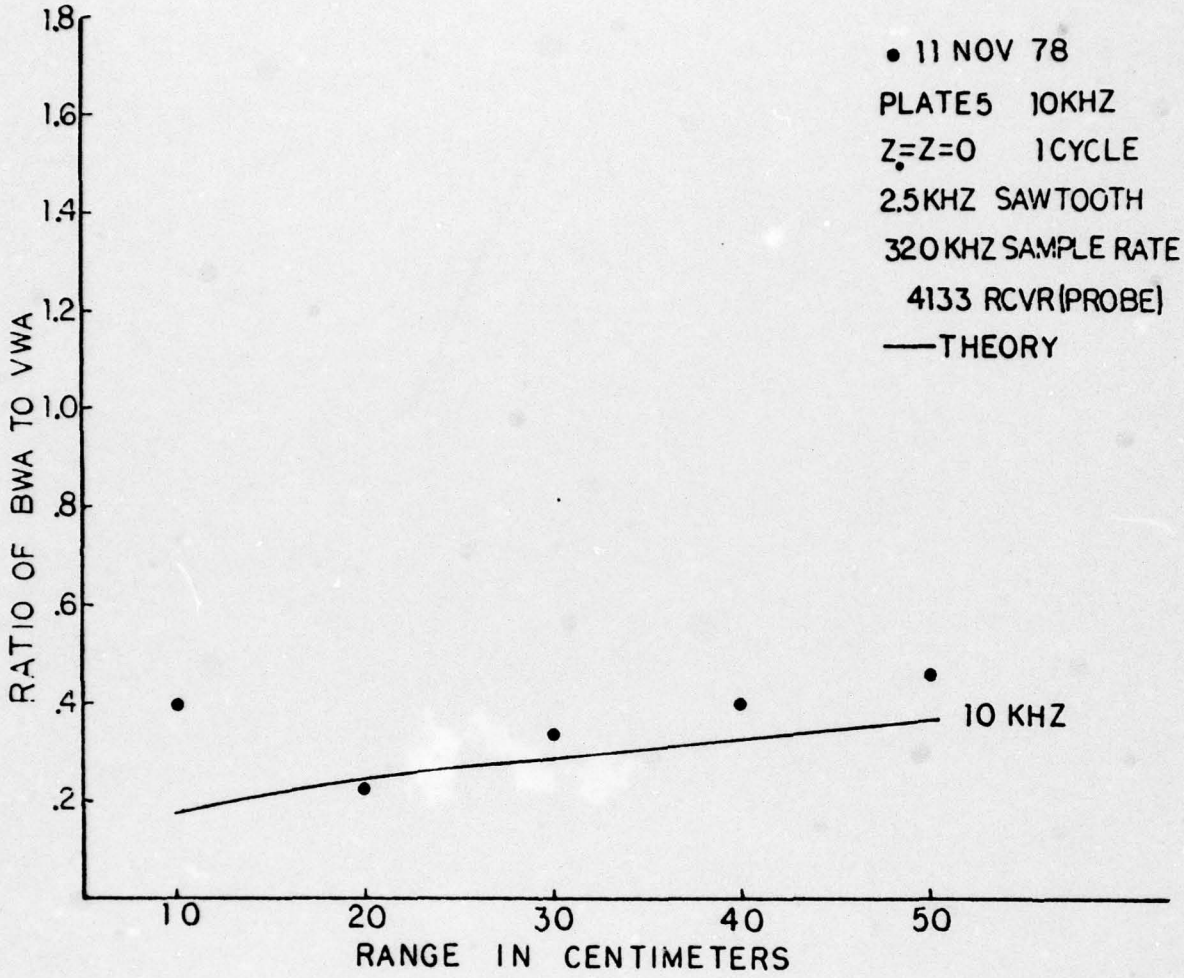

Figure 70. Ratio Of BWA To VWA vs. Range (10 kHz)

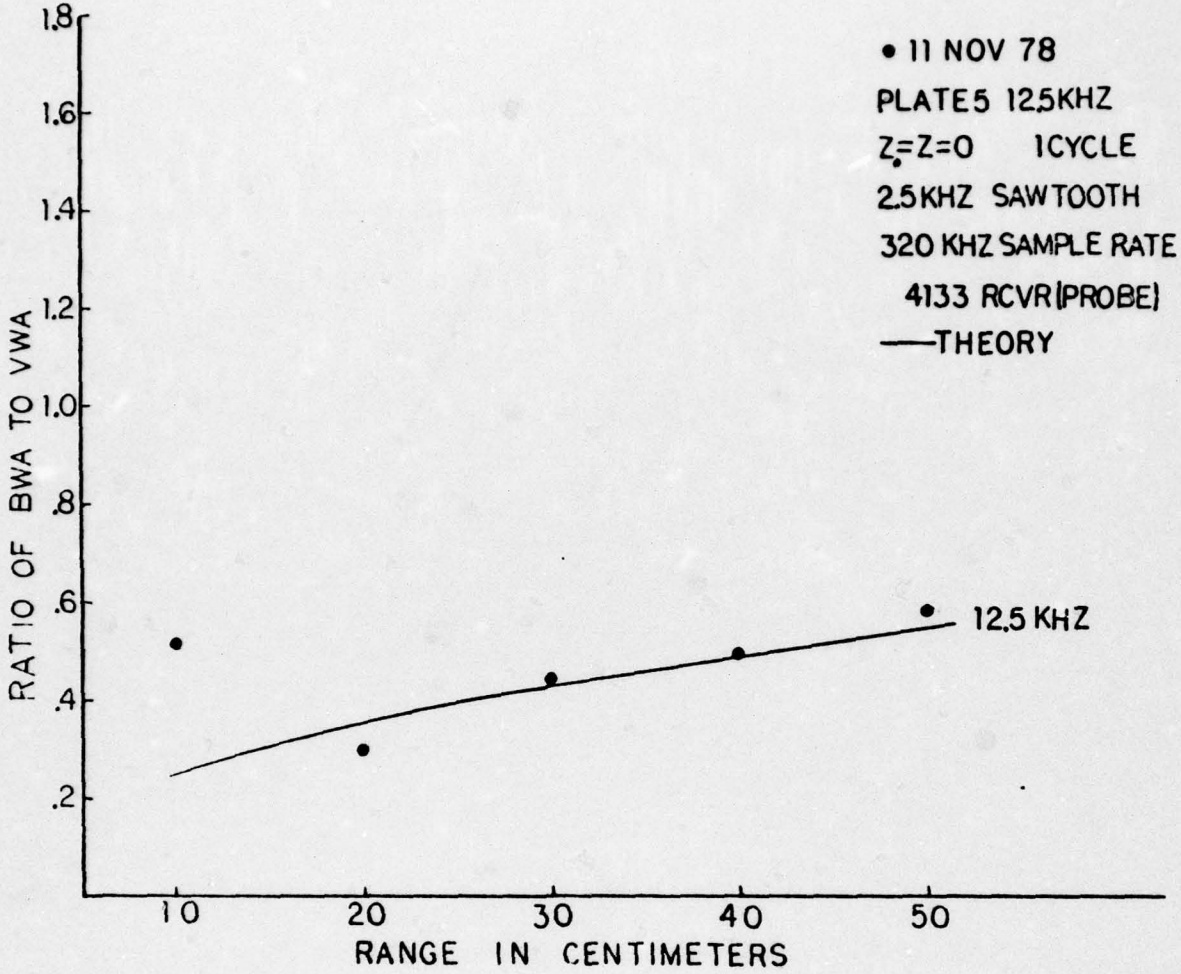

Figure 71. Ratio Of BWA To VWA vs. Range (12.5 kHz)

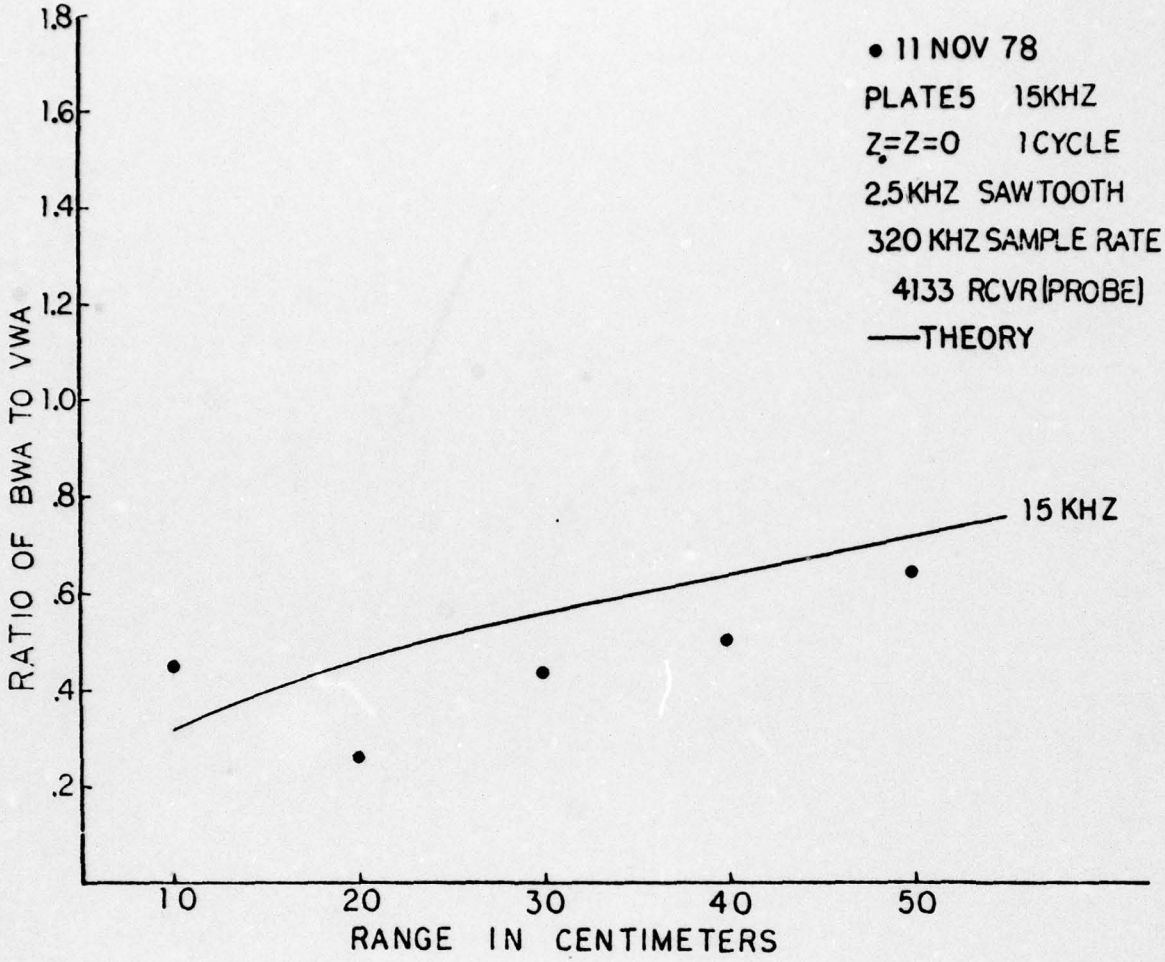

Figure 72. Ratio Of BWA To VWA vs. Range (15 kHz)

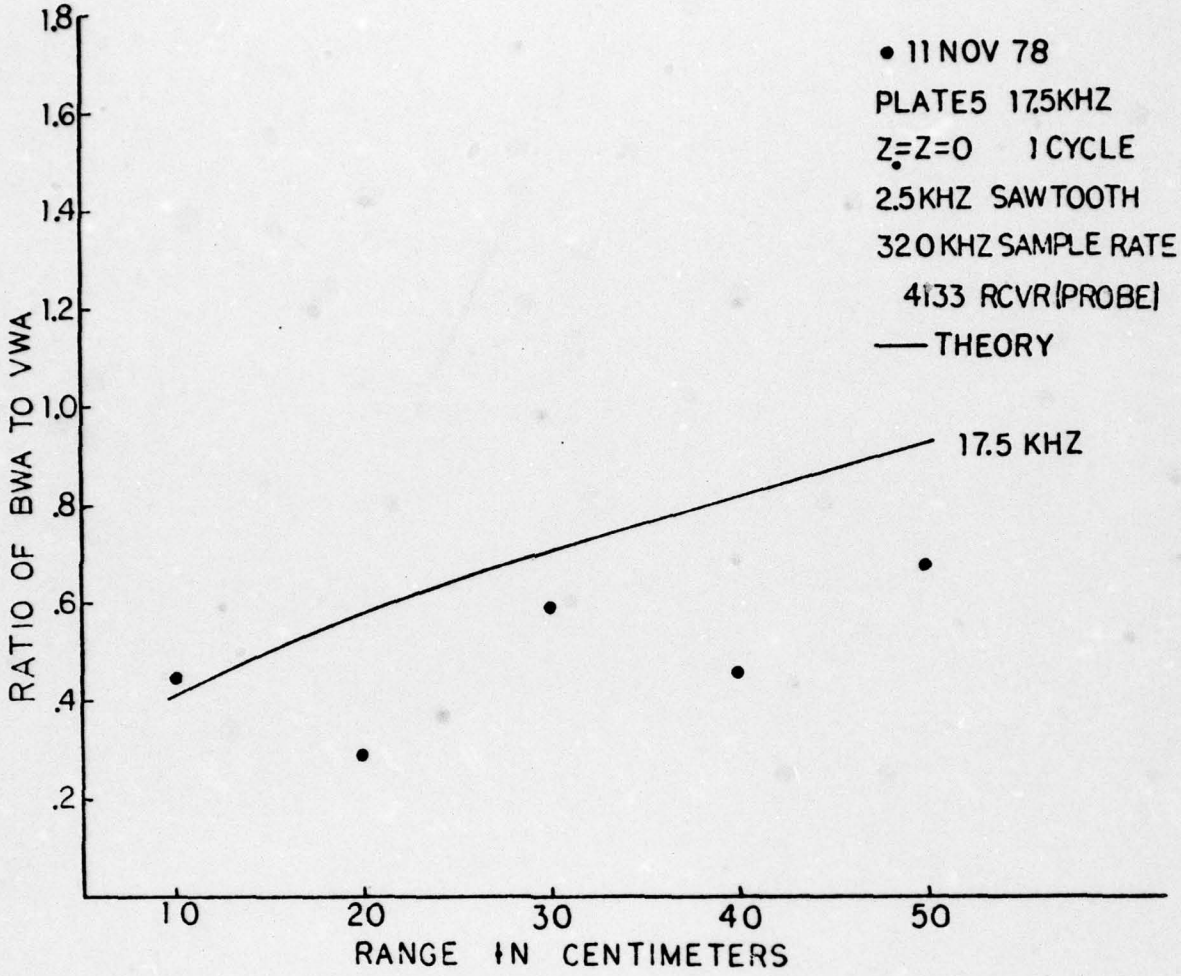

Figure 73. Ratio Of BWA To VWA vs. Range (17.5 kHz)

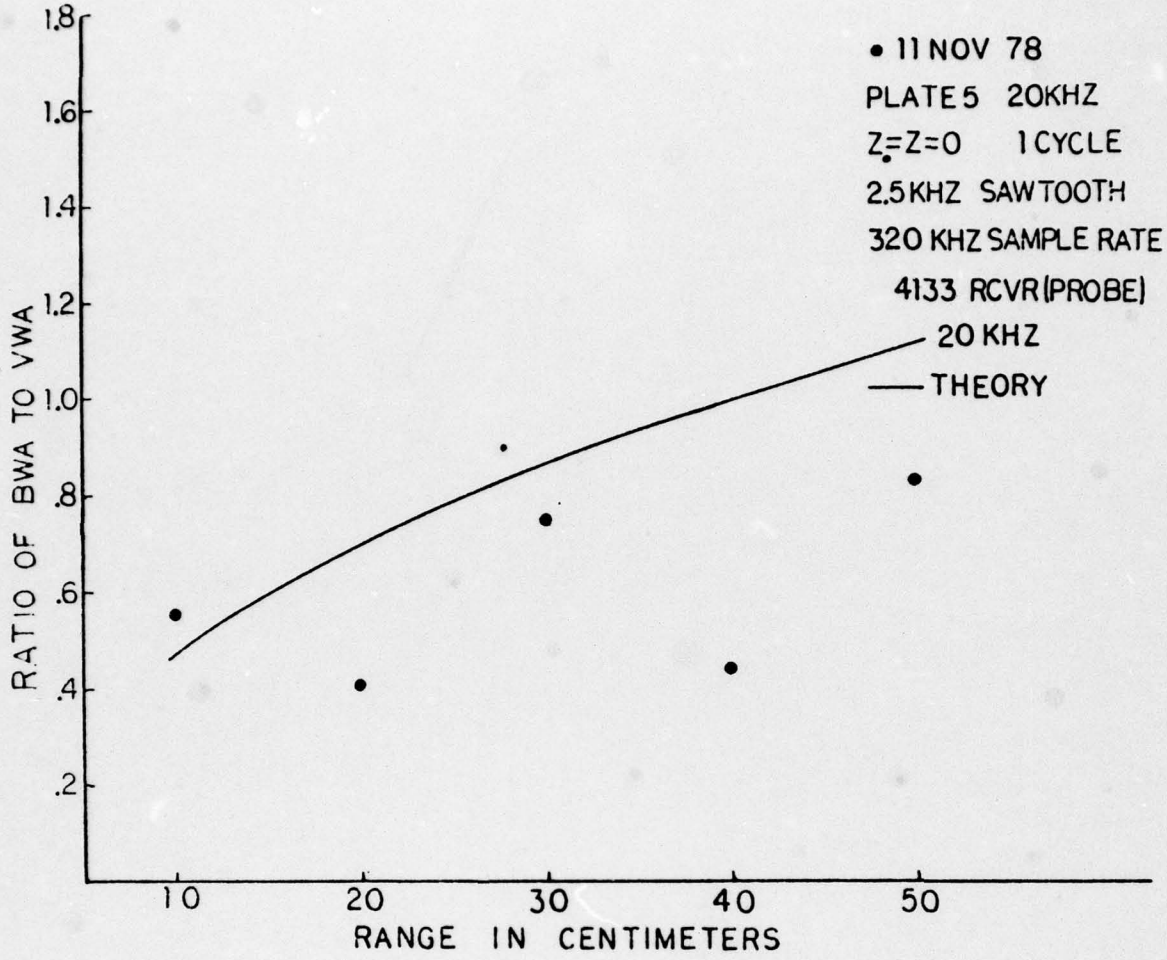

Figure 74. Ratio Of BWA To VWA vs. Range (20 kHz)

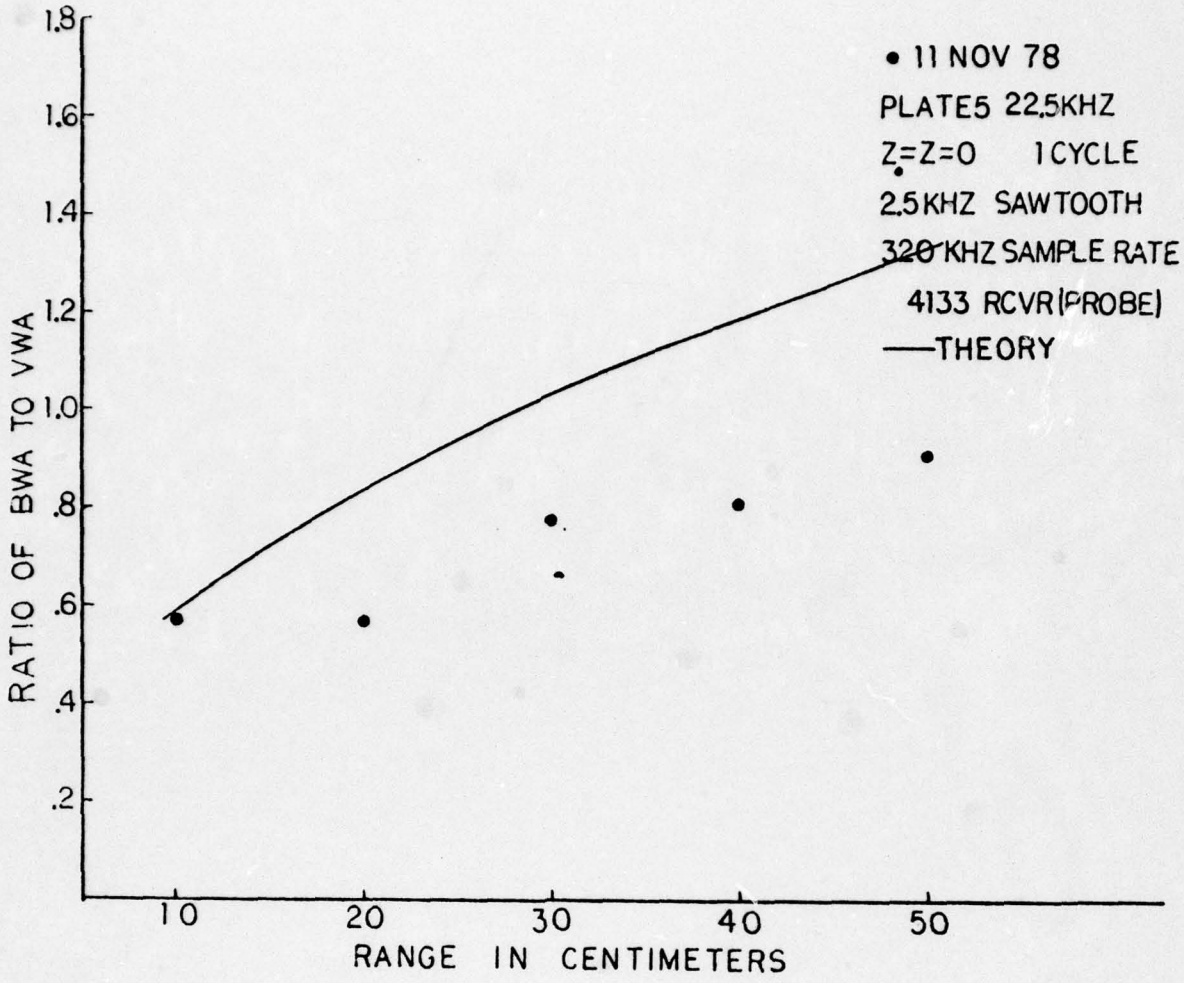

Figure 75. Ratio Of BWA To VWA vs. Range (22.5 kHz)

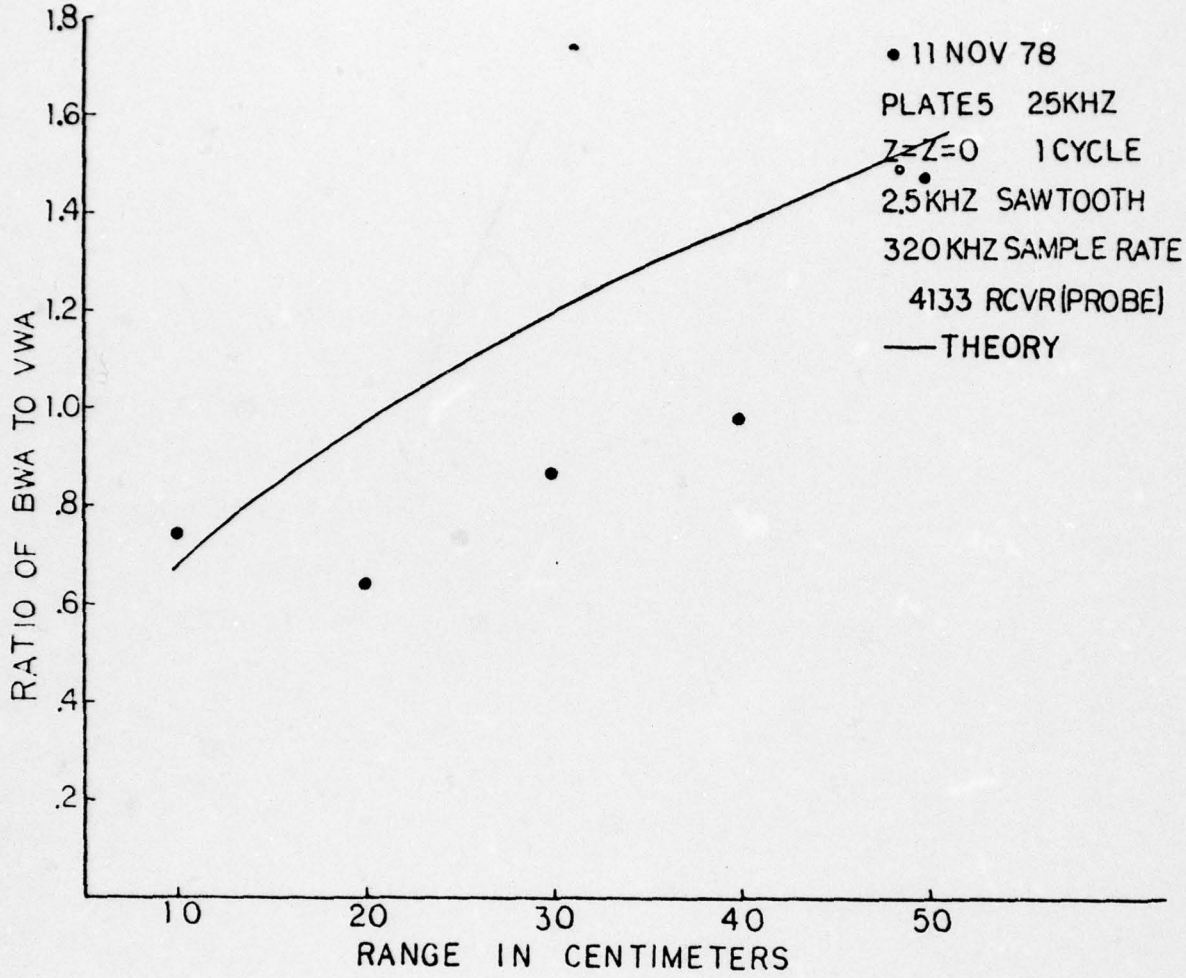

Figure 76. Ratio Of BWA To VWA vs. Range (25 kHz)

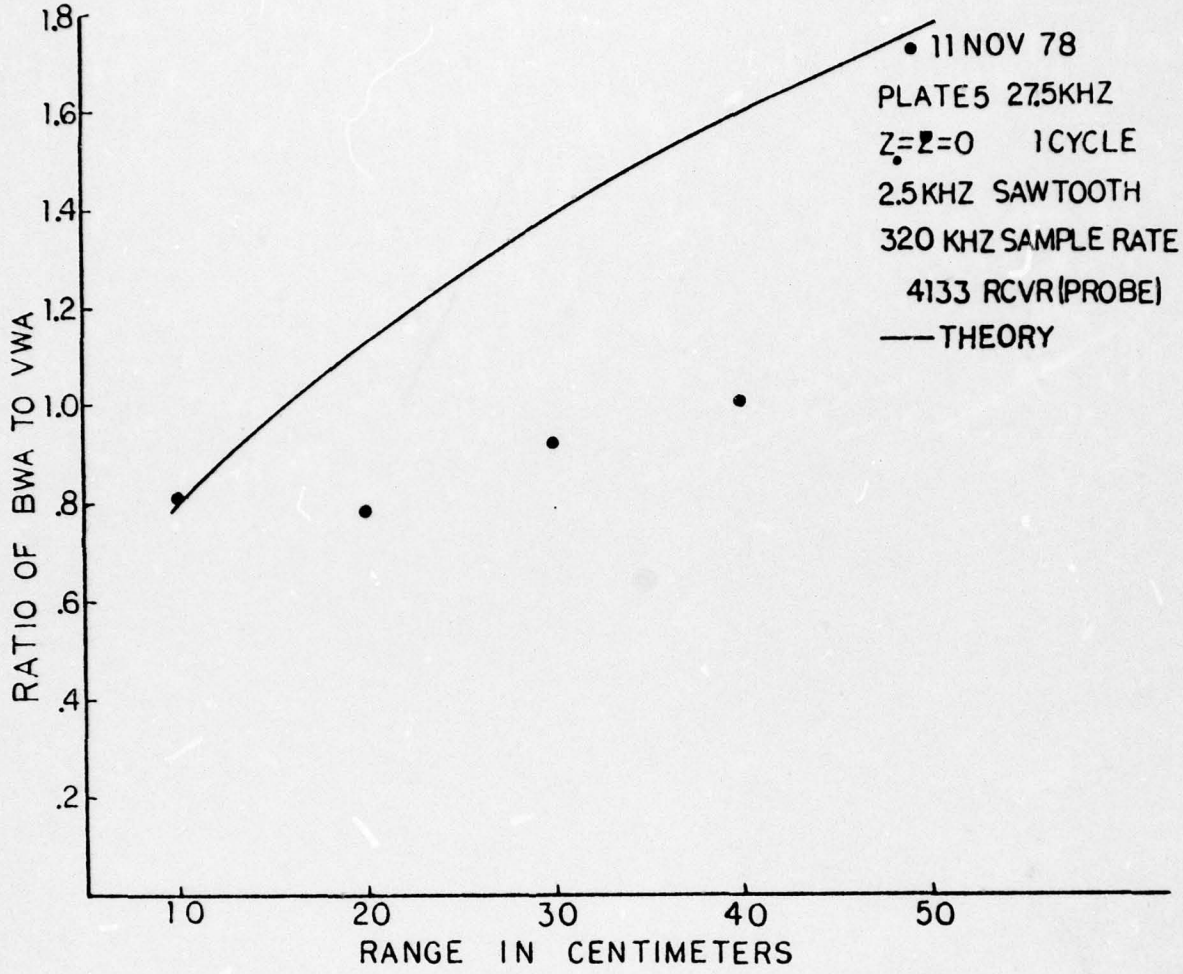

Figure 77. Ratio Of BWA To VWA vs. Range (27.5 kHz)

BIBLIOGRAPHY

1. Biot, M.A., "Generalized Boundary Condition For Multiple Scatter in Acoustic Reflection," The Journal of the Acoustical Society of America, v. 44, p. 1616-1622, 1968.

2. Biot, M.A., "Lagrangian Analysis of Multiple Scatter in Acoustic and Electromagnetic Reflection," Acad. Roy. de Beligique, Bull, Classe des Sci., v.59, p. 153-169, 1973.

3. Tolstoy, I., "Applications of Normal Coordinate Theory to Very Low Frequency Propagation," The Journal of the Acoustical Society of America, 63, S60 (1978).

4. Tolstoy, I., "The Scattering of Spherical Pulses By Slightly Rough Surfaces," The Journal of the Acoustical Society of America, accepted for publication in winter/spring of 1979.

INITIAL DISTRIBUTION LIST

		No. Copies
1.	Library, Code 0142 Naval Postgraduate School Monterey, California 93940	2
2.	Department Chairman, Code 61 Department of Physics and Chemistry Naval Postgraduate School Monterey, California 93940	2
3.	Professor H. Medwin, Code 61Md Department of Physics and Chemistry Naval Postgraduate School Monterey, California 93940	6
4.	Lcdr. James M. Bailie 504 Pondview Circle Virginia Beach, Virginia 23452	1
5.	Manager Anti-Submarine Warfare Systems Project Office Attn: Cdr. J. Hagy ASW 13 Department of the Navy Washington, D.C. 20362	1
6.	Dr. J.C. Novarini Av. Cordoba 4190 1188 Cap. Fed. Buenos Aires Argentina	1
7.	Director of Defense Research and Engineering Office of the Secretary of Defense Washington, D.C. 20301 ATTN: Office, Assistant Director (Research)	1
8.	Defense Documentation Center Cameron Station Alexandria, Virginia 22314	2
9.	Director Naval Research Laboratory Washington, D.C. 20375 ATTN: Library, Code 2620	6

10. Office of Naval Research
Arlington, Virginia 22217
ATTN: (Code 480) 3
ATTN: (Code 460) 1
ATTN: (Code 102-OS) 1
ATTN: (Code 102IP) 6

11. Commander
Naval Oceanographic Office
Washington, D.C. 20390
ATTN: Code 1640 1
ATTN: Code 70 1

12. NODC/NOAA
Rockville, MD. 20882 1

13. Dr. I. Tolstoy
Knockvennie, Castle Douglas 1
S.W. Scotland

14. Dr. Ralph Goodman, Scientific Director
NORDA - NSTL Station 1
Bay St. Louis, Mississippi 39520